

CrossMark
click for updatesCite this: *J. Anal. At. Spectrom.*, 2016,
31, 35

Received 11th November 2015

DOI: 10.1039/c5ja90061a

www.rsc.org/jaas

Atomic spectrometry update – a review of advances in environmental analysis

Owen T. Butler,^{*a} Warren R. L. Cairns,^b Jennifer M. Cook^c and Christine M. Davidson^d

1	Air analysis
1.1	Review papers
1.2	Sampling techniques
1.3	Reference materials and calibrants
1.4	Sample preparation
1.5	Instrumental analysis
1.5.1	Atomic absorption and fluorescence spectrometry
1.5.2	Atomic emission spectrometry
1.5.3	Mass spectrometry
1.5.3.1	Inductively coupled plasma mass spectrometry
1.5.3.2	Other mass spectrometry techniques
1.5.4	X-ray spectrometry
1.5.5	Other spectrometric techniques
2	Water analysis
2.1	Sample preconcentration and extraction
2.2	Speciation and fractionation analysis
2.3	Instrumental analysis
2.3.1	Atomic absorption spectrometry
2.3.2	Laser based spectroscopy
2.3.3	Inductively coupled plasma mass spectrometry
2.3.4	Vapour generation techniques
2.3.5	X-ray spectrometry
3	Analysis of soils, plants and related materials
3.1	Review papers
3.2	Sample preparation
3.2.1	Sample storage and pre-treatment
3.2.2	Sample dissolution and extraction
3.2.3	Preconcentration procedures
3.3	Instrumental analysis
3.3.1	Atomic absorption spectrometry
3.3.2	Atomic emission spectrometry
3.3.3	Atomic fluorescence spectrometry
3.3.4	Inductively coupled plasma mass spectrometry
3.3.5	Laser induced breakdown spectroscopy

3.3.6	X-ray spectrometry
3.4	Analytical quality assurance
4	Analysis of geological materials
4.1	Reference materials and data quality
4.2	Solid sample introduction
4.2.1	Laser ablation inductively coupled plasma mass spectrometry
4.2.2	Laser-induced breakdown spectroscopy
4.3	Sample dissolution, separation and preconcentration
4.4	Instrumental analysis
4.4.1	Atomic absorption and emission spectrometry
4.4.2	Inductively coupled plasma mass spectrometry
4.4.3	Other mass spectrometric techniques
4.4.3.1	Thermal ionisation mass spectrometry
4.4.3.2	Secondary ion mass spectrometry
4.4.3.3	Accelerator mass spectrometry
4.4.3.4	Isotope ratio mass spectrometry
4.4.4	X-ray spectrometry
5	Glossary of terms
6	References

This is the 31st annual review of the application of atomic spectrometry to the chemical analysis of environmental samples. This update refers to papers published approximately between August 2014 and July 2015 and continues the series of Atomic Spectrometry Updates (ASUs) in Environmental Analysis¹ that should be read in conjunction with other related ASUs in the series, namely: clinical and biological materials, foods and beverages;² advances in atomic spectrometry and related techniques;³ elemental speciation;⁴ X-ray spectrometry;⁵ and metals, chemicals and functional materials.⁶ In the field of air analysis, highlights within this review period included: the development of a new laser fluorescence instrument for the ultratrace determination of mercury vapour; single particle ICP-MS studies and the coupling of elemental analysers to mass spectrometers for the improved characterisation of carbonaceous aerosols. In the arena of water analysis, methods continue to be developed: for the extraction and preconcentration of elements, As, Cr, Hg and Sb species and

^aHealth and Safety Laboratory, Harpur Hill, Buxton, SK17 9JN, UK. E-mail: owen.butler@hsl.gsi.gov.uk

^bCNR-IDPA, Università Ca' Foscari, 30123 Venezia, Italy

^cBritish Geological Survey, Keyworth, Nottingham, NG12 5GG, UK

^dUniversity of Strathclyde, Cathedral Street, Glasgow, G1 1XL, UK



determination of elemental constituents in colloidal and NP fractions. Emerging elements of interest include Gd derived from MRI agents discharged at low level from medical facilities in water courses. Instrumental developments reported included the use of MC-ICP-MS for isotopic tracer studies and a review of TXRF techniques and associated preconcentration procedures for trace element analysis. In the period covered by this update several articles have explored the analysis of soil extracts for geochemical prospecting. There has been widening interest in the use of CS-AAS and in the application of techniques capable of direct sample analysis such as slurry sampling ETAAS and ETV-ICP-AES. Portable XRF instrumentation is now being used in many disciplines to quantify trace elements in soils – bringing a need for better transfer of analytical knowledge to non-specialist users – and the growing use of portable XRF in proximal sensing is also noteworthy. Recent research indicates that geological applications still drive many of the instrumental and methodological advances in LA-ICP-MS. Fundamental studies continued to shed light on the processes involved and hence ways of improving the analysis of laser-produced aerosols and to minimise matrix and fractionation effects. A new technique LA-DOF-MS (distance of flight) was described. The utility of LIBS and portable XRF for *in situ* survey work continues to show promise but issues such as appropriate calibration regimes and data processing protocols will still need to be addressed.

1 Air analysis

1.1 Review papers

Useful *review papers* were published that provide a summary of the current and emerging technologies for the characterization of the elemental component in atmospheric particles⁷ (22 references); brown carbon aerosols⁸ (377 references) airborne nanoparticles⁹ (91 references) and in nanomaterials (57 references).¹⁰ Given the overlap in measurement science and the fact that airborne particles can deposit into the seas, then this review¹¹ (142 references) on the analysis of major and trace elements in marine particles is also recommended. Particles and fumes from smoking can contribute to the degradation of air quality and here so it was interesting to note a review of the development of standardised methods to test cigarette smoke¹² (70 references) and a review of analytical methods to test the chemical components of e-cigarette cartridges and refill fluids¹³ (47 references). Researchers in the UK have considered potential methods¹⁴ (9 references) for the determination of total halogenated compounds in H₂ for use in membrane fuel cells and have proposed that ICP-MS provides the best currently available analytical solution.

1.2 Sampling techniques

Evaluation of existing *personal air sampler systems* to monitor workers' exposure to airborne particles continues to be of growing interest. A US research group¹⁵ evaluated whether the relative orientation of the widely used 37 mm closed faced cassette sampler when worn by a worker had an influence on the sample mass that was collected and found that it did not.

Sampling pumps attempt to maintain a constant, known airflow during sampling exercises otherwise sampling volume will be unknown and hence worker concentration exposure indeterminate. Despite integrating pulsation dampers within pump designs, nevertheless, periodic pulsations remain, for example due to reciprocating motion of a piston stroke. The EN standard 1232 recommends that the amplitude of pulsations be <10% of the mean flow rate and provides a way of assessing such deviations. Researchers at NIOSH¹⁶ have now developed an alternative assessment approach which they consider to be more representative of real-world pump performance and have noted that, for a range of pumps tested, pulsation measurements that were 1.5–2.2 times higher than those measured using the codified EN approach. Findings from this study will be reported to the consensus committees to be considered when this EN standard and other similar EN/ISO standards are up for revision. Deposit of particles to the internal surfaces of the widely used 37 mm closed faced cassette sampler can result in measurement results that are biased low if only the filter itself is analysed. For this reason, recent guidelines recommend that these surfaces be wiped and the wipe material employed be analysed alongside the filter. This is a cumbersome procedure and in response acid digestible cellulose acetate cassette inserts have been developed that fit inside samplers that are bonded to the filter. In summary they act as a liner thus preventing particle losses to walls. Researchers at NIOSH¹⁷ have undertaken a study, through parallel measurements of airborne levels of Pb and Sn in a solder manufacturing plant, to show that using these new inserts gave comparable results to the current practice of analyzing filters with their corresponding sampler surface wipe.

Exploiting *new developments in sampler technologies* for the improved assessment of worker exposure to airborne pollutants is of interest to a number of research groups. Elemental carbon is typically used as a marker for worker exposure to diesel fumes but analytically it is not possible, with combustion-based laboratory techniques, to differentiate between carbon in diesel fume samples from carbon derived from coal dust samples. Aerosols in a coal mine environment, where diesel powdered equipment is used, exhibit an aerodynamic bimodal particle distribution with a distinct accumulation mode peak at ~0.12 µm, attributable primarily to diesel fume emissions and a coarse mode peak at ~6 µm attributable primarily to coal particles with a minimum between modes at ~0.8 µm. Work commissioned by MSHA¹⁸ in the USA exploited this bimodal distribution through the design and validation of two new sharp cut cyclones operating at a nominal 0.8 µm cut size that would allow the preferential sampling of diesel fume over coal dust. NIOSH researchers¹⁹ established procedures (extraction methods and IC/ICP-MS analysis) to estimate the respiratory deposition of the nano fraction of selected metals in welding fume using a recently developed nanoparticle respiratory deposition (NRD) sampler. It was noted that a large fraction of the sample mass, 30–60% of the Cr, Mn and Ni content, lay within this nanoparticle fraction of <300 nm. Canadian researchers²⁰ have evaluated the capabilities of a recently commercialized aerosol-to-liquid particle extraction sampler



coupled to ICP-MS for the monitoring of trace metals in indoor air. This sampler, working on an electrostatic precipitation process, charges particles as they pass through the sampler, focuses them onto an electrode which is constantly washed using water resulting in sample being collected in a suspension reservoir which can then be taken away for digestion and analysed. The key advantage of this approach over a more conventional filter-based sampler is that higher air flow rates are achievable *i.e.* 300 L min⁻¹ vs. 1–20 L min⁻¹. This is due to the absence of back pressure in the system that would be present in filter based systems and hence load on the air pumping system. Further refinements are required such as inlets to enable this sampler to sample specific particle size ranges and to assess sampler efficiencies over different particle size ranges.

New *ambient air samplers* continue to be developed. A high volume aerosol-into-liquid sampler at 200 L min⁻¹ was developed to preconcentrate coarse particulate matter (PM_{2.5–10}) into a slurry sample.^{21,22} Copper was chosen as an element of interest for system evaluation given the reported association between this metal and ROS activity of PM and its potential to contribute therefore to overall PM induced toxicity. The soluble Cu concentration in these slurry samples were measured *in situ* with ISE and results obtained compared favourably with off-line measurements by ICP-MS. This monitoring system achieved near-continuous measurements, at 2–4 h intervals, for up to 7 days and application of this system to measure other water soluble metallic species by deploying other ISEs is envisaged. Working on a similar principle but at a lower flow rate of 16 L min⁻¹, a near-continuous – at 60 min intervals – PM₁₀ sampling system was deployed by Korean researchers²³ to study the elemental composition of Asian dust particles. Here 16 elements (Al, As, Ca, Cd, Co, Cr, Cu, Fe, K, Mn, Ni, Pb, Se, Ti, V and Zn) were determined off-line in the collected slurry samples by ICP-MS. A PM_{1.0/2.5/10} trichotomous sampler has been developed²⁴ to determine if airborne particles in the saddle point between the coarse and fine particle modes are derived from coarse or fine particles. This sampler consisted of a standard high volume sampler with two virtual impactors – one with a cut size of 2.5 µm and the second with a cut size of 1.0 µm – inserted between the PM₁₀ inlet and the sample filter. Filter portions were analysed: following leaching, by IC to determine SO₄²⁻, a species primarily found in the fine aerosol mode and analysed directly by PIXE to determine Ca, Fe, Si, and S species which are normally associated with coarse mode aerosols *i.e.* resuspended soil particles. Application of this sampler to Phoenix, Arizona, representing an arid region, showed that particles in this saddle point – specifically the 1 to 2.5 µm particle size range – consisted of ~75% of particles from the coarse mode and ~25% from the fine mode. The Hg isotopic signature may provide insight into tracking the sources and pathways of both airborne particulate matter and Hg_p in the atmosphere. A new sampler has been developed²⁵ that thermally liberates Hg from particulate matter sampled onto a quartz filter and collects the effluent in an acid-trapping solution. An aliquot of BrCl was then added to ensure that the collected Hg is in an ionic Hg²⁺ form. Total Hg concentrations were determined

using CVAFS and isotopic ratios determined using CV-MC-ICP-MS. System verification was undertaken by spiking precleaned blank quartz sample filters with aliquots of aqueous Hg standard (NIST 3133) or powdered soil CRMs (CRM 021, 024 from Sigma Aldrich and IERM GBW07405) which were subsequently analysed. The average Hg recovery was determined to 99 ± 6% (2SD, *n* = 90). The corresponding Hg isotopic ratio determined in this solid matrix samples using this thermal release approach were found to be in good agreement with those obtained with a standard addition protocol – solid test samples doped with various aqueous aliquots of NIST 3133 as the isotopic dopant – indicating the absence of matrix interferences. Initial field studies with this new system indicated that different Hg isotopic compositions do exist in the atmosphere and that further studies are therefore warranted.

Validation of samplers commonly used for volatile gaseous species is of interest to many. A European research group²⁶ has evaluated the performance of the Raschig-tube (RT) and the Drechsel impinger (DI) sampler against the well-established filter pack (FP) technique for the sampling of acidic gaseous species (CO₂, HBr, HCl, HF, HI and SO₂) emitted from volcanos. Analytically IC (for anionic Br, Cl, F and S species), ICP-MS (for Br and I species) and titrations (for dissolved CO₂) were used to perform measurements. The RT sampler approach is based upon the creation of a large interaction surface for sampling gaseous species through the continuous dosing of many little glass rings with a 1 M NaOH solution achieved by rotating this bundle of glass rings within the body of the sampler. The mass per unit time collection efficiency of this sampler was far superior to the DI sampler – 13-fold – not only due to the larger surface area available for absorption but also to higher sampling flow rates that were achievable. The fact that a smaller absorption solution volume was required was an additional bonus resulting in a more concentrated solution for analysis. That said, since both RT and DI samplers use caustic solutions for trapping purposes, the FP is logistically the more practical to use since handling corrosive reagents is probably the last thing one would want to do at the rim of an active volcano! Bio-methylation and volatilisation of trace elements is a process that requires more study so as to gain a fuller understanding of biogeochemical cycle of certain metals. A paper has been published which presents a robust and versatile gas trapping method using classical impinger samplers filled with nitric acid that preserved gaseous As, Se and S species once trapped.²⁷ The novel value of this work lay in the extensive trapping efficiency studies conducted wherein volatile As (DMA, MMA and TMA), Se (DMSe and DMDSe) and S (DMS, DMDS) species were generated, either by a reductive hydride generation process or *via* the use of purchased gas standards, and subsequently passed through three impinger samplers connected in series. Trapping efficiencies were calculated as the ratio between total elemental amounts of analyte in the impinger traps and the total elemental amounts of introduced volatile analyte as determined using ICP techniques. In the case of the As species the injected quantity was calculated as the difference between starting and residual quantities left in the hydride generation chamber. In the case of the Se and S species, direct inject of gas



standards into the ICP was performed. Speciation analysis of trapped species in the nitric acid filled impingers was undertaken using HPLC-HR-ICP-MS with identification by retention-time matching in conjunction with ESI-MS/MS analysis. The reported trapping efficiencies were DMA ($110 \pm 4\%$), MMA ($104 \pm 12\%$), TMA ($89 \pm 6\%$), DMSe ($96 \pm 2\%$), DMDSe ($50 \pm 11\%$), DMS ($101 \pm 5\%$) and DMDS ($74 \pm 8\%$). Furthermore it was ascertained that volatile Se and S species, one trapped, transformed into stable and specific non-volatile forms thus preserving the speciation information. Researchers²⁸ in the US examined, in the field, the performance of the widely used KCl-coated denuder for trapping GOM by challenging them to a known concentration of HgBr_2 . It was noted that such denuders had 95% collection efficiency for HgBr_2 in zero air (challenge gas standard supplied in air prescubbed of Hg_0 and O_3) but that capture efficiencies dropped drastically to 20–54% when ambient air was used. Subsequent tests carried out back in a laboratory setting revealed that O_3 and absolute humidity facilitated the re-release of a portion of the trapped HgBr_2 as Hg_0 thus explaining the low recoveries obtained in the field. Based upon these findings the authors concluded that atmospheric GOM measurements to date are probably underestimated and that the check system they have used should be used on other Hg sampling and monitoring systems deployed elsewhere.

Sampling using *passive samplers* is another approach. Two review papers considered the use of plants as biomonitors. In the first concise review (15 references),²⁹ passive sampling of the air by lichens, mosses and the leaves and bark of trees were considered. The second review (123 references)³⁰ was more specific and considered the use of conifer needles as passive samplers of inorganic pollutants. A French research consortium³¹ have designed a new continuous dust deposition sampler for unattended operation over extended sampling periods. In summary, an inlet funnel is connected to a 25-place filter carousel that can be rotated so that at periodic planned intervals, a fresh filter can be placed underneath this inlet. An automated combined funnel wall vibration and wash system is used to ensure that particles deposited from the atmosphere end upon the filter. Filtration is then carried out under gravity leaving insoluble particles on the filters for subsequent collection and analysis. The autonomy of the instrument can range from 25 days for a 1 day sampling interval to ~ 1 year for a bi-weekly sampling interval. The collection efficiencies³² of twelve widely used dust deposition samplers were tested for large particles in the size range 0.5–1 mm in a controlled wind tunnel facility at wind velocities over the range 1 to 5.5 m s^{-1} . The best eight samplers demonstrated collection efficiencies in the range 60–80% whilst the four worst performers could only demonstrate efficiencies in the range 5–40%. The authors concluded that better design considerations of inlet and outlet flow geometries are therefore required. In a similar study³³ three passive dust samplers were tested for their collection efficiencies for particles in the range 250–4140 nm. The evaluation was carried out in the field in parallel with a wide range particle spectrometer used to provide highly temporally resolved particle number and size distribution reference data. Two of the

samplers sets demonstrated collection efficiencies of $91.5 \pm 13.7\%$ and $103 \pm 15.5\%$ but the third sampler demonstrated poorer performance at an efficiency of $54 \pm 8.0\%$. Chinese researchers³⁴ have developed a new passive sampler for Hg_0 using a pulverised S-impregnated carbon material. Both laboratory and field testing was carried out. In the laboratory a stable Hg_0 atmosphere in the range 5–10 ng m^{-3} was generated using a permeation tube system and verified using an online analyser (Lumex RA-915). Five replicate samplers could be tested in parallel over a range of environmental conditions – relative humidity (25–90%), temperature (-10 to 35°C) and wind velocity (0.5 to 5.0 m s^{-1}). Sorbent beds (0.3 g) were analysed for their Hg content using a combustion-based analyser (Milestone DMA-80) in accordance with USEPA method 7473. Sorbent blanks were 0.58 ± 0.09 and $0.71 \pm 0.11 \text{ ng g}^{-1}$ from laboratory and field studies. The method LOD was determined to be 0.18 ng m^{-3} for an 8 day deployment in the laboratory chamber dropping to 0.05 ng m^{-3} for a 30 day field deployment. The average RSD of replicate samplers was 11% (laboratory) and 9% (field). An average uptake rate of $0.225 \pm 0.022 \text{ m}^3 \text{ d}^{-1} \text{ g}^{-1}$ was determined in field trials and results correlated favourably from active measurements made in parallel ($R^2 = 0.509$, slope = 0.991, 95% CI range of 0.895–1.086). Temperature or humidity did not have significant influence on the sampling rate but wind correction was important when comparing passive sampling data between sites with large variations in wind speeds.

1.3 Reference materials and calibrants

The international *database* for certified reference materials, COMAR, developed in the late 1970s to assist analytical laboratories to find appropriate RMs and a useful overview article has now been published³⁵ (16 references).

Whilst the determination of metals in airborne particles using plasma-based instrumentation is now well established and codified in a number of standardised methods, biased results can be obtained if a suitable dissolution procedure is incorrectly used. The extent of this bias can be assessed if *matrix matched RMs* were to be used and it is therefore welcome now to see three new RMs added to the existing rather limited portfolio of materials. For the analysis of metals in ambient air particles, French researchers³⁶ prepared a new CRM by simply pressing known masses of a well homogenized fly ash material (nominal 15 mg) into a fibre filter. The certification was based upon a single laboratory approach using ID-ICP-MS for Cd, Ni and Pb and a standard addition calibration approach for As. A microwave assisted digestion procedure involving a $\text{HNO}_3/\text{H}_2\text{O}_2$ acid mixture was used and this material is aimed at laboratories working to procedures set out EN 14902. In the reviewer's eyes this material could also be potentially useful for those undertaking stack air analysis to requirements set out in EN 13528. However given that the starting material was a fly ash derived from an incineration process, it would be informative to obtain elemental data following the addition of HF acid to the digestion mixture. British researchers³⁷ have described the preparation and certification of two bulk welding fume RMs for use in laboratories undertaking the analysis of metals in workplace air



to procedures set out in ISO 15202. These materials were certified at a nominal 10 mg test portion using an alternative interlaboratory certification approach. Here various hotplate, hotblock and microwave assisted dissolution procedures, codified in this ISO standard and deemed suitable for the dissolution of such materials, were used alongside an ICP-AES finish. Both certification exercises followed data handling and statistical requirements codified in ISO guide 35. The IRMM CRM BCR-723 (Pd, Pt and Rh in road dust) is widely used in supporting measurements in assessing the extent of PGE emissions from catalytic converters and new compositional data can be found in this paper.³⁸

Nanoparticle RMs are now required to support measurement initiatives in this growing arena. An Anglo-American university consortium³⁹ has described the synthesis and characterization of isotopically-labelled Ag NPs for future tracer studies. In summary monodispersive suspensions of citrate-stabilised Ag NPs, with target sizes of 17, 20 and 30 nm were synthesized by the controlled reduction of AgNO₃ solutions with NaBH₄. Both natural (¹⁰⁷Ag : ¹⁰⁹Ag = 52% : 48%) and enriched isotopic (¹⁰⁷Ag = 99.2%) Ag NPs were prepared. Characterisation techniques used included DLS, TEM and A4F and the particle size distributions showed good reproducibility between the laboratories and stability over 12 months of storage. In order to produce spherical monodispersive Ag NPs with diameters up to 100 nm, a seeded growth process has been advocated.⁴⁰ Here Au seed particles produced with a spark discharge generator were carried by N₂ through a three-zone tube furnace. In the first zone, Ag was evaporated and particle growth and shaping took place in the subsequent zones. An on-line SMPS system was used to monitor the generated aerosol and variables such as furnace temperature, Au seed particle size and concentration and carrier gas flow rates were examined. Off-line techniques such as AFM and TEM were also used to characterize the morphology of the generated Ag NPs. The mobility diameter of the monodispersive aerosol could be varied in the range of 50 to 115 nm by changing the furnace temperature or the Au seed particle size. A European research group⁴¹ has synthesized isotopically enriched ²⁹Si NPs for use as potential ID spikes for the quantification of natural silica NPs. Initially ²⁹SiCl₄ was prepared by heating ²⁹Si in a Cl₂ gas stream and a ²⁹Si tetraethyl orthosilicate intermediate obtained following a careful cooling and dilution procedure. A basic amino acid catalysis route was then used to form the NPs which were characterized using DLS, SAXS and TEM. The research group led by Detlef Günther⁴² have fabricated custom engineered and compacted nanoparticles as potential calibration materials for quantification using LA-ICP-MS. Here a flame spray technique was used to produce a nanomaterial with a customised elemental composition. Liquid organic precursors of Al, Ca, Fe, Mg, Si and Ti in a concentration similar to the matrix of the well-known NIST SRM 610 glass standard were mixed with a selection of REE (Ce, Gd, Ho and Tb); precious metals (Ag, Au, Pt, Rh and Ru) and Pb at concentrations of ~400–500 mg kg⁻¹. This precursor mixture was sprayed, collected as a nanopowder, compacted to pellets and characterised by LA and solution-based ICP-MS. In summary they demonstrated that this flame spray approach

allows production of customised doped calibration materials for micro-analytical techniques.

An advanced gravimetric system was reported for the production of *gaseous CRMs* of mixtures of He isotopes.⁴³ Three artificial He isotope reference mixtures were prepared with absolute isotope ratios $R(^4\text{He}/^3\text{He})$ of 18.905 ± 0.036 ; 98.78 ± 0.21 and 209.82 ± 0.44 ($k = 1$). The internal consistency between the mixtures was verified using a high precision single-focus magnetic sector MS system with a dynamic inlet system. Chemiluminescent analysers used *in situ* for measuring NO and NO₂ in ambient air are generally calibrated with certified gas standards of NO in a balance of N₂. Degradation of this NO standard, *via* oxidation to NO₂, has now been reported.⁴⁴ If left uncorrected the authors suggest that a systematic under-reporting of NO₂, a pollutant of concern in many urban locations, of up to 20% is possible.

1.4 Sample preparation

Automobile catalyst emissions can release not only Pd, Pt and Rh particles into the environment but also Ir, Os and Ru. All these trace elements can be challenging to measure thus the publication of improved methods is most welcome. Chinese researchers³⁸ report a method that involves both the use of ID-ICP-MS and N-TIMS (for Os determination) and applied it for the comprehensive characterization of both CRM BCR-723 (Pd, Pt and Rh in road dust) and road dust samples. Samples were digested with inverse aqua regia in a Carius tube. A solvent extraction step with CCl₄ then separated Os from the other elements prior to the use of an ion exchange process to remove interferents (Cd, Hf, Mo and Zr). Analysis of BCR-723 yielded reproducible results and well-defined average Ir; Os; Pd; Pt; Re and Ru of 0.23 ± 0.12 ; 0.37 ± 0.04 ; 4.6 ± 0.8 ; 79.8 ± 6.0 ; 6.5 ± 0.1 and 1.1 ± 0.13 (ng g⁻¹, 95% CI, $n = 10$). The ¹⁸⁷Os/¹⁸⁸Os ratio was determined to be 0.537 ± 0.022 (95% CI, $n = 10$). In a similar vein, European researchers⁴⁵ using ID-SF-ICP-MS and a combination of both cation and anion exchange chemistry validated their procedure using IRMM CRM BCR-723 and IAEA CRM 450 (algae). For the SI-traceable results complete uncertainty budgets were calculated that yielded expanded uncertainties ($k = 2$) of ~1% for analyte masses in the ng range and the reported LOD were 12 pg for Pd and 7 pg for Pt.

Sample preparation procedures for *emerging nanomaterials* have been developed. A SWCNT material produced by the laser ablation of a renewable biochar in the presence of Co and Ni catalysts was characterized for residual catalyst as well as trace metal impurity content (Cr, Fe, Hg, Mo and Pb) using ID-ICP-MS following sample digestion.⁴⁶ Several digestion procedures were examined including a multi-step microwave-assisted acid digestion, dry ashing at 450 °C and microwave-induced combustion with oxygen. Results were benchmarked against those derived from both NAA and SS-CS-AAS. The multi-step microwave-assisted acid provided to be the most reliable although Cr results were biased low mostly likely due to the formation of a refractory Cr carbide. A similar comparative study has been published looking at procedures to dissolve Ti NPs.⁴⁷ Here the performance of a HNO₃/HF microwave-assisted



acid digestion approach was compared against that using a KOH fusion in a muffle furnace and it was found that the fusion approach provided the more consistent results. Conventional FFF technique for particle size separation use narrow bore channels hence the sample mass that can be injected is typically <1 mg to avoid system overload. A variation of this technique, sedimentation field flow fractionation in a rotating coiled column,^{48,49} enabled up to 1 g of street dust to be processed and it was shown that the metals of a predominately anthropogenic origin – Cd, Cr, Cu, Ni, Pb, Sn and Zn – were found to concentrate mainly in the <1 µm size fraction. French researchers⁵⁰ investigated the elemental recoveries for metal oxide NPs – Al₂O₃, CeO₂, TiO₂, SiO₂ and ZnO – analysed by direct injection ICP-MS and the influence of particle size, agglomeration state and sample matrix. They noted for the NPs tested that an alkaline sodium hydroxide matrix presented the best results; that method performance was satisfactory for primary particles <50 nm but that recoveries decreased when particles were >80 nm especially those particles of a more refractory phase such as TiO₂ anatase. A generic sample preparation scheme for inorganic engineered NPs for subsequent detection, characterization and quantification by A4F coupled to DLS and ICP-MS techniques has been published.⁵¹

Physiologically-based *extraction test*⁵² with two simulated lung fluids, Gamble's and Hatch's solution, and simulated gastric and pancreatic solutions were applied to determine the bioaccessibility of As, Cd, Cr, Hg, Mn, Ni, Pb and Zn in urban particulate matter with analysis undertake using both ICP-AES AND ICP-MS. The effect of the extractant agent employed, extraction time, sample to extractant ratio, sample particle size and elemental properties were evaluated. The authors concluded that the extractable portions are affected not only by their mobility in the test material itself but also by the sample preparation procedure itself. Iron is an essential micronutrient for phytoplankton growth and is supplied to the remote areas of the oceans mainly through atmospheric dust. The amount of soluble Fe content is a major source of uncertainty in modelled dissolution and deposition models coupled with a wide variety of published leach methods. The authors of a new continuous flow leach procedure⁵³ claim that this method can be run with low sample mass, <10 mg, compared to the standard method, based upon BCR protocols, which uses up to 1 g of material. This is very useful given the limited mass of sample that is usually collected. Reproducibility studies were conducted on two well characterized sedimentation dust and ash and ranged between 8–22% as compared to 6–19% for the standard method. Sonication is often used to remove particles trapped on air filter samples for subsequent chemical and toxicological studies. The energy of an applied ultrasonic wave to a sample can cause localized hot spots at elevated pressures, production of free radicals and potential formation of artifact compounds. For those readers that employ ultrasonication in their studies, a read of this paper,⁵⁴ that details the operation of this technique and possible consequences of its use, is therefore recommended. American researchers⁵⁵ compared multi-solvent extraction (MSE) and spin-down extraction (SDE) procedures on PM_{2.5} particulate matter collected on filter and noted

remarkable compositional variance between the respective PM extracts for all the components tested including metals, water soluble ions and elemental/organic carbon. Mass closure was greater than >90% for MSE but was lower for SDE due to a process-based loss of sample mass. Lessons learnt included the importance of standardizing filter extraction objectives. A microwave assisted extraction procedure⁵⁶ used a Na₂CO₃–NaOH leachate to extract total Cr^{VI} from airborne particles collected on a Teflon filter prior to analysis *via* the widely used 1,5-diphenylcarbazide adduct at 540 nm. Recoveries from NIST SRM 2700 (hexavalent Cr in contaminated soil) were 106 ± 17%; total Cr^{VI} in NIST 1648a (urban particulate matter) was determined to be 26 ± 3 mg kg^{−1} and the method LOD was 0.33 ng m^{−3}. The total Cr^{VI} concentrations measured in New Jersey urban air was 1–1.6 ng m^{−3}. The same research group⁵⁷ undertook a study to ascertain whether the use of an enriched Cr^{III} ID spike, advocated in EPA method 6800, was useful in tracking the extent of Cr^{III} to Cr^{VI} interconversion during extraction of air samples and rather predictably noted that this ID protocol could only be applied to the soluble fraction of Cr species.

Improvements in sample preparation have been advocated. A method based upon pyrohydrolysis of airborne particulate matter collected on glass fibre filters for the subsequent determination of Br and I has been reported.⁵⁸ Sample filters were ground using an agate mortar, homogenized and placed on an alumina platform, mixed with a solid V₂O₅ powdered catalyst, fired at 950 °C and the resultant effluent trapped in water prior to analysis by ICP-MS. Quantitative recoveries of 104% (Br) and 95% (I) were obtained when NIST SRMs 1633b (Constituent Elements in Coal Fly Ash) and 2709 (San Joaquin Soil) were analysed and the method LoQ was 0.05 µg g^{−1} for Br and 0.006 µg g^{−1} for I. The authors concluded that their elegant approach was suitable for routine analysis and provided a clean solution for subsequent ICP-MS analysis. An improved method⁵⁹ for the ¹⁴C analysis of water-soluble organic carbon in aerosol samples employed a water extraction step followed by a freeze drying preconcentration step prior to AMS analysis. Reference test samples with known ¹⁴C content were prepared from NIST SRM 4990 (oxalic acid) and IAEA CRM C6 (sucrose). Accurate results were now possible using only 10 µg C containing samples, typical of low-loaded air filter samples, and an improvement on current methods which typically required >250 µg C samples.

1.5 Instrumental analysis

1.5.1 Atomic absorption and fluorescence spectrometry. A tutorial review paper⁶⁰ (105 references) considered the development of the *HR-CS-ETAAS* technique for the direct analysis of solid samples and complex materials including the analysis of atmospheric particles. The authors concluded that the advent of this technology has enabled the direct determination of non-metals and that with solid state detectors all spectral events taking place in the regional around the analyte signal can be directly observed. This greatly assists with method optimization and allows chemometric approaches to be used to handle spectral interferences. Looking forward they see a need for



detector systems that would enable the monitoring of a much wider spectral window thus facilitating the potential of the technique for multi-element applications. The absorption of CaF molecule at a characteristic line of 606.440 nm has been employed in a study for the determination of fluorine in coal.⁶¹ The LOD and M_0 were 0.3 and 0.1 ng F. Recoveries from NIST SRM 1635 (trace elements in coal) with a certified F value and from the following materials with indicative F values – SARM CRM 18 (coal-Witbank) and CRM 20 (coal-Sasolburg); IRMM BCR CRM 40 (coal) and 180 (gas coal) – ranged between 90 and 104%. The determination of Pd, Pt and Rh in a challenging automobile catalyst matrix⁶² required the addition of a chemical modifier ($\text{NH}_4\text{F}\cdot\text{HF}$), an elevated temperature program and the use of a solid standard IRMM ERM EB504 (PGE in used automobile catalyst) to obtain accurate results. Method precision was determined to <10%, which was most favourable, given that test sample sizes were as low as 0.05 mg and the LOD achieved were $6.5\ \mu\text{g g}^{-1}$ for Pd, $8.3\ \mu\text{g g}^{-1}$ for Pt and $9.3\ \mu\text{g g}^{-1}$ for Rh.

The development of a new laser-based *fluorescence* system for the ultra-trace determination of $\text{Hg}(0)_g$ has been reported.⁶³ The system utilizes sequential two-photon laser excitation with detection of blue-shifted laser-induced fluorescence to provide a highly specific detection system that precludes detection of any other species other than atomic mercury. This includes gas-phase oxidized Hg, so called reactive gaseous Hg (RGM). Currently the achievable detection capability is $15\ \text{pg m}^{-3}$ at a sampling rate of 0.1 Hz *i.e.* averaging 100 measurements with a 10 Hz laser system, without any need for sample trapping and preconcentration. Further improvements are planned including the addition of a pyrolysis chamber for the measurement of total gaseous Hg and RGM by difference with good sensitivity and time resolution.

1.5.2 Atomic emission spectrometry. Japanese workers⁶⁴ employed an ETV unit with a tungsten boat furnace sample cuvette and ICP *optical emission spectrometry* for the direct determination of chlorine in metallic nanopowders and fine powder samples. A modifier of either aqueous or alcoholic KOH was used together with an external calibration approach using aqueous calibration standards. A LOD of $170\ \text{ng g}^{-1}$ was achieved and sample throughput was ~ 30 per hour. Precision was determined to be 8.7% following analysis of 16 replicates of a 100 ng chlorine containing sample. Various miniaturized OES systems based upon dielectric barrier discharge micro-plasma have recently been developed which have been used for the determination of elemental species in gaseous samples. A review⁶⁵ discusses progress to date and offers future perspectives for trace elemental analysis. A miniaturized OES system was developed that uses a needle-plate electrode discharge as the light source.⁶⁶ Using a Pt/CNT fluorine-doped tin oxide electrode, this system was used to measure H_2 at room temperature using the 656 nm emission line. Under optimum conditions, this emission intensity was linearly correlated to the H_2 concentration in the range 0.17–4% (v/v). Testing has now been extended to include other species such as O_2 and Na.

The LIBS technique is now seen as a useful technique for *in situ* measurements for process monitoring. Carbon capture

and storage relies upon the long-term isolation of CO_2 from the atmosphere and here attendant technologies will be required for the reliable measurement, monitoring and verification of the integrity of compression, distribution and storage systems. American researchers⁶⁷ detail laboratory scale work that they have carried out in assessing the potential of LIBS for this application and they also discuss its potential for measurements in high pressure and temperature conditions. Chinese researchers⁶⁸ have explored the potential of using LIBS for the rapid measurement of unburned carbon in fly ash in coal-fired power plants using characteristic emission from the CN molecule. This approach overcame the spectral interference between Fe 247.98 nm and C 247.86 nm and the diminishing intensity of C 193.09 nm line when measured in air. An LOD of 0.16% (m/m) was achieved with precision <5% thus meeting requirements of this power generation sector. Both direct and indirect LIBS have been deployed at a French research centre⁶⁹ to measure Cu emissions in the exhaust duct of their casting operations. In the direct mode, a representative portion of the duct effluent was sampled isokinetically and passed through an analytical cell upon which the laser was focused whilst in the indirect mode this particulate effluent, once passed the analytical cell, was then trapped on a quartz filter and then interrogated by the laser. A second sampling line was employed to take parallel filter samples which were analysed off-line by ICP-AES following digestion. These sampling lines conformed to specifications set out in EN 14385, the standardised European method for stack air monitoring. Using this parallel sampling approach it was then possible to calibrate both laser-based approaches against a standard reference method using real-world matrix samples. The LOD was determined to be $\sim 20\ \mu\text{g m}^{-3}$ and future efforts will examine the potential to measure other metals that are regulated under emission directives.

Fundamental developments in the LIBS technique are also being investigated. The quantitative analysis of gaseous samples, by LIBS is limited due to its relatively lower signal reproducibility compared to that of solid samples. The research group at Malaga University⁷⁰ have devised a sequential process consisting of optical catapulting (OC), optical trapping (OT) followed by LIBS as a means of increasing instrumental sensitivity. The OC stage serves to put the particulate material under inspection in an aerosol form, the OT stage permits the isolation and manipulation of individual particles from this aerosol which are subsequently analysed by LIBS. In one study conducted the LOD for the analysis of alumina particles was calculated to be 200 ag Al. Fluorine and chlorine do not produce atomic or ionic line spectra of sufficient intensity to permit their detection by LIBS. They do however combine with alkali-earth elements to form molecular species with more sensitive characteristic spectral lines.⁷¹ In this study⁷² the spatial confinement *i.e.* the analytical zone was optimised which enabled the pulse-to-pulse RSDs to be reduced to <4% for the determination of nitrogen and oxygen in a gas stream, comparable to RSDs encountered in the analysis of solid materials. For more information on fundamental developments in atomic spectrometry readers are directed to our companion review.³



1.5.3 Mass spectrometry

1.5.3.1 Inductively coupled plasma mass spectrometry. New methods based upon the use of ICP-MS are being reported. Atmospheric dust has a substantial impact on climate and knowing its composition helps to determine dust sources and climate processes. Here rapid elemental screening on small test samples would be advantageous. German researchers⁷³ have determined up to 46 major and trace elements in dust samples, using *in situ* 200 nm femtosecond laser ablation-inductively coupled plasma mass spectrometry (LA-ICP-MS). This method was used on very small test portions of 4–7 µg and was sufficiently sensitive thus enabling LODs down to fg and ng g⁻¹, to be achieved. The technique was found to be especially useful for measurements of small amounts of dust on filters, and for 2D-distribution maps of selected elements to identify minerals or contamination. A novel gas-to-particle conversion gas exchange technique for the direct analysis of metal carbonyl gas by ICP-MS has been proposed.⁷⁴ Here particles are generated in a conversion chamber from Cr(CO)₆, Mo(CO)₆ and W(CO)₆ gaseous species following oxidation with O₃ or agglomeration of metal oxide with NH₄NO₃ which is formed by the *in situ* reaction of NH₃ with O₃. A gas exchange device was then used to remove residual NH₃ and O₃ and to provide an Ar carrier gas to the plasma. The achieved detection limits were 0.07–0.3 ng m⁻³ which were 4–5 orders of magnitude lower than those of conventional techniques, such as GC-ECD and FT-IR, used to measure carbonyl species and comparable or slightly better than those obtained with an GC-ICP-MS approach. This new technique holds promise for monitoring of gas quality in the semiconductor industry and in gases from engines and waste incineration.

The use of ICP-MS for isotopic measurements continues to be investigated. Review articles on the performance of ICP-based system to determine Cd⁷⁵ (47 references) and Pb⁷⁶ (70 references) have been published. The Pb isotopic analysis of Antarctic snow using MC-ICP-MS with a torch-integrated sample introduction system (TISIS) has been reported.⁷⁷ With this instrumental setup, accurate and precise determination of isotope ratios was possible at Pb concentrations as low as 0.5 ng mL⁻¹ and sample volumes of 0.2 mL (equating to 100 pg Pb). The repeatability of the ²⁰⁷Pb/²⁰⁶Pb ratio was 0.16‰ for a nominal 10 ng mL⁻¹ Pb solution. With a freeze drying technique it was possible to preconcentrate samples 100-fold starting with a 20 g snow sample. Procedural blanks were 0.5 ± 0.3 pg g⁻¹ enabling the determination of isotope ratio in snow samples containing Pb as low as 5 pg g⁻¹. Isotopic fingerprinting of single particles is of increasing value in nuclear auditing and safeguarding processes. In this study, sp-MC-ICP-MS was proposed for the precise determination of individual particles in suspension using Er oxide as surrogate for U oxide.⁷⁸ This was a suitable surrogate as the U isotope ratios, at different enrichment levels, could be covered by a corresponding Er isotopic range. From the histogram of the pulse intensities, the particle diameter was estimated to ~226 nm with a Er mass of 7 × 10⁻¹⁶ g. Two data processing strategies, point by point (PBP) and linear regression slope (LRS) were employed in the data

analytics. Results showed that precisions of the ¹⁷⁰Er/¹⁶⁶Er, ¹⁶⁸Er/¹⁶⁶Er and ¹⁶⁷Er/¹⁶⁶Er determined by the PBP method were 5.5%, 4.6% and 3.9% respectively. Due to the weak signal intensity for ¹⁶⁴Er the precision and accuracy of ¹⁶⁴Er/¹⁶⁶Er ratio measurements were substantially poorer. The relative errors of these ratios measurements after mass bias correction were 0.2–0.4%. By the LRS method, measured ratio precisions improved to <0.3% and allowed ¹⁶⁴Er/¹⁶⁶Er and ¹⁶²Er/¹⁶⁶Er measurements to be performed. The authors concluded that this proposed technique was suitable for the assay of particles in the size range of 130–3000 nm and combines fast screening, sensitive detection and isotopic identification of an individual particle.

The characterisation of nanoparticles by ICP-MS remains a fertile topic for research. Two reviews,^{79,80} (35 and 52 references) presented the historical development of FFF-ICP-MS techniques, their current status and future prospects. The research group led by Detlef Gunther⁸¹ has investigated the potential of a high temporal resolution ICP-TOF-MS in conjunction with a microdroplet generator for the simultaneous mass quantification of different NPs in a mixture. Here calibration with monodisperse droplets consisting of standard solutions allowed for the quantification of NPs without the need for NP reference materials. On the basis of this mass quantification, the sizing of the calibrant NPs was simultaneously determined with an accuracy of 7–12%. In another study⁸² two different sample introduction systems for the analysis of NP suspensions were investigated. For accurate sp-ICP-MS analysis it is crucial to ascertain the transport efficiency of nebulized sample to the plasma. Here, using the waste collection method, efficiencies were 11–14% for Ag NP suspensions and 9–11% for Au NP suspensions by pneumatic nebulisation. In contrast the transport efficiency using a microdroplet generation was 100%. British researchers⁸³ modified a HDC-ICP-MS system to facilitate the injection of NIST-traceable standards into the post-column effluent so that quantification by standard addition could be carried out. Combining the simultaneously acquired particle sizing data and mass concentration data allowed accurate quantification of the particle number concentration to be made in a single analytical run. A US based consortium⁸⁴ has developed a method that estimated the size detection limit – the *D*_{min} value – for various NPs when sp-ICP-MS is used. There was the assumption that each NP sample consists of only one element and the lowest *D*_{min} values of <10 nm were obtained for elements such as Ce, Ir and U; *D*_{min} values of 11–20 nm for elements such as Ag, Au, Cd and Pb; *D*_{min} of 21–90 nm for elements such as Co, Ni, Ti and Sn and *D*_{min} values > 200 nm for elements such as Ca, Se and Si. Parameters that influence these *D*_{min} values include instrument sensitivity, nanoparticle density and instrumental noise and that *D*_{min} values can be reduced by analyte isotope selection and the use of DRC/CCT to facilitate the removal of isobaric interferences. A validation exercise then compared estimated *D*_{min} values against *D*_{min} values experimentally derived by sp-ICP-MS for the following three nanoparticles in a range of aqueous matrices: Ag (13 nm vs. 21 ± 4 nm); CeO₂ (10 nm vs. 19 ± 8 nm) and TiO₂ (91 nm vs. 130 ± 28 nm) which showed reasonable agreement. Other work has been reported that included: application⁸⁵ of a *k*-means clustering



algorithm to signal processing of raw sp-ICP-MS data that improved discrimination of particle signals from background signals; improving⁸⁶ the detection and characterization of engineered NPs by sp-ICP-MS using short dwell times; investigations⁸⁷ into calibration approaches and non-linear detector responses and development⁸⁸ of a data evaluation tool for the calculation of particle size, concentration and size distribution from raw sp-ICP-MS data.

1.5.3.2 Other mass spectrometry techniques. Developments in IRMS techniques for the isotopic analysis of *gaseous species* have been published. A technique for compound specific analysis of stable carbon isotope ratios of ambient VOCs was developed.⁸⁹ It was based upon the selective sampling of VOCs onto sorbent cartridges which are recovered and separated by a TD-GC-MS followed by on-line oxidation in a combustion interface prior to IRMS. The method allowed measurements of isotope ratios of VOCs present in ambient air at low pptv to ppbv concentrations with an accuracy of typically better than 0.5‰. An on-line IRMS system⁹⁰ for analysis of single substituted isotopologues ($^{12}\text{C}^{16}\text{O}^{17}\text{O}$, $^{12}\text{C}^{16}\text{O}^{18}\text{O}$, $^{13}\text{C}^{16}\text{O}^{16}\text{O}$) in nanomolar CO_2 extracted from stratospheric air samples has been developed. The $\Delta^{17}\text{O}$ excess was derived from isotope measurements on two different CO_2 aliquots: unmodified CO_2 and modified CO_2 after complete oxygen isotope exchange with CeO_2 at 700 °C. This exchange and measurement process took 15 minutes, a major improvement over previously off-line methods that took up to 3 hours. Other IRMS related papers of interest included: the development⁹¹ of a high temperature interface to convert organic Cl to HCl prior to MS/IRMS analysis; a device to extraction trapped ancient air from large ice samples;⁹² separation and purification of Ar/ O_2 mixtures by cryogenic means rather than the conventional chromatographic approaches;⁹³ an investigation into the matrix effects of gases other than He have on measured ^{13}C and ^{18}O isotopes ratios of CO_2 ;⁹⁴ a bracketing calibration protocol that makes reference gas measurement potentially redundant thus saving cost and time⁹⁵ and an elemental analyser-IRMS instrument⁹⁶ that provided high-precision, rapid simultaneous measurements of $^{13}\text{C}/^{12}\text{C}$, $^{15}\text{N}/^{14}\text{N}$ and $^{34}\text{S}/^{32}\text{S}$ ratios as well as elemental concentrations. Studies have shown that nitrous acid (HONO) chemistry can play an important role in O_3 production but that the detailed chemical mechanism of HONO production and identification of its sources are poorly characterised. A novel approach⁹⁷ for the ambient measurement of HONO using ion drift chemical ionization MS employed SF_6^- , generated *in situ*, to form the F^- -HONO analytical adduct by an F transfer reaction. The typical sensitivity achieved was 200–300 cps per ppb resulting in a LOD of 10–20 ppt HONO for a 1 s integration. This instrumental sensitivity coupled with the high temporal resolution will assist in the future mechanistic studies that are required.

There have been developments in MS techniques for analysis of *airborne particulates*. The hyphenation of a thermal-optical carbon combustion analyser to a PI-TOF-MS allowed deeper insight into the organic composition of primary particles and the formation mechanism of secondary organic aerosols.⁹⁸ Here the combination of PI-TOF-MS was beneficial as the data offered a more detailed insight into the molecular composition of

evolved gaseous species following determination of bulk carbon parameters in the preceding combustion step. A new particle trap laser-induced incandescence mass spectrometer for the examination of the black carbon mixing state within aerosols has been developed.⁹⁹ Total aerosol composition was analysed with the laser stitched off and the aerosol particles externally mixed with black carbon can be analysed with the laser switched on. By difference the chemical composition of particles internally mixed with black carbon could be measured. Entrained flow gasification is a promising technique where biomass is converted to a syngas such as CO and H_2 which can then be used as building blocks, *via* further catalysis, to biofuels of chemicals. To better understand the mechanisms involved, on-line measurements¹⁰⁰ involved soot particle aerosol mass spectrometry and the main advantage compared to other techniques was that particle composition – ash-forming elements, organics, PAH and soot – was obtainable at high time resolution. Improvements in particle sample introduction into online mass spectrometers included: a new aerodynamic lens inlet system¹⁰¹ designed to transmit and allow the analysis of individual particles in the 4–10 μm size range with a peak detection efficiency of $74 \pm 9\%$ for 6 μm particle.

Characterisation of *individual particles* released from nuclear facilities and processes can be a useful tool for auditing and safeguarding purposes. The direct isotope ratio analysis¹⁰² in individual U–Pu mixed particles with various U/Pu atomic ratios were analysed without prior chemical separation by TIMS. In the analysis, peaks of Am, Pu and U ion signals were successfully separated by continuously increasing the evaporation filament current when applied to model particles mixtures consisting of μm -sized RM particles with U/Pu ratios of 1, 5, 10, 18 and 70. The use of TIMS combined with a FT technique can be an efficient method for determining the isotope ratio of individual U particles but erroneous conclusions can be derived from averaged ratio results if a number of particles are perceived to be a single particle – so called particle mixing. In a refinement of this approach,¹⁰³ prior microsampling using SEM was deployed to identify and thus isolate individual particles thus minimise the potential for this particle mixing effect. The efficacy of this approach was proven by the successful analysis of a mixture of NIST SRM 950a (U_3O_8) and NBL CRM U100 (Uranium Isotopic Standard) particles. The contribution¹⁰⁴ of three traffic-related components – abrasion, exhaust and resuspension – to kerbside and urban background PM_{10} and PM_1 levels was quantified based upon the analysis of individual particles collected on B-substrates using a two stage cascade impactor (0.1–1 μm and 1–10 μm) by SEM-EDS. In total 160 urban air samples were collected, and 111 003 individual particles examined and classified into 14 particle classes as to their origins! Results showed that traffic-related contribution to PM_{10} load was 27% at an urban background sampling site away from roads rising to 48% at kerbside. For PM_1 load the values were 15% and 38%. The relative contribution of the different traffic components to PM_{10} was 15% from abrasion processes, 27% from exhaust and 58% from resuspension and for PM_1 these figures were 8%, 38% and 54%. Compared to previous work, the authors observed significantly lower portion of



exhaust particles, undoubtedly due to increasingly stringent emission legislation, but the high abundance of resuspension particles highlights the need for more health effects and mitigation studies.

1.5.4 X-ray spectrometry. The use of *multifunctional systems involving X-ray techniques* has been reported for the analysis of airborne particulate matter. Both X-ray diffraction and scattering on a single platform have been used to examine the structure, composition and thermal properties of TiO₂ particles in the 1 to 10 nm size range.¹⁰⁵ A new system¹⁰⁶ has been deployed, that combined SWAXS with a single stage multi-orifice low-pressure impactor (SS-MOLPI), as a process analytical tool for the quasi-online analysis of NPs generated by electrical discharge in an inert gas. The SS-MOLPI allowed quick sampling of aerosol particle directly from the process gas stream onto an adhesive tape substrate which could then be transferred to the SWAXS for rapid analysis. The entire process took only a few minutes and provided information on primary particle size, aggregation state, morphology and crystalline properties in a single run. Information provided was thus comparable to that obtained by SEM/TEM and XRD but was more affordable and quicker. A new apparatus for the simultaneous application of PIXE and XRF for the elemental analysis of atmospheric aerosol samples has been described.¹⁰⁷ Here the relative strength of PIXE to interrogate light elements (Al to Zn) and XRF to interrogate higher elements (Fe and above) neatly complement each other. Improved elemental analysis methods for the characterization of atmospheric particulate matter on filters have been reported.¹⁰⁸ These included: a revised microwave assisted acid digestion protocol that used less than 2 mL acid mixture with a FIA-SF-ICP-MS method that measured 44 elements with a daily throughput of up to 30 samples; and an EDXRF method that could quantify 15 elements per filter at a rate of 4 samples per hour. The EDXRF method employed a FP calibration protocol and daily calibration checks were carried out with NIST SRM 2783 (Air Particulate on Filter Media) with recoveries in the range 85–115%. As an additional validation check, in a study involving the determination of metals in diesel fume samples, filters were analysed initially by EDXRF and then digested and analysed by ICP-MS. The EDXRF/ICP-MS ratios, obtained for elements amenable for analysis by both techniques, were Ca (0.8 ± 0.2); Ce (1.1 ± 0.0); Cu (0.9 ± 0.2); Fe (1.1 ± 0.4); Mg (1.2 ± 0.3); Ni (1.0 ± 0.3); P (0.7 ± 0.2); Pt (1.1 ± 0.2); S (1.2 ± 0.3) and Zn (1.2 ± 0.2).

Speciation of airborne particles by X-ray techniques continues to be investigated. Iron is often the most abundant metal in airborne particles and can act as a catalyst in the formation of radicals and in the generation of reactive oxygen species, hence it is an element of interest in respiratory health effects studies. XANES was used to study the local order and valence state of Fe in urban PM_{2.5} collected on filters.¹⁰⁹ Based upon a comparison with model compounds, fayalite (Fe²⁺) and ferrihydrite (Fe³⁺), Fe in samples was prevalent as Fe³⁺ whereas EAFS data attributed this valent state to a nanocrystalline phase of ferrihydrite. The authors noted that ferrihydrite has never been shown to be associated with suspended urban dusts in previous literature or specific studies to investigate its toxicology. Aerosol deposition

of P to the oceans is a key source of nutrient for biological productivity. To study its potential bioavailability in the Mediterranean, NEXAFS was used to examine aerosol samples in both European and North African air masses.¹¹⁰ It was found that European derived aerosols delivered on average 3.5 times more soluble P than aerosols originating from North Africa. This soluble P source was dominated by organic P compounds derived it was concluded from a bacterial source. The composition of Se in atmospheric urban particle was investigated by XANES.¹¹¹ It was noted that Se^{IV} was the dominant oxidation state in ambient aerosols followed by Se⁰, Se^{II} and Se^{VI}. The Se^{IV} oxidation state was only observed in particles derived from gasoline, diesel and coal fly ash whilst a combination of Se⁰, Se^{II} and Se^{IV} was found in particles originating from biomass burning. Understanding the speciation of metals in workplace aerosols is required for better exposure assessment and health effects studies. The Zatka sequential extraction method has been developed to speciate Ni aerosol samples in refineries using model Ni compounds but its performance on real-world dust samples is somewhat unknown. In this study,¹¹² XANES was used to examine samples prior to extraction and it was noted that the Zatka method can overestimate the soluble Ni fraction and it may underestimate the sulfidic and metallic fractions in some samples. Importantly, XANES was able to identify component sulfidic nickel species which should assist in more accurate exposure assessments and more refined epidemiological analysis of respiratory cancers in workers processing such ores. A Canadian study¹¹³ investigated the impact of humid indoor air conditions on the bioaccessibility of Zn in dust and the transformation of Zn species during weathering. House dust samples were subjected to an oxygenated humid environment in a sealed chamber for up to 5 months. Bulk and μ XAS was used to interrogate the Zn species and test samples were subjected to a gastric acid extraction procedure, before and after, each storage experiment to determine Zn bioaccessibility. It was noted that under these humid conditions that there was a significant increase in Zn bioaccessibility with redistribution from inorganic Zn to Zn adsorbed on humates. The results helped explain the greater bioaccessibility of certain metals in house dust compared to soil samples. Interested readers are invited to read our companion XRF review.⁵

1.5.5 Other spectrometric techniques. There is growing interest in *laser-based techniques for gas monitoring* because they can be portable and can offer a non-invasive or stand-off monitoring capability with high sensitivity, selectivity and high time resolution. The application of absorption spectroscopy using quantum cascade lasers (QCLs) has been reviewed (150 references)¹¹⁴ and covered applications such as molecular gas spectroscopy, industrial process control, combustion diagnostics and medical breath analysis. Two pulsed mid-IR QCLs were deployed to make in-line simultaneous measurements of NO and NO₂ in the cooling stack of a power plant.¹¹⁵ Despite the harsh environment, water content up to 235 g m⁻³ and average particle loads of 15.8 mg m⁻³, in the flue gas, LODs of 219 ppb for NO and 164 ppb NO₂ were achieved. The authors employed¹¹⁶ the same open path technology at the kerbside and achieved a LOD of <1 μ g m⁻³ for both species for a 1 minute



integration and using a path length of up to 428 m. The results obtained correlated well with those obtained using the reference chemiluminescence method and the fast response time allowing emissions from different vehicle classes to be distinguished was most advantageous. The development and demonstration of a ground based mobile differential adsorption lidar (DIAL) system for monitoring CO₂ emission plumes from industrial sources has been reported for the first time¹¹⁷ but further improvements in detection limits will be required to quantify smaller fugitive emissions. A newly developed isotope ratio laser spectrometer for CO₂ analysis has been tested during a tracer experiment at a German pilot plant for CO₂ storage.¹¹⁸ In this experiment 500 tonnes of CO₂, with a $\delta^{13}\text{C}$ value significantly different from background value, was injected in a supercritical state into a reservoir in the ground. This new instrument was then used to monitor the breakthrough of the isotope tracer through a stainless steel riser tube installed in an observation well. Measurements compared favourably with those derived from IRMS measurements and it is believed that this new capability, with its high temporal resolution, can contribute to future CO₂ capture and storage projects by assisting in the assessment of the long-term integrity of reservoirs.

Measuring *carbonaceous particles using thermal-optical analysis*, that thermally fractionates the content of such particles in an oven into organic and elemental carbon, is widely as a reference method. Oven temperature accuracy is therefore rather important and it has now been demonstrated that temperatures measured by oven thermocouples can vary by as much as 50 °C from instrument to instrument. A new temperature calibration kit has now been evaluated¹¹⁹ and the same device was then used to calibrate different instruments as part of an interlaboratory trial¹²⁰ resulting in significant improvement in measurement precisions. A thermal-optical carbon analyser has been modified¹²¹ to now include a seven-wavelength light source/detector system covering the range 405–980 nm so that carbonaceous material can be examined optically as it undergoes combustion. It is hoped that this new modification will assist in a better understanding of this fractionation process leading to more accurate carbon measurements and hence more value to aerosol monitoring programs.

The *aethalometer*, an instrument which collects airborne particulate matter onto a filter while continuously measuring its light transmission, has been widely deployed to measure black carbon in high time resolution. Here the measurement relies on ideally a linear relationship between attenuation and black carbon on the filter. At higher filter loadings this response becomes non linear and correction procedures such as an algorithm build into the instrument calibration have been used to compensate. An improved system, the “dual-spot” aethalometer has now been developed to undertake this correction in real-time.¹²² This was achieved by measuring concurrently the attenuation of light on two sample spots on the filter which are sampled at different flow rates. This resultant continuous difference in sample loading is then used in a new algorithm to develop this time correction model. The AE51 μ -aethalometer was designed as a smaller wearable version and researchers¹²³

have examined the potential for saving the filters for subsequent off-line SO₄²⁻ measurements by IC for personal exposure assessment purposes. The estimated LOD for a 24 hour time integrated sample was estimated to 1.4 $\mu\text{g m}^{-3}$ and results compared favourably with those obtained by collocated filter-pack sampling ($R^2 = 0.87$, slope = 1.02). Comparing optical based methods, such as the aethalometer, against thermal-based reference methods has been the focus of two reported studies.^{124,125}

A *round up of new instrumental techniques and interesting applications* included a demonstration¹²⁶ of the first continuous measurements of $\delta^{18}\text{O-CO}_2$ in air by FTIR which showed good measurement stability of <0.1‰ (over a day) and <0.25‰ (over 9 minute averages). Whilst this precision is not as good as that obtainable by IRMS, the ability to perform highly time resolved measurements could be exploited to explore the dynamics of atmospheric gas processes. A study¹²⁷ aimed at determining the Fe^{III/II} ratio of the Fe-bearing minerals contained in the Harmattan dust, a northeasterly Saharan winter wind that blows over the West African subregion, by ⁵⁷Fe Mössbauer spectroscopy, determined that this dust was seriously deficient in soluble Fe^{II} needed in the soil for healthy crops and plants. Silver NPs are the most commonly used nanoparticles in consumer products. A study¹²⁸ investigated the feasibility of SERS as a method for the detection and quantification of Ag NPs. By using ferbam, ferric dimethyl-dithiocarbamate, as an indicator molecule that binds strongly onto NPs, detection and discrimination was based upon a signature SERS response of Ag-ferbam NP complexes. Particles in the 20–200 nm range were detectable with highest signal intensity for particles in the range 60–100 nm and a linear relationship was noted between the Raman intensity and Ag NPs concentration over the range 0–20 mg L⁻¹. The authors concluded that SERS could be a promising analytical tool in the future not only for the determination of Ag NPs in consumer products but in other environmentally relevant matrices.

2 Water analysis

2.1 Sample preconcentration and extraction

The majority of *review articles* focussed on specific methodologies rather than groups of analytes or matrices, reflecting the proliferation of microextraction techniques now available. Al-Saidi and Emara¹²⁹ (74 references) covered recent developments in DLLME for the determination of inorganic analytes whilst Hagarova¹³⁰ (84 references) (in Slovakian) covered the use of supramolecular solvents for the extraction of metals. A very similar theme, the use of ionic liquids in microextraction techniques¹³¹ (112 references) was reviewed for the preconcentration of metals. Although the majority of papers considered in the timely review of nm-sized materials for the SPE of trace elements¹³² (265 references) covered water analysis, virtually every possible matrix from human hair to crude oil had also been analysed. A review¹³³ (84 references) of microextraction techniques for the determination of organomercury and organotin compounds in environmental samples reflected how laborious current standard methods are. Great strides



have been made in the elimination of toxic organic solvents from preconcentration methods, as evidenced by the latest approaches for “green” chemistry preconcentration methods¹³⁴ (46 references) specifically applied to the determination of trace elements in seawater. This author appreciates not having to use MIBK or CCl₄ anymore, but does wonder just how environmentally friendly ionic liquids, 1-undecanol, and other “green” reagents really are. The most significant developments in analyte preconcentration for water analysis are summarised in Tables 1 and 2.

2.2 Speciation and fractionation analysis

This year has been particularly blessed with *review articles*; authoritative reviews on the determination of dissolved Fe in seawater¹⁶¹ (138 references) and on coupled techniques for As speciation in food and water¹⁶² (243 references) are of particular interest. Other review articles covered As, Cr, Sb and Tl speciation in water and sediments by LC-ICP-MS¹⁶³ (103 references) and speciation analysis of Cr by HPLC-ICP-MS since 2000 with particular emphasis on traceability and metrology¹⁶⁴ (98 references). The onward march of nanomaterials and their characterisation is underlined by the reviews on FFF coupled to ICP-MS⁸⁰ (51 references) and the application of NPs and nanostructured materials to elemental speciation¹⁶⁵ (62 references).

By coupling IC with an HG-AFS instrument for the on-site determination of *arsenic species* in sulfidic waters,¹⁶⁶ it was possible to separate in just 25 minutes As^{III} and thioarsenite from As^V and its monothio-, dithio-, trithio- and tetrathio-forms (7 species in total). Separation was achieved on an IonPac® AS 16 analytical column using a KOH mobile phase gradient at a flow rate of 1 mL min⁻¹. Peak identification was based upon the retention times observed for standard solutions of the target analytes. Calibration was carried out against an As^V stock solution since all peaks were reduced to arsine gas and the dissolution of the standards typically resulted in the formation of more than one species. Because samples were stable only for <2 h, use of a mobile laboratory was necessary. There was good agreement between the total As concentration and the sum of the individual species concentrations. Using this method the LOD was 1–3 µg L⁻¹ depending on the daily baseline response. Strangely, the authors managed to publish their results without reporting any significant method validation. A screening method¹⁶⁷ for the selective trapping and determination of As^{III} and As^V with WDXRF detection involved first passing a 50 mL sample (pH 5–9) through an Empore™ chelating disk to remove Pb since the PbL α line can interfere with the AsK α line. The pH was adjusted to 2–3 and 1 mL of 0.06 M APDC added to form a complex with As^{III}. The resulting solution was passed at 12.5 mL min⁻¹ through a PTFE disk placed on top of an Empore™ Cation-SR cation-exchange disk to trap chelated As^{III} on the top disk and the As^V on the bottom disk. Both disks were washed with 0.5 mL of a pH 3 HCl solution, separated and dried at 100 °C for 15 minutes prior to WDXRF analysis. The LODs were 0.8 and 0.6 µg L⁻¹ for As^{III} and As^V, respectively. Recovery of As^{III} and As^V spikes from local mineral waters was 98–104% for both species. In an interesting method¹⁶⁸ that did not use

chromatography, labile inorganic and organic As species were trapped in a ferrihydrite gel layer of a DGT unit for direct determination using XANES spectroscopy. They did not recommend extraction into 1 M HNO₃ and analysis by HPLC-HG-AFS because 20% of the arsenate was converted to arsenite and a significant amount of DMA into MMA or As^V during extraction. Even worse results were obtained for extraction into 1 M NaOH. This reviewer is surprised that they did not try extraction solutions such as their mobile phase (20 mM phosphate buffer at pH 6.5) or a nitrate buffer with added EDTA in which As species are stable.

Methods for the determination of *arsenic plus other elemental species* are always welcome. A method¹⁶⁹ for the separation and determination of As^{III}, As^V, DMA, MMA, Cd^{II}, Cr^{III} and Cr^{VI} in one chromatographic run involved addition of 3 mL of concentrated ammonium phosphate buffer (pH 7) containing 10 mM EDTA to a 7 mL sample before incubation at 70 °C for 15 minutes to ensure the formation of anionic EDTA complexes of Cr^{III} and Cd^{II}. A 50 µL aliquot was injected onto a Hamilton PRP-X100 anion-exchange column and the species separated using a mobile phase of 40 mM NH₄NO₃ (pH 8.6) at a flow rate of 1.0 mL min⁻¹. With ICP-MS detection, the LODs for the individual species ranged from 0.07 (Cr^{VI}) to 0.12 (Cd^{II}) µg L⁻¹ and spike recoveries ($n = 9$) from 91–97% (Cr^{III}) to 105–116% (Cd^{II}). A slightly different philosophy was used to determine As^{III}, As^V, Sb^{III}, Sb^V, Se^{IV} and Se^{VI} in water samples.¹⁷⁰ The same analytical column was used but EDTA solution was the mobile phase rather than being added to the sample. All the species were separated within 11 minutes using a mobile phase with a constant pH of 4.7 (adjusted with formic acid) and organic modifier content (97 : 3 EDTA : CH₃OH). The EDTA concentration was held at 5 mM for the first 4.5 minutes, stepped up to 30 mM EDTA in 1 minute and then held at 30 mM for 11 minutes. The flow rate was 1.5 mL min⁻¹ and the sample injection volume 50 µL. With SF-ICP-MS detection, the LODs ranged from 0.02 µg L⁻¹ for As^{III} and Sb^V to 0.4 µg L⁻¹ for Se^{VI}. The sum of the species concentrations measured in NIST SRM 1643e (trace elements in water) and the HPS CRM-SW (elements in seawater) agreed well with the certified data for total concentrations. Spike recoveries from pure water and two hot spring samples ranged from 94% (Sb^V) to 123% (Sb^{III}) ($n = 3$). The fluxes of volatile species of As, S and Se above a peat bog were quantified²⁷ by trapping in concentrated HNO₃ in 3 sequential liquid traps attached to a 60 L h⁻¹ air pump for 24 h. Trap solutions as well as surface water samples were analysed for As, S and Se species by HPLC-ICP-SF-MS. The air trap samples were diluted 1 + 49 with ultrapure water whereas the water samples were analysed directly to prevent speciation changes during sample manipulation. Slightly different HPLC separations were required for the two sample matrices; both methods used a 250 × 4 mm id OmniPac® PAX-500 mixed mode column with an eluent A of 30 mM NH₄NO₃ pH 7.5 containing 1% v/v CH₃OH. The differences lay in eluent B (50 mM Na₂CO₃–NaHCO₃ pH 8.5 containing 25% v/v CH₃OH for air trap samples and H₂O adjusted to pH 8.4 for water samples) and the flow rates (0.5 and 1 mL min⁻¹, respectively). The instrumental LODs ranged from 0.17 (methane selenic acid) to 13 µg L⁻¹ (dimethyl sulfone) for



Table 1 Preconcentration methods using solid phase extraction for the analysis of water

Analytes	Matrix	Substrate	Coating or modifying agent	Detector	Figures of Merit ($\mu\text{g L}^{-1}$ unless otherwise stated)	Method validation	Reference
Al, Cd, Co, Cu, Fe, Ni, Mn, Pb, Zn	Seawater	NOBIAS chelate-PA1	None	ICP-SF- MS	LOD, 0.9 (Pb) pmol kg^{-1} to 0.3 (Al) nmol kg^{-1} 120 g seawater sample	NRCC CRMs CASS-5 (nearshore seawater) and NASS-5 (seawater), GEOTRACES RMs GS (surface seawater), and GD (deep water seawater) (Environmental waters)	135
As^{V} , Cr^{VI} , Se^{VI}	River, rain and lake water	MWCNT	3-(2-Aminoethylamino)- propyltrimethoxysilane	ICP-MS	LOD 15 (As) to 38 (Cr) 4 mL sample	IERM CRMs GSBZ50009-88 GSBZ50027-94 and NRCCRM CRM GBW3209 and GBW3210	136
As, Sb, Se	Tap and lake water	Iron oxide silicon nanoparticles	CeO_2 coating to trap <i>in situ</i> generated hydrides	ICP-AES	LOQ 0.26 (Sb) to 0.44 (As) 50 mL sample	ERM CA021a (soft drinking water)	137
Be	Seawater	Silica gel	Interference removal with EDTA solution	ICP-MS	LOD 0.2 pmol kg^{-1} 250 mL sample	NRCC CRM SLRS-5 (river water)	138
Cd, Cu	Environmental water samples	Glass beads with a nano- TiO_2 surface	1-Octyl-3-methylimidazolium hexafluorophosphate and trapping of chelates with 2-[(5- bromo-2-pyridyl)azo-5-(diethyl- amino)phenol] Dithiazone	FAAS	LOD 0.1 (Cd) and 0.3 (Cu), 100 mL sample	Spike recovery	139
Cd, Co, Ni, Pb	Environmental water samples	Graphene		WD- XRF	LOD 1.1 (Co) to 6.1 (Pb), 100 mL sample	Spike recovery and comparison with ICP-MS results	140
Cd, Co, Cu, Mn, Ni, Pb	Water	Poly(methyl methacrylate) lab on a chip	Cl^-	ICP-MS	LOD 3.48 ng L^{-1} (Pb) to 20.68 ng L^{-1} (Mn), 50 μL sample	Spike recovery and NIST SRM 1643e (artificial saline water)	141
Co, Cu, Pb	Environmental water samples	Co-precipitation of a zinc hydroxide suspension	Metal complexes with 1-(2- pyridylazo)-2-naphthol	FAAS	LOD 1.5 (Cu) to 2.4 (Co), 40 mL sample	Spike recovery	142
Cu, Pb, REEs	Water, seawater and sediments	Graphene oxide	TiO_2	ICP-MS	LOD 0.13 (Eu) to 2.64 (Pb), 7 mL sample	Spike recovery (waters), NRCCRM CRM GBW07301a (stream sediment)	143
Fe, Zn	Seawater, lake, mine and tap water	MWCNT		HR-CS- ETAAS	LOD 0.5 ng L^{-1} (Zn) and 4 ng L^{-1} (Fe), 150 mL sample	NIST SRM 1643e (trace elements in water), ERM- CA011b (hard drinking water)	144
Hg	Seawater, ground water	Poly(acrylamide)- grafted poly(propylene) sheet	Ag nanoparticles	ED-XRF and CV- AAS	LOD 6 (CV-AAS) and 30 (ED- XRF), 25 mL sample	Spike recovery	145
Hg	Water	Polydimethylsiloxane microfluidic chip	Au nanoparticles	ICP-MS	LOD 0.07, 20 μL sample	NIST SRM1641d, (mercury in water)	146
Mo	River, thermal, mine and tap water	Carbon nanotubes	L-Tyrosine	ICP-AES	LOD 40 ng L^{-1} , 2 mL sample	NIST SRM 1643e (trace elements in water)	147
Mo, Nb, Ti, V, W, Zr	Seawater	SeaFAST column	Ethylenediamine triacetic acid and iminodiacetic acid	ICP-MS	LOD 1.27 pmol kg^{-1} (Nb) to 4970 pmol kg^{-1} (V) 50 mL sample	NRCC CRM NASS-6 (seawater)	148
REEs	Tap and seawater	Amberlite XAD-4 resin	2,6-Pyridine dicarboxaldehyde	ICP-AES	LOD 0.006 (Yb) to 0.15 (Nd), 50 mL sample	SPS RMSW2 Batch 127 (elements in surface waters)	149



Table 1 (Contd.)

Analytes	Matrix	Substrate	Coating or modifying agent	Detector	Figures of Merit ($\mu\text{g L}^{-1}$ unless otherwise stated)	Method validation	Reference
REEs	Seawater and water samples	Amberlite XAD-4 resin	8-Hydroxy-2-quinoline carboxaldehyde	ICP-AES	LOD 0.01 (Yb) to 0.42 (Pr), 25 mL sample	SPS RM SW2 Batch 127 (elements in surface waters)	150
^{99}Tc	Water	TEVA@resin		ICP-MS	LOD 0.005 ng L^{-1} , 100 mL sample	Spike recovery	151

Table 2 Preconcentration methods using liquid phase extraction for the analysis of water

Analytes	Matrix	Method	Reagents	Detector	Figures of merit	Method validation	References
Ag, Au	Water and ore samples	Magnetic DLLME	1,3-(Propyl-1,3-diyl)bis-(3-methylimidazolium)bis-(tetrachloroferrate (III)) and 4,4'-bis(dimethylamino)thiobenzophenone (chelating agent)	ETAAS	3.2 (Au) and 7.3 (Ag) ng L^{-1} , 25 mL sample	Spike recovery (96–104%)	152
As^{III} and As^{V} (by difference)	Water	SPE-DLLME-SFOD	Diethyldithiophosphate (chelating agent), acetone and 1-undecanol	ETAAS	LOD 2.5 ng L^{-1} (As^{III}), 100 mL sample	NIST SRM 1643e (trace elements in water) and spike recovery	153
As^{V} (As^{III} by difference)	Water	LLME	Arsenomolybdate complexes, and tetradecyl(trihexyl) phosphonium dicyanamide	ETAAS	LOD 1.9 ng L^{-1} , 5 mL sample	NIST SRM 1643e (trace elements in water) and spike recovery	154
Au	Water and hair	DLLME	Benzyltrimethyltetradecyl ammonium chloride dehydrate (ion pairing agent) and 1-hexyl-3-methylimidazolium hexafluorophosphate	ETAAS	LOD 2.0 ng L^{-1} , 20 mL sample	Spike recovery, NRC CRM MA-1b (gold ore)	155
Cd	Water, seawater, beer, wine	CPE	Ag nanoparticles, APDC and Triton TM X-114	ETAAS	LOD 1 ng L^{-1} , 20 mL sample	NIST SRM 1640a (trace elements in natural water), NRCC CRM NASS-6 (sea water), spectrapure standards RM SPS-SW2 batch 125 (surface water)	156
Hg	Water, seawater and fish	Single drop ME lab in syringe	$\text{Pd}(\text{NO}_3)_2$, L-ascorbic acid, SnCl_2	VG-ETAAS	LOD 0.48 $\mu\text{g L}^{-1}$, 3.5 mL sample	Spike recovery (water) and ERM CE278 (mussel tissue) and IAEA-CRM 350 (tuna homogenized)	157
Ho, Yb	Water	Emulsification ME	1-(2-Pyridylazo)-2-naphthol (chelating agent), C_2Cl_4	ICP-AES	LOD 0.364 $\mu\text{g L}^{-1}$ (Ho) and 0.252 $\mu\text{g L}^{-1}$ (Yb), 10 mL sample	Spike recovery	158
REEs	Tap, river and seawater	DLLME	Acetone and CCl_4	ICP-MS	LOD 0.68 (Tb) to 26.6 (Ce) ng L^{-1} , 5 mL sample	Spike recovery	159
Si	Water	Ion associated complexation	Hexaammonium heptamolybdate tetrahydrate, N -[4-bis[4-(dimethylamino)phenyl]methylene]-2,5-cyclohexadien-1-ylidene]- n -methyl, chloride (crystal violet)	ED-XRF	LOD 9 ng mL^{-1} , linear range 0.02–1.0 $\mu\text{g mL}^{-1}$, 5 mL sample	Spike recovery and comparison with ICP-AES	160



air trap samples and from 0.10 (Se^{VI}) to 22 (Se^{VI}) $\mu\text{g L}^{-1}$ in water samples. The method was validated by measuring spike recoveries from the two matrices. Total elemental values determined by ICP-MS or ICP-AES agreed with the sum of the species concentrations.

A study¹⁷¹ of the fractionation of *Gadolinium* in Japanese river waters used sequential SPE. Humic and fulvic acid complexes of Gd were trapped on a strong anion-exchange column (QAE-Sephadex A-25) together with the MRI contrast agent diethylenetriamine-*N,N,N',N',N'',N''*-penta acetato aquo gadolinium(III) (Gd-DTPA). Free Gd^{III} was not retained and was trapped on a separate iminodiacetic acid-type chelating resin (EmporeTM). After the Gd-DTPA complex had been eluted with 4.0 mL of a 50 mM tetramethyl ammonium sulfate solution, the Gd humic and fulvic acid complexes were dissociated with 2 mL of 1 M HNO_3 and the Gd desorbed. Free Gd^{III} was eluted from the iminodiacetic acid-type chelating resin with 5.0 mL of 3 M HNO_3 and all eluates analysed for Gd by ICP-MS. The method LOD was in the low ng L^{-1} range for a 500 mL sample and its accuracy verified in spike recovery experiments. Whereas no free Gd or contrast agents were detected in a sample from a remote area, an urban sample contained 0.82 ± 0.09 ng ($n = 4$) Gd in the contrast agent fraction. In both rivers, the humic and fulvic acid fraction contained 3.6 ± 0.2 ng Gd ($n = 4$), taken to be the Japanese background level.

The determination of *mercury species* in aquatic samples continues to be of interest. A method for the determination of thimerosal (sodium ethylmercurithiosalicylate) and its breakdown products (EtHg and Hg^{2+}) in pharmaceutical effluents discharged to river waters in Argentina¹⁷² involved separation on a Zorbax SB-Aq C_{18} -RP (1.6 mm \times 150 mm, 5 μm particle size) analytical column. An eluent system of 0.1% formic acid followed by 0.1% formic acid + 0.1% 2-mercaptoethanol at a flow rate of 1.0 mL min^{-1} was used. The Hg species concentrations were determined by CV-AFS after UV photo-oxidation of the HPLC eluent. The LODs ranged from 0.07 $\mu\text{g L}^{-1}$ for Hg^{2+} to 0.09 $\mu\text{g L}^{-1}$ for thimerosal and EtHg , sufficient to detect EtHg and Hg^{2+} in the river water and industrial effluents. Thimerosal, however, was not detected. The accuracy of the method was validated by comparing the speciation results with total Hg measurements. A highly sensitive and automated HPLC-AFS method¹⁷³ for the determination of MeHg and Hg^{2+} in waters involved preconcentration onto a column packed with thiourea- and thiol-functionalised silica and separation on an EclipseXDB C8 (4.6 \times 150 mm, 5 μm) analytical column with a mobile phase of 1.5 mM APDC in a 75% (v/v) methanol : water solution at a flow rate of 1 mL min^{-1} . An LOD of 40 pg L^{-1} (MeHg) using UV oxidation CV-AFS was obtained for a 200 mL sample. Accuracy was determined by spiking a number of water samples (sewage, river and seawater) with MeHg and determining MeHg in the CRMs NIES no. 13 (human hair) and IAEA-085 (human hair).

A method for the determination of *iodine and selenium species* in groundwater¹⁷⁴ used anion-exchange chromatography coupled to ICP-MS. A 10 minute separation of I^- , IO_3^- , Se^{IV} and Se^{VI} was achieved using a Hamilton PRP X100 anion-exchange column and a aqueous mobile phase of 3 mM ammonium citrate and 30 mM ammonium perchlorate at pH 8.5 with 2% v/v

CH_3OH as an organic modifier. The LODs ranged from 4.3 ng L^{-1} for I^- to 23 ng L^{-1} for Se^{VI} . Method validation was carried out using spike recoveries from a groundwater. The method was deemed suitable for baseline monitoring of candidate sites for a Chinese high-level radioactive waste repository.

The determination of *nanoparticles* in environmental samples is becoming increasingly important as NPs are now finding uses in all walks of life. Although most methods rely on coupled techniques for their quantification and characterisation, there is still scope for simple fractionation methods to separate the particulate phase from the ionic phase. Although CPE is extensively used to preconcentrate trace elements, it has also been employed¹⁷⁵ to separate silver NPs from dissolved AgI species. Both silver NPs and AgI were extracted from a 20 mL sample acidified with 0.1 mL of 0.1 M HNO_3 into the Triton-X114 micellar phase. To extract only the silver NPs, 0.2 mL of 1 M ammonium thiocyanate was added to complex the AgI to prevent its extraction into the surfactant phase. The AgI concentration was calculated by difference. With ETAAS detection, the LOD was 2 ng L^{-1} . The accuracy of the method was tested by carrying out spike recovery experiments in a range of waters including NIST SRM 1640a (trace elements in natural water). The use of HDC to resolve engineered NPs in water samples was demonstrated¹⁷⁶ through use of a PL-PSDA cartridge, type 1 column (80 cm length and 7.5 mm id) with a separation range of 5 to 300 nm. The mobile phase was 1 mM NaNO_3 containing 0.0013% (w/w) SDS and 0.0013% (w/w) TritonTM X-100 at pH 7.5. Under these conditions a mixture of polystyrene, silver and gold NPs were detected on-line with DLS to determine the retention times of the different NPs. These results and those obtained by AUC with off-line fraction collection, DLS and sp-ICP-MS agreed well with the manufacturer's declared size for the NPs. In the sp-ICP-MS analysis, 20 μL of a 100 ng L^{-1} solution of NPs was injected onto the column. The 75 μL fractions were collected and analysed off-line after a further 1 + 99 dilution to ensure single particle conditions. Under these conditions, 10 nm gold NPs were below the LOD but 20 nm silver NPs were detectable. To further show proof of concept, the column was connected directly to an ICP-MS instrument to detect a 4 $\mu\text{g L}^{-1}$ spike of 20 nm radius silver NPs in river water. Asymmetric flow FFF was coupled with ICP-MS for the determination of engineered NPs in tap and domestic waste water.¹⁷⁷ Samples were spiked with various quantities of gold (20 and 60 nm) and silver NPs (10, 60 and 70 nm) capped with either citrate or polyvinylpyrrolidone to reduce the formation of agglomerates or aggregates. This also had the side effect of reducing solubility of the NPs thus maintaining their particle size. The FFF device was fitted with a 10 kDa cutoff membrane with a spacer/channel height of 350 μm . The mobile phase was 0.005% (w/v) NaHCO_3 with a flow rate of 0.8 mL min^{-1} at the detector. The capped NPs were stable in tap water for up to 2 h but domestic waste water had to be diluted at least fivefold to reduce matrix effects. Using an injection volume of 100 μL , the LODs of 30 for Ag and 15 $\mu\text{g L}^{-1}$ for Au were not low enough to determine the current suspected levels of NPs in tap or domestic waste water. Spike recoveries were $\sim 100\%$ for all the different types of NP but the measurement uncertainty



seemed to depend on particle size, with 70 nm silver NPs having the worst expanded uncertainty of 51% for a 0.13 mg L^{-1} spike based on 4 replicate measurements.

The formation of *thiomolybdate species* in geothermal and euxinic saline lake bottom waters¹⁷⁸ was studied using ion pair chromatography coupled with ICP-MS. The mono, di, tri and tetra thiomolybdate species as well as molybdate were separated on a RP polymeric column (Dionex, IonPac NS1, $10 \mu\text{m}$, $250 \times 4 \text{ mm}$) thermostated at 30°C . The mobile phase (1 mL min^{-1}) contained an aqueous component (2 mM tetrabutylammonium hydroxide as an ion pairing agent and 1 mM sodium carbonate) and an organic solvent (2-propanol) the proportion of which was increased from 10 to 25% in 10 minutes. The LOD was 10 nM of molybdate. To investigate thiomolybdate formation, a lake water sample was spiked to 250 nM of ammonium molybdate in the field and subsamples taken after 60 minutes and flash frozen with liquid N_2 to preserve the species. Thiomolybdate formation was dependent on sulfide availability and pH but all the species were formed with tetrathiomolybdate the most dominant one. To see if these species were formed in nature, 47 samples of geothermal waters from Yellowstone National Park were taken and preserved in the same way. Dithiomolybdate, trithiomolybdate or tetrathiomolybdate were detected in almost half of these waters and constituted 12–38% of the total Mo measured in acidified sub-samples.

Although most methods for the speciation analysis of *tin* in waters focus on the determination of butyltin compounds, procedures for other species are being developed. A method¹⁷⁹ for the determination of Sn^{II} and Sn^{IV} was based on the on-column complexation of ionic Sn with DTPA. The Sn–DTPA complexes were retained on a porous polymethacrylate strong anion-exchange resin and eluted with a mobile phase containing 20 mM NH_4NO_3 and 3 mM DTPA at pH 6.0. Complete separation was achieved within 5 minutes at a flow rate of 1 mL min^{-1} . The LODs for a $50 \mu\text{L}$ injection and ICP-MS detection were $0.3 \mu\text{g L}^{-1}$ for Sn^{II} and $0.1 \mu\text{g L}^{-1}$ for Sn^{IV} . The method was sufficiently sensitive for the detection of these analytes in contaminated water from an industrial site. Recoveries for a mixed $20 \mu\text{g L}^{-1}$ spike in water samples were 96.8–103%. A rapid derivatisation-free HPLC-ICP-MS method¹⁸⁰ for the detection of MBT, DBT and TBT in water, sea water and sediments used stir bar sorptive extraction preconcentration. All the analytes were separated in $<8 \text{ min}$ using a CN bonded silica analytical column with a mobile phase of ethanol–formic acid–water (16 : 8 : 76, v/v) containing 5 mM mercaptoacetic acid at pH 2.5. When a C_{18} -coated stir bar was used in the preconcentration procedure, enrichment factors of up to 127 could be achieved, resulting in LODs ranging from 15.6 (TBT) to 29.4 (MBT) ng L^{-1} . The accuracy of the method was assessed by analysis of the NRCC CRM PACS-2 (marine sediment) as well as by spike recovery from lake, river and seawaters. A method¹⁸¹ for the determination of TBT in surface water at the European framework directive limit of 0.2 ng L^{-1} was based on GC-ICP-MS. Response curves were constructed for TBT extraction using SPE with a C_{18} stationary phase. To determine TBT at the required level, preconcentration from a sample volume of between 250 and 1000 mL was necessary. The analyte could be

eluted with CH_2Cl_2 , ethylacetate, THF or MeOH. Ethylation of TBT should take place at pH 5, so that it could be carried out either before or after preconcentration. A LOQ of *ca.* 0.06 ng L^{-1} was achieved when carrying out the analysis under these constraints.

2.3 Instrumental analysis

2.3.1 Atomic absorption spectrometry. One of the main innovations in AAS is the development of continuum source instruments that do not rely on hollow cathode lamps and so can operate in multi-elemental mode much more easily. A fast sequential method¹⁸² for the determination of Ca, Cd, Cu, Fe, K, Mg, Mn, Ni, Na, Pb and Zn in environmental samples and drinking water used a high resolution continuum source instrument coupled with FI, which reduced the sample uptake to $<1 \text{ mL}$ per element for triplicate measurements. The linear range was expanded through use of multiple lines, elemental multiplets (such as that for Fe) and side pixel registration (for Mg). The resultant linear working range of $0\text{--}120 \text{ mg L}^{-1}$ for Mg meant that sample dilutions were not required. Concentrations of Cd, Cu, Fe, Mn, Ni, Pb, and Zn in river, sea, mineral, bottled and tap waters were below the instrumental LOD but those of Ca, K, Mg and Na were in good agreement with the levels given on the labels of the mineral and bottled waters. Recoveries of spikes from water samples ranged from 92% (Cd) to 110% (Pb). Accuracy at higher concentrations was checked by analysing NIST SRM 1575a (pine needles); the results were in good agreement with the certified values.

2.3.2 Laser-based spectroscopy. The use of *laser-induced luminescence spectroscopy* for the determination of U in groundwater has been reviewed¹⁸³ (47 references). The two main detection methods for U^{VI} were TRLFS, and the measurement of the ratio between the U^{VI} luminescence and the Raman scattering intensity of water as a kind of internal standard to correct for variations in laser pulse energy and drift in the voltage to the PMT. Results were generally in good agreement with those obtained by ICP-MS and radiochemical spectrometry with LODs as low as $0.03 \mu\text{g L}^{-1}$ when an excitation wavelength of 266 nm was used.

A review¹⁸⁴ (86 references) of the use of *LIBS* for water analysis noted that although LIBS should not require much sample pretreatment, an improvement in LODs and stability is necessary to meet water monitoring requirements. The LODs for LIBS were improved by combining it with DLLME.¹⁸⁵ Chromium, Cu, Mn, Ni and Zn were extracted as APDC complexes and then deposited onto an aluminium sample holder. By extracting a 9 mL sample into $100 \mu\text{L}$ of tetrachloromethane, followed by deposition of a $10 \mu\text{L}$ drop, LODs of between 107 (Ni) and 19 (Cr) $\mu\text{g kg}^{-1}$ were achieved. This presented a 3.7–5.6 times improvement over those obtained with no preconcentration. In an alternative approach,¹⁸⁶ Zn^{2+} was deposited onto a Cu electrode *in situ* and the Zn then measured by underwater LIBS. Emission was detectable at the 5 mg L^{-1} concentration level and the calibration was linear up to 50 mg L^{-1} .

2.3.3 Inductively coupled plasma mass spectrometry. In a survey¹⁸⁷ of the *niobium* content of mineral and freshwaters by



ICP-SF-MS it was possible to obtain a LOD of 0.02 ng L^{-1} in low resolution mode ($R = 500$) if the instrumental sensitivity was greater than $1.2 \times 106 \text{ cps per ppb of } ^{115}\text{In}$. Under these conditions, replicate measurements of a 1 ng L^{-1} standard ($n = 20$) gave an RSD of 3.8%. Accuracy was checked against a 5 ng L^{-1} in-house standard. Measured Nb concentrations ranged from 0.37 ng L^{-1} for a bottled mineral water to 417 ng L^{-1} in a geothermal water. An indicative value of 2.8 ng L^{-1} was obtained for the NRCC CRM SLRS-5 (river water).

Vertical distribution profiles of *dissolved platinum* in the Sea of Japan were obtained¹⁸⁸ using SPE followed by IDA-ICP-MS. On board ship, 12 L seawater samples were filtered and acidified to 0.024 M HCl . In the laboratory, a 1 L aliquot was acidified to 0.5 M HCl and equilibrated with a ^{192}Pt -enriched standard for 24 h. The Pt was retained on a minicolumn packed with Biorad AG1 X-8 anion exchange resin. Following removal of the matrix with 6 mL of 0.05 M HCl and 6 mL of ultrapure water, the Pt was eluted with 25 mL of 5 M HNO_3 and 5 M HClO_4 , the eluent evaporated to $<0.1 \text{ mL}$ and then redissolved in 1.5 mL of $5\% \text{ HCl}$ for quantification by ICP-MS. The LOD was $0.015 \text{ pmol L}^{-1}$ and the precision ($n = 3$) $0.23 \pm 0.026 \text{ pmol L}^{-1}$. The authors note that the levels of Pt in ocean water are similar to those reported 20 years ago suggesting that Pt has a conservative behaviour in the ocean and that the anthropogenic Pt effect seen on land has yet to reach the Sea of Japan.

In the multi-element analysis of drinking water by ICP-MS, an excess of HCl or other agents containing Cl is often added to the sample to preserve any Hg^{2+} in solution but this has the drawback of increasing Cl-based polyatomic interferences at the As, Cr and V masses. In an ICP-MS-MS procedure,¹⁸⁹ oxygen was introduced into the octopole reaction cell thereby shifting the analyte masses by 16 amu. Mercury did not react in the cell so continued to be determined at m/z 202. The instrumental LODs ranged from 1.6 (As) to 38 (Hg) ng L^{-1} and results for the NIST SRM 1643e (trace elements in water) were in agreement with the certified values.

The *uncertainty contributions* associated with the determination of trace elements in seawater by ICP-MS after matrix separation and preconcentration have been investigated¹⁹⁰ by using Toyopearl AF-Chelate-650 resin to preconcentrate Co, Fe, Pb and V and ICP-MS to determine their concentrations in the NRCC CRM NASS-6 (seawater) and two GEOTRACES RMs. The experimental design allowed a thorough investigation of the uncertainty contribution for each parameter to the overall expanded uncertainty of the measurement. The largest contributions were the uncertainties from the precision of the peak area measurement (for NASS-6 from 10% for Fe to 88% for Pb) and those associated with the slope of the calibration curve (again for NASS-6 from 10% for Pb to 81% for Fe). The results obtained were in good agreement with the certified or consensus values, demonstrating the suitability of the analytical method used for the investigation.

Most advances in *IR analysis* revolve round strategies for analyte preconcentration or separation from matrix elements to reduce fractionation and mass bias effects. The Mg coprecipitation method for Si in natural waters is widely used for seawater analysis but the addition¹⁹¹ of a 1 M MgSO_4 solution to

the sample in the ratio of 20 : 1 sample : MgSO_4 made it applicable also to river and estuarine waters. An improved recovery of 98.0% of Si from low silicate waters was achieved by using NH_4OH (approximately 7 M) instead of 1 M NaOH (80% recovery) with a coprecipitation time of 6 h, this meant that only one extraction was required. The direct coupling of IEC with MC-ICP-MS promises to be a faster method¹⁹² as demonstrated through use of an ICE-AS1 IEC column ($9 \text{ mm id} \times 250 \text{ mm}$) with a mobile phase of $0.01\% \text{ HCl}$ at a flow rate of 0.8 mL min^{-1} . The Si peak was separated from other matrix components in 10 minutes. The mass-independent bias was corrected by using a bracketing calibration solution in nutrient-free seawater. To demonstrate the applicability of this method, the Si isotope ratios of NRCC CRMs MOOS-3 (seawater) and SLRS-5 (river water) were successfully determined.

In a procedure for the preconcentration of *mercury* adapted for measurement of Hg isotope ratios in seawater,¹⁹³ filtered seawater was acidified with 10 mL of concentrated HNO_3 per L of sample. The sample was then purged with N_2 overnight to remove I_2 , acidified to a concentration of 0.1 M with HCl and treated with BrCl to release the organically-bound Hg. The BrCl was then neutralised with $\text{NH}_2\text{OH} \cdot \text{HCl}$ and Hg retained on a Biorad AG1-X4 anion-exchange resin. For a 10 L sample, the resin was washed with 40 mL of 0.1 M HCl followed by 80 mL of water and the Hg eluted with 10 mL of a $0.05\% \text{ L-cysteine}$ solution in $1\% \text{ sodium citrate}$. Mercury was detected using MC-ICP-MS with CVG as the sample introduction system. The preconcentration recovery was $98 \pm 6\%$. It was suggested that Hg isotope ratios may be used to distinguish between anthropogenic mercury sources in seawater. In an alternative purge-and-trap method,¹⁹⁴ Hg in seawater was purged as Hg^0 from the sample and then trapped in three amalgamation tubes filled with gold-coated glass beads. The trapped Hg was thermally desorbed and re-trapped in a KMnO_4 solution, before analysis by CV-MC-ICP-MS to determine the Hg isotope ratio. During measurement of the NIST SRM 3133 (Mercury (Hg) Standard Solution), the external precision for $\delta^{202}\text{Hg}$ was 0.06% ($2\text{SD}, n = 310$).

2.3.4 Vapour generation techniques. The advantages of *vapour generation* for trace element analysis are well known but the technique is applicable to only a small number of elements. An alternative approach is photochemical vapour generation in which a UV reactor is used to catalyse the generation of volatile species. Such a technique¹⁹⁵ for the production of CH_3Br used a photochemical generator fitted with a 19 W low pressure mercury vapour lamp. Use of a solution of $2\% \text{ v/v}$ acetic acid containing $3000 \text{ } \mu\text{g mL}^{-1} \text{ NH}_4\text{Cl}$ gave a VG efficiency of 95% and a LOD at m/z 79 of 0.14 ng mL^{-1} , which was superior to that (2.4 ng mL^{-1}) obtained using solution nebulisation ICP-TOF-MS. However, the analytical gains to be made by extending this method to elements that are known to undergo hydride or CVG are more dubious. For example, CVG has been applied to Sn^{196} with ICP-MS detection and Hg^{197} with ETAAS detection to obtain LODs ($\text{LOQ for Sn } 0.02 \text{ } \mu\text{g L}^{-1}$, $\text{LOD Hg } 0.02 \text{ } \mu\text{g L}^{-1}$) similar to those obtainable by traditional VG. One advantage of CVG was that more stable reagents could be used to volatilise the target analyte, e.g. stannic instead of stannous chloride for Sn and



HCOOH for Hg. However, this was at the cost of increased analysis time such as the 32 s irradiation time required for Sn with CVG compared to the quasi instantaneous determination of traditional VG.

The hydride generation of *thallium*¹⁹⁸ with NaBH₄ was enhanced by the addition of rhodamine B (3.5×10^{-5} M) and KI (0.018 to 0.024 M) to the sample. These enhancing/catalysing agents resulted in a 7-fold signal enhancement. Under optimum conditions a LOD of $1.5 \mu\text{g L}^{-1}$ was obtained with AAS detection. The method was validated by spike recovery experiments in tap and river water samples, good agreement was obtained with the certified values for NIST SRM 1643e (trace elements in water).

2.3.5 X-ray spectrometry. The use of T-XRF for water analysis was reviewed¹⁹⁹ (175 references) with special attention paid to sample preparation, instrumentation, matrix effects, potential errors and the figures of merit. Readers are directed to our companion ASU review⁵ on advances in X-ray fluorescence spectrometry for more specific information on XRF in all its guises.

3 Analysis of soils, plants and related materials

3.1 Review papers

Multi-technique reviews have highlighted the growing contributions²⁰⁰ of X-ray spectroscopy and ICP-MS to the understanding of P cycling in soil (397 references); the application²⁰¹ of AAS, AES and AFS in the analysis of conifers and conifer-derived products (106 references); and laser-based approaches for algal biomass analysis²⁰² with particular emphasis on LIBS and, to a lesser extent, LA-ICP-MS (136 references). In a review²⁰³ (112 references) of the advantages and limitations of atomic spectrometric techniques for authentication of organically grown food, it was concluded that chemometric analysis of multi-element and stable isotope data generated by several complementary techniques represented the best option for classifying the agricultural origin of plant products.

Country-specific reviews included a description of the substantial contribution made by Brazilian researchers²⁰⁴ (217 references) to the field of flow analysis and a summary of Turkish studies²⁰⁵ (146 references) that applied atomic spectrometry to investigate the uptake of potentially toxic elements by plants.

3.2 Sample preparation

3.2.1 Sample storage and pre-treatment. The *collection, preservation and pre-treatment of samples* can have a marked influence on results obtained by atomic spectrometry. Amaral *et al.*²⁰⁶ used HPLC-ICP-MS to investigate the effects of four storage regimes on As speciation in tissue of the tropical grass *Brachiaria brizantha*. Portions were: (a) freeze dried, milled in liquid N₂ and then stored at room temperature; (b) freeze-dried and stored at 4 °C; (c) stored at –18 °C; or (d) stored at –80 °C. None of the samples showed a marked change in As speciation over a 12 month period, but highest recoveries were always

obtained following storage regime (a) and this was the only portion from which DMA could be extracted. Loppi *et al.*²⁰⁷ showed that painstaking removal of extraneous particles from lichen using nylon tweezers under a binocular microscope – a process that took 3–4 h to prepare a 200 mg sample – almost halved the measured concentrations of the lithogenic elements Al and Fe, presumably due to the removal of adhering soil-derived material. In forensic science,²⁰⁸ double-sided tape could be used to mount small samples of soil (10 ± 4 mg) typically recovered in criminal investigations for analysis by either LA-ICP-MS or LIBS without introducing significant blank signals from either the adhesive or the tape. Similarly, Arnoldussen and van Os²⁰⁹ showed that portable XRF could be used to study lacquer-peel soil sections from archaeological sites without interference from the fixing and mounting agents used.

The *suitability of ferrihydrite gel DGT samplers*¹⁶⁸ combined with extraction procedures and solution techniques such as HPLC-HG-AFS for determination of As species in soil solution has been questioned. Use of XANES to measure As species directly in the gel showed that the species distribution changed significantly during extraction, *e.g.* about 20% of arsenate was converted to arsenite.

3.2.2 Sample dissolution and extraction. *Sample preparation methods used in the determination and speciation of arsenic in rice* have been reviewed²¹⁰ (76 references) and a new method²¹¹ proposed based on enzyme-assisted microwave extraction prior to CE-ICP-MS. This gave excellent separation of DMA, MMA, As^{III} and As^V, and LODs in the range 0.15–0.27 ng g^{–1}.

An *optimised pyrohydrolysis method*²¹² was designed for the extraction of I from organic-rich samples such as seaweed prior to ICP-MS or AMS analysis. Use of ¹²⁵I as a yield tracer was recommended.

A *closed-vessel conductively heated digestion system*²¹³ gave ICP-AES results close to certified values (recoveries 87–104%) for Al, B, Ca, Cu, Fe, K, Mg, Mn, P, S and Zn in NIST SRMs 1515 (apple leaves), 1575a (pine needles) and IRMM BCR 679 (white cabbage). When applied to sugarcane leaf – a potentially important source of bioethanol – the method gave results similar to those obtained using microwave-assisted digestion.

Several *comparisons of sample extraction methods* have been published. Amongst the most interesting were a study²¹⁴ featuring the determination of MeHg in IAEA CRM 405 (estuarine sediment).

405 (estuarine sediment) by GC-AFS following: (a) microwave-assisted extraction with 0.5% (v/v) 2-mercaptoethanol in 5% (v/v) methanol; (b) acid leaching with 3 M HNO₃/1 M CuSO₄ at room temperature, dichloromethane extraction and back extraction into water by evaporation; (c) alkaline digestion with 25% (w/w) KOH in methanol at 75 °C, dichloromethane extraction and back extraction into water by evaporation; or (d) acid leaching with 3 M HNO₃/1 M CuSO₄ at room temperature, dichloromethane extraction and back extraction into 1 mM Na₂S₂O₃. Recoveries of >90% were obtained with procedures (b) and (d) but (d) was preferred because it took less time to perform (95 vs. 180 minutes). Other workers²¹⁵ compared four methods for extraction of As species from freeze-dried roots of the hyperaccumulator plant *Pteris vittata*. The methods were:



sonication with 2 mM NaH₂PO₄ + 0.2 mM Na₂EDTA at pH 6.0; acid digestion with 1% HNO₃; sonication with 1 + 1 methanol–water; and sonication with 1 + 1 ethanol–water. Analysis of the extracts by HPLC-ICP-MS indicated that ethanol–water was the most efficient extractant. Following further optimisation, the final recommended procedure was sonication of 0.05 g sample for 0.5 h (fronds) or 2 h (roots) in 10 mL 1 + 3 ethanol–water mixture. In a study²¹⁶ of various combinations of HNO₃ and HCl for determination of Cd, Cr, Cu, Pb and Zn in herbal plants by FAAS, oven-dried leaves were digested either following dry ashing, using a hotplate, or with microwave-assistance. Highest recoveries were obtained with dry ashing followed by 4 + 1 HNO₃–HCl (v/v).

Improvements in *microwave-assisted extraction procedures* included²¹⁷ generation of UV irradiation *in situ* in the digestion vessel to reduce acid consumption without compromising digestion efficiency in the analysis of seaweed by ICP-MS. Results obtained for As, Cd, and Pb when 0.7 g samples were treated with 2 M HNO₃ were comparable to those obtained using conventional microwave digestion with concentrated HNO₃ and to certified concentrations for aquatic plant IRMM CRMs BCR 670 and BCR 060. The efficiency of acid digestion of biological samples, including plants, with 2 M HNO₃ was also improved²¹⁸ by performing the digestion under 7.5 bar of O₂ and cooling the vessel with an external air flow. Results obtained for Ca, Cu, Fe, K, Mg, Mn, Mo, Na and Zn in NIST SRMs 1515 (apple leaves), 1577 (bovine liver) and 8435 (whole milk powder) were statistically similar to certified values. The optimal extractant in a MAME procedure²¹⁹ that did away with acid altogether was a mixture of 1.25% (w/v) SDS and 0.1% (v/v) Triton X-100. The method could be used in the determination of pseudototal Cd, Cr, Cu, Ni and Pb in sediment by ETAAS without the need to add chelating agents to improve extraction efficiency. New MAE methods have also appeared. That for Cr species²²⁰ in soil and sediment used 0.1 M EDTA, 1% tetrabutyl ammonium bromide and HF, followed by ion-exchange separation and quantification by ICP-AES. A MAE method for As species in ornithogenic sediments²²¹ used 1.0 M orthophosphoric acid and 0.1 M ascorbic acid, with separation and quantification by HPLC-HG-AFS.

Developments in *ultrasound-assisted extraction procedures* included the application of a rapid, small-scale ultrasonic probe-based method²²² previously optimised for dust, to extract Hg from industrial soil (20 mg soil, 1 mL 8 M HCl, 3.2 min sonication), and a new ultrasonic bath-based method²²³ for the extraction of ten trace elements from estuarine sediment (100 mg sediment, 1 mL 7.5 M HF + 1 mL 3.5 M HNO₃, sonication time 15 min). An ultrasonic probe-based method²²⁴ for extraction of Hg species from fish and plant tissue (0.5 g sample, 8 mL 2% tetramethylammonium hydroxide, sonication time 5 min) gave quantitative recoveries for IRMM CRMs BCR 060 (aquatic plant) and BCR 482 (lichen).

Research continues to improve *methods for estimation of the available trace element fraction in soils*. Duval *et al.*²²⁵ found a relationship between Mo extracted into 0.3 M ammonium oxalate and foliar uptake for the N₂-fixing legume *Galactia elliottii* but not for oak (*Quercus myrtifolia*). Workers in Brazil²²⁶

used the radionuclide ¹⁰⁹Cd as a tracer to show that extraction with a mixture of 1 M acetic, 0.72 M citric, 0.49 M lactic and 0.12 M oxalic acids gave a better estimation of Cd available to rocket (*Eruca sativa*) than extraction into DTPA, Mehlich-1 or Mehlich-3 reagents. An ammonium phosphate method²²⁷ was optimised for extraction of labile As species from soil for determination by HPLC-ICP-MS. A two-level Plackett–Burman factorial design was used to identify variables affecting extraction efficiency, and then these were each optimised in turn using a univariate approach to give the final recommended method in which 0.1 g soil was extracted with 30 mL of 40 mM NH₄H₂PO₄, at 70 °C for 120 min. Ultrasound and microwave-assisted versions²²⁸ of standard soil extraction methods using 0.01 M CaCl₂, 0.43 M acetic acid and 0.05 M EDTA were developed using IRMM CRMs BCR 483 (sewage sludge amended soil) and BCR 700 (organic rich soil) as test substrates. The CaCl₂ and EDTA extractions could each be performed in 2 min by UAE or 5 min by MAE (*cf.* 3 h and 1 h by conventional shaking), and the acetic acid extraction in 15 min with either approach (*cf.* 16 h).

There has been interest in *partial soil extractions for geochemical prospecting*. Of 11 extraction procedures²²⁹ applied to the determination of 30–55 elements in 15 soils overlying the Talbot VMS Cu–Zn prospect in Canada, weaker leachates such as deionised water detected anomalies with greater contrast than strong acid digests. A similar conclusion was reached by workers in China²³⁰ who found that whereas extraction with 2% HCl and determination of Bi, Cu, Pb and Zn in leachates by ICP-MS gave a good indication of the location of the Jiaolongzhang polymetallic deposit beneath *ca.* 100 m of soil overburden, total digestion did not.

Advances in *human bioaccessibility tests* have continued with the development of an automated in-line dynamic extraction system²³¹ used in the determination of bioaccessible Cr, Cu, Ni, Pb and Zn in forest and garden soil. To validate the method, the residue remaining after extraction was digested with aqua regia and the sum of the bioaccessible and residual fractions compared with the result following a separate MAE on whole soil. Recoveries were 96–110%. Growing interest in extraction tests that estimate bioaccessibility of potentially toxic elements following inhalation was reflected in two studies. Boisa *et al.*²³² used a novel simulated epithelial lung fluid to extract Pb from the <10 µm diameter particle size fraction of urban soil and mining waste. Sysalova *et al.*⁵² applied established bioaccessibility tests – Hatch's solution and the PBET – to the determination of bioaccessible As, Cd, Cr, Hg, Mn, Ni, Pb and Zn in various size fractions of urban particulate matter.

In a *sequential extraction procedure for P* in volcanic soil²³³ modified to include an additional fraction, 'recalcitrant organic P', both air-dried subsamples and subsamples that had been heated at 300 °C were analysed. The 'recalcitrant organic P' fraction was estimated from the difference between results for the two subsamples. The sum of the steps of the modified method corresponded better with total P concentrations than those of the original procedure, which accounted for <40% of analyte present.

Two *automated flow-through fractionation procedures for As* have been described. A modified (3-step) BCR sequential



extraction²³⁴ and HG-AFS system with on-line UV photo-oxidation for degradation of organic As species and reduction of As^V to As^{III} was optimised using an As-enriched soil and then applied to four agricultural soils impacted by mining activities. Results were generally within 10% of those obtained by conventional batch extraction. A four step sequential extraction procedure²³⁵ involving 0.05 M ammonium sulfate, 0.05 M ammonium dihydrogen phosphate, 0.2 M ammonium oxalate and finally 0.2 M ammonium oxalate + 0.1 M ascorbic acid at 96 °C, was combined with HG-ICP-AES for on-line speciation of As^{III} and As^V in soil. Results similar to batch extraction were obtained and the overall As recovery (sum of the 4 steps plus off-line *aqua regia* digestion of the residue) obtained for NIST SRM 2710a (Montana soil) was excellent.

3.2.3 Preconcentration procedures. Numerous preconcentration procedures for specific analytes continued to be reported.

Methods for the analysis of soils, plants or related materials, or those developed for other sample matrices that used soil or plant CRMs for validation, are summarised in Tables 3–5.

3.3 Instrumental analysis

3.3.1 Atomic absorption spectrometry. In *simultaneous multi-element ETAAS*, the use of permanent chemical modification²³⁶ (200 µg Zr + 20 µg Ir) and Te internal standard improved the LODs for As from 1.48 to 0.59 µg L⁻¹ and for Se from 1.96 to 0.35 µg L⁻¹. The method was applied successfully to IRMM CRM BCR 402 (white clover) and river sediment samples.

New procedures involving *slurry sampling ETAAS* included a matrix-modifier-free method²³⁷ for the measurement of As in soils; a procedure²³⁸ for determination of Bi in sediments using platform atomisation, NbC permanent modifier and Ba(NO₃)₂ chemical modifier; and a method²³⁹ for the determination of As, Cd, Cr, Cu, Ni and Pb in moss. The latter involved sonication of pulverised moss (1–50 mg) with 0.2 M HNO₃ and 0.01% Triton X-100 for 25 seconds prior to injection into the furnace. Chemical modifiers used were: 3 µg Mg(NO₃)₂ + 5 µg Pd for As and Cu; 70 µg NH₄H₂PO₄ + 4 µg Mg(NO₃)₂ for Cd and Pb, and 20 µg Mg(NO₃)₂ for Cr. No modifier was required for Ni determination.

A comprehensive tutorial review⁶⁰ (105 references) of *HR-CS-ETAAS* summarised progress to date and provided guidelines for future method development. Researchers at IAEA, Monaco, optimised slurry sampling HR-CS-ETAAS methods for the determination of Hg in sediment and fish²⁴⁰ and for As, Cd, Co, Cr, Cu and Ni in sediment.²⁴¹ In both cases calibration based on solid CRMs rather than liquid standard solutions improved accuracy, yielding results similar to certified values for other CRMs.

A *fast sequential HR-CS-FAAS* method¹⁸² for determination of Ca, Cd, Cu, Fe, K, Mg, Mn, Na, Ni, Pb and Zn in soil and water used secondary lines and side-pixel registration to extend the calibration range for elements present at high concentration. Results obtained for NIST SRM 1575a (pine needles) were in agreement with certified values at 95% CI for all the elements except Cd, Ni and Pb for which the certified concentrations were below the LODs of 1.1 (Cd), 2.0 (Ni) and 6.2 mg kg⁻¹ (Pb) for a 250 mg sample.

Coufalik and Komarek²⁴² provided an overview (48 references) of the use of *TD-AAS for mercury speciation analysis* in solid samples. Particularly useful was their inclusion of a summary of desorption temperatures reported for key mercury species.

3.3.2 Atomic emission spectrometry. Articles purporting to *compare the performance of ICP-AES and X-ray techniques* – but actually comparing sample pre-treatment procedures – have been published for determination of trace elements in mosses²⁴³ and soil.²⁴⁴ The moss study²⁴³ used HNO₃–HCl–HF to digest samples for ICP-AES but HNO₃–HCl–H₂O₂ for TXRF spectrometry because the sample digest was dried and analysed in a quartz reflector and this was damaged if HF was used. Lower values obtained for Cr and Fe by the X-ray technique likely resulted from their presence in refractory forms that only HF could dissolve. In contrast, the soil study²⁴⁴ obtained higher concentrations for most elements when XRF spectrometry was applied directly to solid samples than for ICP-AES analysis of sample digests. This can be readily explained by the inappropriate choice of *aqua regia* extractant for the ICP-AES procedure – a reagent well-known to give only incomplete digestion of soils.

Table 3 Preconcentration methods involving coprecipitation used in the analysis of soils, plants and related materials

Analyte(s)	Matrix	Carrier	Detector	LOD (µg L ⁻¹)	CRMs or other validation	References
Cd, Co, Cu, Fe, Mn, Ni, Pb	Herbal plants	Lutetium hydroxide	FAAS	1.7–7.2	NIST SRM 1570a (spinach leaves), NWRI CRM TMDA-70 (fortified lake water)	311
Cr	Drinking water, soil extracts, wastewater	APDC/Ce ^{III}	FAAS	2.1	NRCCRM CRM GBW 07309 (stream sediment)	312
Cr, Cu, Fe, Pb, Zn	Foods, water	2,9-Dimethyl-4,7-diphenyl-1,10-phenanthroline	FAAS	0.28–3.1	NIST SRM 1515 (apple leaves), NRCCRM CRM GBW 07605 (tea)	313
Cr, Cu, Pb	Tea, tobacco, water	2-[4-[2-(1H-indol-3-yl)ethyl]-3-(4-chlorobenzyl)-5-oxo-4,5-dihydro-1H-1,2,4-triazol-1-yl]-N-aryl methylidene acetohydrazide	FAAS	2.1 for Cr 0.56 for Cu 0.86 for Pb	HPS CRM-SA-C (sandy soil C)	314



Table 4 Preconcentration methods involving liquid-phase microextraction used in the analysis of soils, plants and related materials

Analyte(s)	Sample matrix	Method	Reagent(s)	Detector	LOD ($\mu\text{g L}^{-1}$)	CRMs or other validation	Reference
As	Rice	CPE	Ammonium molybdate, Triton X-114	ETAAS	0.01	IRMM CRM 804 (rice flour)	315
Cd	Hair, herbs, spices	IL-UAEME	(4-(2-Pyridylazo)resorcinol), 1-butyl-3-methylimidazolium hexafluorophosphate	FAAS	0.21	NIST SRM 1570a (spinach leaves)	316
Cd	Fruit, vegetables	IL-DMME	Pyrrolidine dithiocarbamate, 1-butyl-3-methylimidazolium hexafluorophosphate, iron oxide nanoparticles	FAAS	0.32	NIST SRM 1570a (spinach leaves)	317
Cd, Co, Cu, Ni, Pb	Sediment	CPE	1-(2-Thiazolylazo)-2-naphthol, Triton X-114	FAAS	0.77–2.8		318
Cd, Cr, Pb	Herbal medicines	UAEME	APDC, toluene	ETAAS	0.002–0.03	Spike recovery	319
Cd, Ni	Artificial saliva extracts of tobacco	IL-UADLLME	APDC, 1-butyl-3-methylimidazolium hexafluorophosphate	ETAAS	0.05 for Cd, 0.14 for Ni	INCT CRM CTA-VTL-2 (virginia tobacco leaves)	320
Cd, Pb	Rice	CPE	8-Quinolinol, Triton X-45	ETAAS	0.018 for Cd, 0.043 for Pb	Spike recovery	321
Co	Rice, water	UAEME	Sodium dodecyl sulfate, chloroform	ETAAS	0.016	NRCCRM CRMs GBW 07605 (tea leaves), GBW 10015 (spinach)	322
Cr ^a	Soil solution, water	CPE	Alizarin-3-methyliminodiacetic acid, OP-5 surfactant	FAAS	1.0	Spike recovery	323
Cu	Sediment, soil	IL-DLLME	1-Hexyl-3-methylimidazolium bis-[(trifluoromethyl)sulfonyl]imide	ETAAS	1.8	NIST SRMs 2709 (San Joaquin soil), 2711 (Montana soil), 2704 (Buffalo river sediment), IAEA CRM 433 (marine sediment)	324
Cu	Water	CPE	7-Iodo-8-hydroxyquinoline-5-sulfonic acid, alkylphenol polyoxyethylene	FAAS	0.6	NRCCRM CRM GBW 08301 (river sediment)	325
Cu, Ni, Pb	Fruit, spices, vegetables	IL-UADLLME	Carbon tetrachloride, 1-butyl-3-methylimidazolium hexafluorophosphate ionic liquid	FAAS	0.17 for Cu, 0.49 for Ni, 0.95 for Pb	NIST SRM 1515 (apple leaves)	326
Ga, In, Tl	Mobile phone LCDs, sediment	CPE	Gallic acid, Triton X-114	FAAS	3.5 for Ga, 1.2 for In, 0.92 for Tl	Spike recovery	327
Hg	Rice, water, wheat	DLLME	Displacement of copper from copper pyrrolidine dithiocarbamate, carbontetrachloride, methanol	ETAAS	0.019	NRCCRM CRM GBW 08508 (rice flour)	328
Hg species ^b	Atmospheric particles, fish, plant, sediment, water	Hollow fibre-LLLME	Na ₂ S ₂ O ₃ solution, toluene, 1-(2-pyridylazo)-2-naphthol	HPLC-ICP-MS	0.003–0.006	NRCC CRM DORM-2 (dogfish muscle)	329
Mo, V	Drugs, soil, water	DLLME	8-Hydroxyquinoline, 1-undecanol	LIBS	30 for Mo 5 for V	NCS CRM ZC 85005 (beef liver)	330
Pb	Medicinal plants	Hollow fibre-LLLME	EDTA, 1-hexyl-3-methylimidazolium hexafluorophosphate ionic liquid, dicyclohexyl-18-crown-6	ETAAS	0.008	Spike recovery	331
Pb	Fruit, herbs, macaroni, plants, tea, vegetable, water	DLLME	5-(4-Dimethylaminobenzylidene) rhodamine	FAAS	1.1	SPS RM WW2 (wastewater), NIST SRM 1515 (apple leaves), NWRI CRM TMDA-51.3 (fortified water)	332
Pb	Soil, tea	CPE	Displacement of zinc from zinc diethyldithiocarbamate	TS-FF-AAS	0.5		333



Table 4 (Contd.)

Analyte(s)	Sample matrix	Method	Reagent(s)	Detector	LOD ($\mu\text{g L}^{-1}$)	CRMs or other validation	Reference
Pd	Soil, vegetables, water	IL-DLLME	1-(2-Pyridylazo)2-naphthol, 1-hexyl-3-methylimidazolium hexafluorophosphate	FAAS	3.2		334
REE	Soil	CPE	Diglycolamide, Triton X-114	ICP-MS	0.0002–0.03	NIST SRM 2709a (San Joaquin soil), IAEA CRM 384 (sediment)	335
Se	Tea	SFODME	APDC, 1-undecanol	ETV-ICP-MS	0.0002 for Se^{IV} , 0.0003 for Se^{VI}	NRCCRM CRM GBW 07605 (tea leaves)	336
V	Milk, vegetables, water, wine	IL-DLLME	4-(2-Pyridylazo) resorcinol, 1-butyl-3-methylimidazolium hexafluorophosphate	ETAAS	0.018	NRCC CRM SLRS-4 (riverine water), NIST SRM 1515 (apple leaves)	337

^a Cr^{III} then reduction, measurement of Cr, and estimation of Cr^{VI} by difference. ^b Hg^{II} , MeHg, EtHg, PhHg.

A fundamental study of the effect of adding N_2 to the plasma in ICP-AES included soil and sediment CRMs in performance assessment.²⁴⁵ The excitation temperature increased when 20 mL min^{-1} of N_2 was introduced to the central channel and matrix interference effects were reduced. The authors recommended this approach be used with, in particular, ETV and LA sample introduction systems.

Notable amongst improvements in solid sampling ETV-ICP-AES was the modification²⁴⁶ of the sample introduction system to incorporate a heated sheath between the spray chamber and the torch to generate hot aerosol. A switching valve placed between the ETV system and the sheath device allowed pyrolysis products generated during the ashing step to be directed to waste before introduction of the analytes generated during the vaporisation step into the plasma. In comparison to conventional systems in which the ETV module is connected directly to the torch, the new apparatus allowed soil samples as large as 13 mg to be analysed thereby increasing sensitivity for a suite of over 30 analytes by up to 5-fold and improving LODs by up to an order of magnitude. A conventional solid sampling ETV-ICP-AES system²⁴⁷ was used to measure the pathfinder elements Ag, Al, Ba, Cu, Hg, P, Pb, S and Zn in soil profiles for mineral exploration in Canada. This allowed the underlying ore body to be readily located. A procedure for the analysis of rice,²⁴⁸ which included cooling steps both before and after the sample vaporisation step and also point-by-point internal standardisation to Ar, gave results statistically similar to those obtained by ICP-MS analysis of rice digests (demonstrated by *F*-tests at 95% CI). The total analysis time of just 5 min per sample included time for grinding and weighing. In what must surely count as a labour of love, Masson²⁴⁹ demonstrated for the first time that ETV-ICP-AES can be used for imaging trace elements in biological tissue. Using a ceramic knife, tobacco leaves were subdivided into >100 individual segments which were cut out and weighed. Portions of each segment were analysed to generate elemental maps for Cd and Mg. The concept may have been proven but the fact that the analysis of a single leaf took

more than a day to complete, at a resolution of about 0.5 cm^2 , suggests that the approach is unlikely to become a major rival to established imaging techniques such as LA-ICP-MS!

The use of $750 \text{ mg L}^{-1} \text{ MgNO}_3$ as a chemical modifier improved²⁵⁰ the LOD for determination of Mn in plants by tungsten coil AES from 0.86 to 0.05 mg L^{-1} . Results for analysis of NIST SRMs 1547 (peach leaves) and 1573 (tomato leaves) were statistically similar to certified values at 95% CI whereas, without modifier, results approximately twice the certified values were obtained.

The performance of MP-AES with nitrogen as plasma gas was assessed for determination of four major and 13 trace elements in HNO_3 digests of sunflowers.²⁵¹ Results were similar to those obtained by ICP-MS, except for As, Co and Mo whose concentrations were below the LODs of the new technique. As the plasma temperature was lower than that of an Ar ICP, it was recommended that atom (as opposed to ion) lines should be used for analysis, together with an ionisation suppressor such as CsNO_3 . In an environmental survey²⁵² of an industrially contaminated area in Hyderabad, India, MP-AES gave results broadly similar to certified values for NRC CRM SO-1 (soil) and data comparable to those obtained by ICP-MS for soils, sediments, and water samples.

Several developments in capacitively coupled plasma microtorch AES have been reported by a research group in Romania. Use of a coiled Rh filament²⁵³ for ETV sample introduction allowed determination of Ag, Cd, Cu, Pb and Zn in six soil and two sediment reference materials with mean recoveries of 95–108%. The LODs were in the range $0.5\text{--}20 \mu\text{g L}^{-1}$. Mercury was successfully determined²⁵⁴ in soil, sediment and fish by CCP-AES following sonically-induced CVG in 0.2 M formic acid. Simultaneous determination²⁵⁵ of As and Sb in soil using HG-CCP-AES gave LODs for both analytes of 0.02 mg kg^{-1} for the most sensitive emission line. Results obtained for CRMs were close to certified values (recoveries 96–104%) and for soil samples were similar to those obtained by HG-ICP-AES.



Table 5 Preconcentration methods involving solid phase extraction used in the analysis of soils, plants and related materials

Analyte(s)	Matrix	Substrate	Substrate coating/ modifying agent or analyte complexing agent	Detector	LOD ($\mu\text{g L}^{-1}$)	CRMs or other validation	Reference
Cd	Soil, rice, tea, vegetables, water, wheat	Alumina	1-(5-Nitrofuran-2-yl) thiosemicarbazide	ICP-AES	0.025		338
Cd	Fish, water	Cation exchange fibre	None (non-selective sorption then selective elution with KI)	CV-AAS	0.0006	NRCC CRM DOLT 4 (dogfish liver), 339 NRC CRM AGAL-10B (river sediment)	
Cd, Co, Ni	Sediment	Polystyrene-divinylbenzene	2-Hydroxyacetophenone	FAAS	0.1 for Cd 0.8 for Co 0.6 for Ni	NIST SRM 2702 (marine sediment)	340
Cd, Cu, Ni	Food, water	Silica gel	Pentaethylene hexamine	FAAS	0.19 for Cd, 0.73 for Cu 0.91 for Ni	INCT CRM CTA-VTL-2 (virginia tobacco leaves), NWRI CRM NWTM-15.2 (water)	341
Cd, Ni, Pb	Sewage sludge, soil, water	Activated carbon cloth	1-(2-Pyridylazo)-2-naphthol	FAAS	0.1–2.8	NWRI CRM TMDA-64.2 (fortified lake water), IRMM CRM BCR 146R (sewage sludge amended soil)	342
Cd, Pb	Fish, sediment, soil, water	$\text{Fe}_3\text{O}_4@\text{SiO}_2$ NPs	Phenyl isothiocyanate	FAAS	0.05 for Cd 0.9 for Pb	NRC CRM LKSD-4 (lake sediment)	343
Cd, Pb	Fish, soil, water	Mesoporous silica	1-(2-Pyridylazo)-2-naphthol	FAAS	0.04 for Cd 0.9 for Pb	NCS CRM DC 73323 (soil)	344
Cd, Pb	Coffee, tea, water	Obsidian	Cetyltrimethylammonium bromide	FAAS	0.37 for Cd 0.89 for Pb	HPS CRM-SA-C (sandy soil C)	345
Cd, Pb	Fruit, walnut	Magnetite NPs	3-Aminopropyltriethoxysilane-2,4-bis(3,5-dimethylpyrazol)-triazine	FAAS	0.01 for Cd 0.7 for Pb	NIST SRMs 1571 (orchard leaves), 1572 (citrus leaves)	346
Cd, Pb	Herbs, meat products, spices, plants, tea, water	Dowex Marathon C	None	FAAS	0.13 for Cd 0.18 for Pb	SPS RM WW2 batch 108 (wastewater level 2), INCT CRM TL-1 (tea leaves)	347
Ce, Cu, Dy, Eu, La, Pb, Yb	Sediment, water	Graphene oxide-titanium dioxide composite	None	ICP-AES	0.13–2.6	NRCCRM CRM GBW 07301a (stream sediment)	143
Co, Cu, Ni	Plants, water	$\text{Fe}_3\text{O}_4@\text{MCM-41}$ NPs	N-(4-Methoxysalicylidene)-4,5-dinitro-1,2-phenylenediamine	FAAS	0.03 for Co, 0.03 for Cu 0.04 for Ni	Spike recovery	348
Co, Cr, Cu, Fe, Ni, Pb, Zn	Fish, mango, mint, water	Amberlite XAD-16	p-Aminobenzene sulfonic acid	FAAS	4.0–6.6	Spike recovery	349
Co, Pb	Fruit	Diethylamine phosphorus containing polymer	1-(2-Thiazolylazo)-2-naphthol	FAAS	4.4 for Co, 1.0 for Pb	NIST SRM 1515 (apple leaves)	350
Cs (^{135}Cs , ^{137}Cs)	Sediment	Amberchrom CG-71	Calix[4]arene-bis(tert-octylbenzo-crown-6) in octan-1-ol	SF-ICP-MS	<0.001		351
Cu	Food, water	Silica gel	Bis(3-aminopropyl)amine	FAAS	0.12	INCT CRM TL-1 (tea leaves), NRCC CRM DORM-3 (fish protein)	352
Cu	Plant, water	Naphthalene	2-(5-Bromo-2-pyridylazo)-5-diethylaminophenol	ETAAS	0.0015	CRMs	353
Cu, Fe, Mn, Zn	Beans, fish, leaves, water	Natural cellulose (almond bark)	<i>Rhizopus oryzae</i> fungus	HR-CS-FAAS	1.2–2.8	NIST SRM 1547 (peach leaves), IAEA CRM 407 (fish tissue)	354
Cu, Fe, Pb	Cosmetics, food, soil, water	Polyhydroxybutyrate-b-polydimethylsiloxane	2-(5-Bromo-2-pyridylazo)-5-diethylamino-phenol	FAAS	1.9 for Cu, 2.2 for Fe, 2.5 for Pb	NIST SRM 1577b (bovine liver), IAEA-336 (lichen), NWRI CRM TMDA-51.3 (fortified lake water)	355
Cu, Ni	Soil, vegetables, water	Amberlite XAD-16	<i>Bacillus subtilis</i>	ICP-AES	0.21 for Cu, 0.33 for Ni	NCS CRM ZC 73014 (tea)	356
Hg	Water	PTFE	APDC	CVAAS	0.02	IRMM CRM BCR 060 (aquatic plant)	357
Ni	Sediment, water	Ethylvinylacetate	None	FAAS	3.8	IJS TRAP-LRM (lake sediment)	358
Pb	Lipstick, pine leaves, water	MWCNTs	Thiourea functionalised ionic liquid	ETAAS	0.13	Spike recovery	359



Table 5 (Contd.)

Analyte(s)	Matrix	Substrate	Substrate coating/ modifying agent or analyte complexing agent	Detector	LOD ($\mu\text{g L}^{-1}$)	CRMs or other validation	Reference
Pb	Fish, fruit	MWCNTs	Poly(<i>N</i> -phenylethanamine)/	FAAS	0.8	NIST SRM 1515 (apple leaves), IAEA 360 CRM 336 (lichen)	
Pb	Water	Cellulose nitrate membrane filters	Brilliant black BN	FAAS	1.5	SPS RM WW2 (wastewater), NRCCRM CRM GBW 07424 (soil)	361
Pd, Rh	Catalytic converter, street dust, rock, water	Nanosponge Mn_2O_3	None	FAAS	1.0 for Pd, 0.37 for Rh	NIST SRM 2556 (used auto catalyst pellets)	362
Sn species ^a	Sediment, water	Stir bar	C18	HPLC-ICP-MS	0.016–0.029	NRCC CRM PACS-2 (sediment)	180
Tc (⁹⁹ Tc)	Soil, water	TEVA®	None	ICP-MS	0.00005	Spike recovery	151
Tc (⁹⁹ Tc)	Seaweed, solidified cement	TEVA®	None	ICP-MS	0.0024	NIST SRM 4359 (seaweed)	363

^a MBT, DBT, TBT (as the chlorides).

A solution-cathode glow discharge AES method²⁵⁶ for determination of Hg incorporated on-line SPE using L-cysteine-modified mesoporous silica for analyte preconcentration. A Hg concentration of $0.24 \pm 0.04 \text{ mg kg}^{-1}$ (certified value $0.28 \pm 0.03 \text{ mg kg}^{-1}$) was obtained for NRCCRM CRM GBW 07310 (stream sediment). The LOD was $0.75 \mu\text{g L}^{-1}$.

3.3.3 Atomic fluorescence spectrometry. A direct on-line HPLC-CV-AFS method²⁵⁷ for the determination of MeHg in water was shown also to be applicable to urine, sediment and biological samples. The method was adapted for each sample matrix to address the different challenges posed. For example, a selective extraction of MeHg into DCM was used for sediments to separate it from the large (typically three orders of magnitude) excess of inorganic Hg present and to avoid contamination of the preconcentration column.

A new cell²⁵⁸ was constructed for the determination of Mg and Mn in water and plants by continuum source tungsten coil AFS. It contained a tungsten coil atomiser and three quartz windows arranged in a T-shape to allow entry of light from a 300 W Xe arc lamp and collection of the fluorescence radiation by a CCD. Following optimisation of the optical alignment, cell purge gas flow rate ($1.0 \text{ L min}^{-1} \text{ Ar/H}_2$) and atomisation current (4.5 A) the LODs were 0.06 mg L^{-1} for Mg and 0.1 mg L^{-1} for Mn. Results for Mg in NIST SRMs 1547 (peach leaves) and 1643e (trace elements in water) were similar to the certified values at 95% CI and Mn recoveries from a series of spiking experiments were 90–105%.

3.3.4 Inductively coupled plasma mass spectrometry. New methods for specific analytes included a procedure²⁵⁹ for estimation of Hf by SF-ICP-MS. Acid digestion (even with HF) was unable to fully recover Hf and Zr from a suite of 60 rock, soil and sediment RMs. However, the recoveries for the two elements were always similar. Therefore, given a known Zr content and the measured Zr/Hf ratio, the Hf concentration could be calculated. An ICP-TOF-MS method²⁶⁰ for determination of Pt in algae and water allowed the impact of hospital waste to be

estimated. Simultaneous measurement²⁶¹ of ²³⁷Np, ²³⁹Pu and ²⁴⁹Pu was achieved by using ²⁴²Pu as a yield tracer for both elements. Results obtained for NIST SRM 4357 (ocean sediment powder) were consistent with those reported in the literature. A novel approach²⁶² for measuring Cr species in soil involved SSID and mass balance. An IC-ICP-MS instrument was used to determine Cr^{III} and Cr^{IV} in soil extracts and ICP-MS to measure Cr in acid digests of extract residues. Species interconversion during sample processing was tracked by using SSID. The sum of detected species, corrected for interconversion, agreed well with certified total Cr concentrations in NIST SRMs 2709a (San Joaquin soil) and 2711a (Montana soil).

Careful optimisation of reaction cell conditions in ICP-MS/MS successfully removed doubly charged interferences from Gd, Nd and Sm in the determination of As and Se in plants.²⁶³ Introduction of $3.5 \text{ mL min}^{-1} \text{ O}_2\text{-H}_2$ to convert ⁷⁵As⁺ to ⁹¹AsO⁺ and ⁷⁸Se⁺ to ⁹⁴SeO⁺ gave excellent results for NIST SRMs 1515 (apple leaves) and 1547 (peach leaves) without the need for mathematical correction based on simultaneous monitoring of the abundances of REEs in the sample. A proposed alternative method²⁶⁴ for quantification of As and Se used CH₃F-He reaction gas and measurement of AsCH₂⁺ and SeCH₂⁺. Results obtained for a suite of plant, marine biota and sediment CRMs were in agreement with certified values at 95% CI.

Transition-metal-ion assisted PVG²⁶⁵ was coupled with MC-ICP-MS and optimised for the determination of Pb using sediment and water CRMs. A 22-fold enhancement in sensitivity was obtained with PVG relative to direct solution nebulisation, yielding a LOD of $0.005 \mu\text{g kg}^{-1}$. Two research groups optimised MC-ICP-MS methods for Cd. A group in Sweden⁷⁵ developed a method applicable to a wide range of sample types – soil, sediment, plant and animal tissues – that was used to study Cd isotope variability in birch leaves during the growing season. A group in China²⁶⁶ studied four species of plant – two grown in soil and two hydroponically. Both methods achieved overall reproducibility better than 0.1‰ for $\delta^{114}\text{Cd}/^{110}\text{Cd}$ measurement.



In a valuable study to establish *lead isotope ratios* in biological CRMs,²⁶⁷ indicative values were reported for NIST SRMs 1515 (apple leaves), 1566b (oyster tissue), 1570a (spinach), 1573a (tomato leaves), 1575a (pine needles); IRMM CRMs BCR 100 (beech leaves), BCR 101 (spruce needles), BCR 670 (aquatic plant); and IAEA CRM 359 (cabbage). Data were obtained by three ICP-based techniques – conventional quadrupole ICP-MS, SF-ICP-MS, and MC-ICP-MS. The precision of the quadrupole instrument was poorest but all three instruments obtained similar $^{208}\text{Pb}/^{206}\text{Pb}$ and $^{206}\text{Pb}/^{207}\text{Pb}$ values for the same sample. Uncertainties arising from use of different methods of mass fractionation correction in Pb isotope ratio measurement by MC-ICP-MS and TIMS were evaluated⁷⁶ based on data acquired for rock, soil and metal samples in a single laboratory over an 18 year period. It was found that precision of measurement had improved by an order of magnitude. An optimised ICP-MS method²⁶⁸ was used to discriminate successfully cigarettes according to their geographic origin. Data for $^{208}\text{Pb}/^{206}\text{Pb}$ and $^{207}\text{Pb}/^{206}\text{Pb}$ in INCT CRM CTA-VTL-1 (Virginia tobacco leaves) were reported for the first time.

Two new ICP-MS methods for determination of $^{135}\text{Cs}/^{137}\text{Cs}$ isotope ratios were applied to the analysis of soils and plants. Both involved selective adsorption by ammonium molybdophosphate followed by ion-exchange chromatography to remove interfering elements such as Ba. The LODs achievable using SF-ICP-MS²⁶⁹ were markedly superior (e.g. 0.16 vs. 40 Bq kg⁻¹ for ^{137}Cs) to those achievable using ICP-MS/MS.²⁷⁰

Two reviews addressed the use of LA-ICP-MS for analysis of biological samples and provide a comprehensive overview and introduction to the field. Becker *et al.*²⁷¹ (127 references) focussed particularly on bioimaging, combining comments on analytical aspects with discussion of numerous applications in both clinical and environmental science. Pozebon *et al.*²⁷² (219 references) placed more emphasis on analyte quantification and IDA, though also covered some bioimaging applications. The development²⁷³ of a LA-ICP-MS method for quantification and mapping of Fe in soybean leaves revealed that differences in analyte distribution were present between transgenic and non-transgenic plants.

A novel DGT probe²⁷⁴ for studying the remobilisation of sulfide and trace metals in anoxic sediments comprised two polyacrylamide gel layers overlain with a 0.45 μm pore size filter membrane. The first gel layer contained AgI to trap sulfide for determination by densitometry and the second a chelating resin to trap metals for LA-ICP-MS. Depth resolution of 100 μm was achieved. A consideration of the uncertainty budget²⁷⁵ associated with LA-ICP-MS imaging of DGT samplers concluded that the relatively low signal stability arising from the LA process was the major contributing factor.

Although the combination of chromatographic separation with ICP-MS is becoming relatively routine, new methods continue to be published. An IC-ICP-MS method²⁷⁶ used an IonPac® AS7 anion-exchange column and HNO₃ gradient elution in the speciation analysis of orthophosphate and *myo*-inositol hexakisphosphate, a stable phosphate monoester formed by degradation of plant litter, in soil solution and plant extracts. An HPLC-ICP-MS procedure²⁷⁷ employed a Purospher® RP-8e

column and a mobile phase containing 0.02 M CH₃COONH₄ + 0.2% (v/v) 2-mercaptoethanol + 1% (v/v) CH₃OH for the determination of MeHg, Hg^{II} and EtHg in leafy vegetables. An ID-GC-ICP-MS procedure²⁷⁸ for Hg speciation in peat soils was used to demonstrate that N₂-assisted distillation could be used successfully to isolate MeHg from relatively unpolluted soils in which this species represented at least 1% of the total Hg present. A review¹⁶³ (103 references) of hyphenated HPLC-ICP-MS methods for the speciation analysis of As, Cr, Sb and Tl in water and sediment samples placed emphasis on the need to preserve species integrity during sample preparation.

As in many other fields, there is interest in the use of ICP-MS to determine NPs in soil and plants. Koopmans *et al.*²⁷⁹ developed a asymmetric flow FFF method with on-line UV-vis spectroscopy and off-line HR-ICP-MS to characterise silver NPs in soil water extracts that could be useful in future studies of soil-NP interactions. Another group²⁸⁰ used macerozyme R-10 enzyme digestion and SP-ICP-MS to study the uptake of gold NPs by tomato plants. Particle size, particle concentration and dissolved Au concentration could all be measured accurately. Tomato plants grown hydroponically could take up 40 nm gold NPs intact and translocate them from roots to shoots.

3.3.5 Laser induced breakdown spectroscopy. A detailed technical review²⁸¹ with 111 references highlighted good practice in LIBS analysis. Advice was included on identification and classification of samples, and on concentration measurement.

A study²⁸² of the influence of sample particle size distribution on the analysis of plants and related materials by LIBS found that emission intensities increased as particle size decreased in pressed pellets of boldo (*Peumus boldus* Molina) leaves. However, the magnitude of the increase depended on laser fluence. Workers in New Zealand²⁸³ used LIBS to measure major and minor elements in pressed pellets of 100 pasture samples. Results correlated well with those obtained by ICP-AES following microwave digestion for B, Ca, Na, Fe, K, Mg, Mn and P ($R^2 > 0.8$), less well for Zn ($R^2 = 0.64$) and poorly for S ($R^2 < 0.4$) and Cu ($R^2 < 0.1$). The provenance²⁸⁴ of the herbal medicine *Blumea balsamifera* from different regions of China was determined successfully by application of PLS-DA models to either complete LIBS spectra or selected spectral lines.

Applications of LIBS in soil analysis included²⁸⁵ the use of a series of ANNs in the determination of Pb. Improved prediction was obtained when different ANN models were optimised for Pb concentrations either above or below a 1% (m/m) threshold and when the type of soil matrix (which could also be estimated by ANN modelling) was taken into account. As LIBS could be used to measure Cu, Mo, Pb concentrations in soils down to typical crustal abundances, the technique was considered²⁸⁶ to have potential application for detecting geochemically anomalous concentrations indicative of underlying ore bodies. The technique has been applied²⁸⁷ for the first time to the determination of the degree of humification of bulk soil organic matter, knowledge of which provides an estimate of the capacity of soil to sequester carbon from the atmosphere under different soil management regimes and thereby make an important contribution to climate change mitigation.



3.3.6 X-ray spectrometry. *Advances in pXRF* were reviewed²⁸⁸ (140 references) in a volume of Elsevier's 'Advances in Agronomy' series. An overview of the development, theory and uses of the technique was presented, along with information on its strengths and limitations.

Brand and Brand²⁸⁹ carried out a very revealing *inter- and intra-instrument comparison of pXRF instrumentation* using six Olympus Innov-X Delta Premium and three Thermo-Niton XL3t GOLD+ systems. Each individual instrument performed differently – a conclusion also reached by Hall *et al.*²⁹⁰ in their study of 41 rock, soil, sediment and ore CRMs – but the performance of all deteriorated over a relatively short period (two-three months). Frequent recalibration by the manufacturer was recommended, which is costly and inconvenient.

Application of pXRF to soil and sediment analysis included a study by Shand and Wendler²⁹¹ on the suitability of the method for analysis of organic-rich soils. They analysed a suite of CRMs and 183 Scottish topsoils with variable organic matter content and demonstrated the need for matrix-specific calibration models. Arne *et al.*²⁹² showed that even with little or no sample preparation or instrument calibration it was possible to obtain results for the pathfinder elements As, Cu and Pb that were fit-for-purpose in gold exploration. In the on-site analysis of samples of dredged waterway sediment, Lemiere *et al.*²⁹³ showed that partial removal of water using a simple hand press significantly improved correlations with results of laboratory-based analysis.

Investigations into the *use of pXRF in archaeological studies* have highlighted the need to transfer good practice from analytical geochemistry²⁹⁴ and the requirement for more appropriate calibration models for archaeological sediments and ceramics.²⁹⁵

There is growing interest in *use of pXRF data for proximal sensing* either alone or combined with other techniques. Field spectroscopic methods and chemometrics²⁹⁶ were used to predict soil quality characteristics normally measured in the laboratory, offering a huge saving in time and labour. Portable XRF equipment was used to estimate soil pH,²⁹⁷ soil organic matter content,²⁹⁸ cation exchange capacity²⁹⁹ and soil salinity.³⁰⁰ Together, VIS-NIR DRS and pXRF data could be used to predict total C and total N content³⁰¹ and to quantify total petroleum hydrocarbon contamination³⁰² in soils. Soil salinity could be mapped using pXRF and VIS-NIR DRS data and Landsat imagery.³⁰³ The scope and enormous potential benefits of integrating field spectroscopy and spatial analysis for assessing soil contamination were summarised by Horta *et al.*³⁰⁴ (240 references).

A μ XRF system for the *analysis of plants*³⁰⁵ was used to measure uptake of Co *in vivo* from the leaves of the aquatic plant common duckweed (*Lemna minor*) floating in dilute CoCl₂ solution. Both benchtop and handheld EDXRF systems³⁰⁶ used for the determination of Ca, Fe, K, Mn, P, S and Si in pressed pellets of sugarcane leaves had similar performance in terms of correlation coefficients for calibration graphs and LODs.

There is continuing research into the best method for *preparing biological tissue for PIXE analysis*. Significant differences were revealed in a comparison³⁰⁷ between element

distributions obtained by μ PIXE analysis of freeze-dried and frozen-hydrated plant and animal samples. Morphological changes such as cell shrinkage were induced by water removal but artefacts could be introduced during cryo-fracturing and mounting of shock-frozen samples.

A *TXRF method*³⁰⁸ involving room temperature trapping of bismuthine and stibine onto quartz substrates coated with palladium NPs gave LODs of 0.20 $\mu\text{g L}^{-1}$ for Bi and 0.50 $\mu\text{g L}^{-1}$ for Sb. Although developed primarily for the analysis of food-stuffs such as milk, the procedure was applied to NIST SRMs 2711 (Montana soil) and 2702 (marine sediment) proving its applicability to these matrices.

3.4 Analytical quality assurance

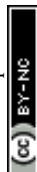
An international proficiency test³⁰⁹ to evaluate *mercury determination in environmental samples* included soil and sediment, together with fish and human hair. Of the 29 participant laboratories, 74% performed satisfactorily for measurement of total Hg concentration ($|z \text{ score}| \leq 2$) but 18% required action ($|z \text{ score}| > 3$). The inter-comparison sought also to include measurement of available Hg in soil and organoHg in soil, sediment and fish, but too few results were returned to permit conclusions to be drawn. Mercury was measured³¹⁰ by TD-AAS in 116 different environmental RMs from ten international suppliers. Each material was analysed at least in triplicate and comparison between different bottles was performed for half of the RMs. Significant mercury heterogeneity was found for some RMs and a list provided of those the authors recommended should be used – and those that should be avoided.

4 Analysis of geological materials

4.1 Reference materials and data quality

New geological reference materials included three samples of Ni ore (0.1–1.0% m/m) and two Ni concentrates (6.0–9.0% m/m) prepared by the Chinese Institute of Geophysical and Geochemical Exploration.³⁶⁴ Certified values for 23 components in the Ni ores and 20 in the concentrate were established following analysis in 19 laboratories. Nickel was mainly determined by volumetric and gravimetric methods, SiO₂ and H₂O⁺ by gravimetry and trace elements by AFS, FAAS, ICP-AES and ICP-MS. Because of the high S content of these materials, storage in sealed containers at low temperatures was recommended. Five Chinese clay CRMs,³⁶⁵ originally certified for only major elements in the late 1980s, were reanalysed for 10 major and 29 minor and trace elements by INAA and EDXRF and WDXRF spectrometries, for which there was good agreement. These methods had better precision and lower LODs than those used for the original certification so these new data should make these clay CRMs much more useful.

The lack of *reference materials for microanalysis* continues to be a major concern. A large Ti-rich natural quartz crystal³⁶⁶ from Shandong province China was characterised for use as a RM in titanium-in-quartz thermobarometry. Pieces of the crystal were analysed by seven different laboratories worldwide using EPMA, LA-ICP-MS and solution ICP-MS to give well-characterised



working values for Al, Fe, Ge, Li, Mn and Ti. Approximate concentrations of B, Be, Cu, Na, Pb, Sn and Zr were also determined but those for Ag, Au, Ba, Ca, K, Mo, Sb and Sr were below the LODs of all three techniques. The RM, with a mean Ti concentration of $57 \pm 4 \mu\text{g g}^{-1}$, was considered to be perfectly suitable for the intended purpose. However, because some of the trace elements, particularly Al and Mn, were not homogeneously distributed, practical use of this quartz as a RM required at least 10 points to be measured along a transect through the entire middle growth zone.

A recent IUPAC Technical Report³⁶⁷ provided a comprehensive overview of *international RMs for isotope ratio analysis*, including materials for which the supply was exhausted or superseded by newer materials. The number of primary isotopic RMs for anchoring stable isotope delta scales now exceeds 30, covering more than 25 elements. There are also over 150 secondary isotopic RMs with a specified delta value, although half of these were produced for isotope measurements of one of seven elements: B, C, H, Li, N, O and S. Tables of relevant RMs for every element for which a zero-scale material has been produced or proposed, listed delta values with uncertainties as given in the original reference. The current recommended delta value was highlighted where there was more than one entry for a particular RM.

New high resolution SIMS U–Pb determinations have confirmed the age homogeneity of *zircon RM* Temora 2 and its value as a geochronological RM.³⁶⁸ The geological processes that lead to the formation of isotopically homogeneous Temora zircons within the host rock, the Middledale Gabbroic Diorite in New South Wales, Australia, were elucidated from a combination of petrographic observations, EPMA major element data and LA-ICP-MS trace element data. It was concluded that sources of future zircons appropriate for use as RMs may lie in igneous suites where Zr saturation is not achieved until late in the crystallisation history. Eocene gem zircons³⁶⁹ from Glen Innes, Australia were assessed for isotopic and chemical homogeneity by ID-TIMS, LA-ICP-MS, SIMS and WDXRF spectrometry. Twelve U–Pb determinations by ID-TIMS of separate 200–400 μm chips measured in two laboratories showed that one of the zircons (Aus22) had remarkable isotopic homogeneity at the sub-per mil level, with a ^{206}Pb – ^{238}U age of $38.8963 \pm 0.0044 \text{ Ma}$ (2σ). This zircon was also very homogeneous for the REEs and other trace elements at the analytical volumes sampled by these techniques and thus suitable as a RM for U–Pb isotope and trace element microanalysis.

In the $^{40}\text{Ar}/^{39}\text{Ar}$ dating technique, neutron fluence monitors (standards) are required for age calculations. For Precambrian samples there are few standards with sufficient grain-to-grain reproducibility and an appropriate age for acceptable argon isotope ratio measurements. Jourdan *et al.*³⁷⁰ presented data for a new muscovite standard WA1ms with an age of $2614.2 \pm 1.5 \text{ Ma}$, an age closer to those of Proterozoic and Archaean samples than those of previously used standards. As muscovite does not contain Ca, it was possible to analyse the samples soon after irradiation because there was no need to wait for ^{37}Ar to decay. In addition, corrections for Ca-related interferences were not required. Its high K content ($\sim 10\%$) resulted in a large Ar signal

even for the minute amounts analysed and so provided better precision for individual measurements.

In an inter-laboratory comparison³⁷¹ organised by the IAEA, six laboratories were asked to quantify 69 impurities in *two uranium ore concentrates*. The main technique employed was ICP-MS with matrix-matched external calibration. As well as establishing consensus values for the two materials, the exercise also served to identify the current state of practice for analysis of this type of matrix. Lessons learnt included issues related to sample dissolution, blank correction and calibration, previously unaccounted polyatomic interferences, and the challenge of estimating measurement uncertainties. Most laboratories significantly underestimated their uncertainties. These ore concentrates will go some way to making more uranium RMs available for identification of the origins of uranium ore concentrates, currently a hot topic in nuclear forensics. In a novel approach to tracing the origin of unknown uranium ore concentrates, Lin *et al.*³⁷² established a database of published REE data of uranium ores from different countries and then transformed the data by a two-step pretreatment to show stronger geographical and geological indications. Of the different multidimensional statistical pattern recognition techniques tested, orthogonal partial least squares discriminant analysis was shown to be the most effective in revealing the fractionations of the HREEs and LREEs. This made it possible to delineate uranium deposits by country and then by deposit type within a country. An unknown uranium ore concentrate could then be attributed to one of ten different countries using a decision tree based on the REE data of uranium ores.

4.2 Solid sample introduction

4.2.1 Laser ablation inductively coupled plasma mass spectrometry. Despite the indisputable progress in laser technology over the last decade, LA-ICP-MS (and other microbeam techniques) still suffers from the limited availability of *suitable calibration standards*. A review³⁷³ (112 references) of common strategies for the calibration of LA-ICP-MS strongly recommended the use of matrix-matched standards and considered various methods that have been employed to prepare such RMs using powdered RMs, synthetic standards or spiked materials. Where matrix-matched standards were not available for whatever reason, solution-based calibration or the use of standard reference glasses were adopted. The utility and limitations of all these approaches were very dependent on the matrix and experimental conditions, as illustrated by examples of their application. One area of topical interest is the development of RMs for the determination of PGEs in sulfide minerals by LA-ICP-MS. Ke *et al.*³⁷⁴ developed a series of synthetic sulfide calibration standards by spiking a mixture of nanoparticulate grains of CuS, FeS₂, NiS and ZnS with a standard solution containing Pd, Pt, Rh and Ru, remilling and fusing the powder in a homemade high temperature furnace designed specifically for this purpose. Argon gas was introduced into the furnace to avoid oxidation of the sulfide mixture during fusion. The differences in results for PGEs in these materials by solution ICP-MS and LA-ICP-MS were generally $<11\%$. Homogeneity,



assessed by the signal intensity of LA-ICP-MS line scans, was <10% RSD. Unfortunately, the lack of a recognised sulfide standard made it difficult to verify independently the accuracy of these standards.

Quantification using non-matrix-matched calibration standards is limited by the occurrence of *elemental fractionation*, which represents the sum of all non-stoichiometric effects occurring during the ablation process, transport and ionisation. In order to separate the relative contributions of processes in the laser plume and ICP, Luo *et al.*³⁷⁵ studied the fractionation behaviour of 63 elements using a modified single volume LA cell. The cell modifications enabled the distance between the gas outlet, a needle with a nozzle tip (id 0.6 mm), and the ablation site to be varied between 1 and 10 mm. This distance was found to be positively correlated with the size of the LA-produced aerosol particles. A high carrier gas flow rate at the ablation site facilitated the production of small aerosol agglomerates or particles. Larger aerosol particles produced in zones of the cell with low helium flow rates were not completely vaporised in the ICP, particularly under conditions of high mass loading. To reduce the ICP-induced fractionation, hot plasma conditions and high carrier gas velocity at the ablation site were required. These results also demonstrated that the position of the sample within a standard LA cell affected the size of the resulting laser aerosol particles.

The use of *fs laser radiation* is one of the most promising approaches for minimising elemental fractionation and matrix effects. Jochum *et al.*³⁷⁶ used a new 200 nm fs LA system with spot sizes of 10–55 μm to analyse RMs with different matrices in an investigation of matrix-related effects. The experiments were also undertaken with 193 nm excimer and 213 nm Nd:YAG laser systems. The short laser pulse duration of the fs LA system resulted in reduced fractionation and matrix effects, especially for volatile, siderophile and chalcophile elements. Any matrix effects were smaller than the analytical uncertainty of the measurements and therefore considered to be negligible. Consequently, 22 RMs with varying matrices could be analysed with a precision of 1–3% and an accuracy of $\pm 10\%$ when a non-matrix-matched calibration based on NIST SRM 610 (trace elements in glass) was used. Although the precision of ns LA-ICP-MS was comparable with that of fs LA-ICP-MS, the overall analytical uncertainty increased to 15–30% for volatile, siderophile and chalcophile elements. Similar conclusions were reached by Li *et al.*³⁷⁷ who ablated silicate reference glasses with either a 193 nm ArF excimer ns laser or a 257 nm fs LA system. The significantly different fractionation behaviours of Co, Cr, Cs, Cu, Fe, K, Li, Mn, Na, Ni, Rb, Si, U and V for NIST SRM 610 and USGS CRM GSE-1G (basalt) observed in 193 nm ns LA-ICP-MS were eliminated using fs LA-ICP-MS at high spatial resolution. The use of fs LA also reduced mass loading effects. Values determined for a range of MPI-DING, NIST and USGS glasses using fs LA-ICP-MS with a laser spot size of 24 μm agreed within $\pm 10\%$ for most elements. The NIST SRM 610 was considered to be unsuitable as an external RM for the analysis of natural silicates using ns LA unless matrix effects were minimised by using Si as an internal standard. The CRM GSE-1G standard was recommended as a better choice.

The influence of ablation cell geometry and laser wavelength on aerosols produced by fs LA was evaluated by d'Abzac *et al.*³⁷⁸ by monitoring $^{56}\text{Fe}/^{54}\text{Fe}$ ratios of particles generated from magnetite, pyrite, haematite and siderite. There was no discernible difference in the ablation mechanisms at the laser wavelengths investigated (198 and 266 nm), indicating that the laser interactions were independent of the sample's optical absorption properties. The HelEx two-volume cell produced smaller particles with a larger range of $^{56}\text{Fe}/^{54}\text{Fe}$ ratios than particles from the Frames single-volume cell, but the composition of the bulk aerosol matched that of the sample, demonstrating stoichiometric fs-LA sampling. The faster washout of the HelEx cell gave a more constant stream of small particles to the ICP, thereby producing a more stable Fe ion signal (0.7% *versus* 1.5% RSE for ^{56}Fe in a 40-cycle single analysis) and consistent instrumental mass bias. The measurement was therefore more precise. Oeser *et al.*³⁷⁹ demonstrated that *in situ* determinations of $\delta^{56}\text{Fe}$ and $\delta^{26}\text{Mg}$ in silicates by fs-LA-MC-ICP-MS could be performed with a measurement reproducibility of better than 0.13‰ (2s) at a spatial resolution of about 50 μm . The fs-LA-MC-ICP-MS determinations (at a wavelength of 194 nm) were largely matrix-independent and agreed, within analytical uncertainties, with data obtained by solution MC-ICP-MS. All the MPI-DING and USGS reference glasses analysed were homogeneous with respect to their Fe and Mg isotopic signatures making them suitable RMs for future *in situ* Fe–Mg isotope studies.

A second-generation custom-built fs LA system³⁸⁰ operating at 196 nm and coupled to MC-ICP-MS was used to assess optimum analytical conditions for the measurement of stable *Si isotope ratios* for a wide range of geological materials. Wet plasma conditions were preferred to provide stable and reproducible ICP conditions. Although precise $\delta^{29}\text{Si}$ and $\delta^{30}\text{Si}$ values of better than $\pm 0.23\%$ (2SD) were obtained if the ablated area was at least $50 \times 50 \mu\text{m}$, the best $\delta^{30}\text{Si}$ precision that could be achieved for single spots of <30 μm diameter was about $\pm 0.6\%$ (2SD). The laser beam was focussed below the sample surface with energy densities of 1–3.8 J cm^{-2} . Using NIST 8546 (pure quartz) as the measurement standard for calibration in a standard-sample-bracketing protocol resulted in accurate and precise data for a range of international RMs. No composition-dependent matrix effects were discernible within the uncertainties of the method.

Recent *hardware developments* included a novel device³⁸¹ for signal smoothing and removal of Hg during the measurement of Pb isotopes by LA-ICP-MS. The device consisted of a stainless steel cylinder with a total volume of 94 cm^3 filled with nine smoothing elements, each comprising seven intersecting corrugated plates 30 mm long. The internal surfaces were coated with a $\sim 10 \mu\text{m}$ thick layer of gold to trap any Hg in the carrier gas. The device did not affect the aerosol transport efficiency significantly and no oscillation of the signal intensity occurred at a laser repetition rate of 1 Hz. Incorporation of this device reduced the Hg background by an order of magnitude and, more importantly, the signal intensity of ^{202}Hg was reduced from 256 to 0.7 mV when ablating the USGS RM MASS-1 (synthetic polymetal sulfide). Feng and Wang³⁸² evaluated four



different designs of mixing devices for on-line ID-LA-ICP-MS for accurate quantification of Pb in NIST SRM 610 (trace elements in glass). The spike solution was introduced either before or after the ablation cell and the mixing efficiencies assessed from the signal sensitivity, plus the accuracy and precision of the $^{207}\text{Pb}/^{208}\text{Pb}$ ratio. The best performance was given by a ball-shaped device with a volume of 35 cm^3 and inserted prior to the ablation cell. The practicalities of on-line double ID for the analysis of solids by LA-ICP-MS was also evaluated by Fernandez *et al.*³⁸³ A liquid aerosol containing an isotopically-enriched spike solution was mixed with the laser-generated aerosol in a Y-piece placed just before the ICP torch, a design rejected by Feng and Wang.³⁸¹ The double ID strategy required the sequential analysis of a certified natural-abundance standard placed alongside the sample in the ablation cell so that the mass fraction of the analyte in the sample could be directly referenced to the certified standard without prior knowledge of the composition of the spike solution. To validate the procedure, Pb, Rb and Sr were determined in silicate glass RMs prepared as fused glass beads and pressed powder pellets. Precisions were 6–21% RSD ($n = 3$) for pressed pellets and 3–21% RSD ($n = 3$) for fused beads. Given that bulk analysis of pellets and beads by LA-ICP-MS (without ID) is a well-known technique, these precisions seem surprisingly poor. As this procedure did not remove the need for matrix-matched standards for accurate data, it is difficult to see the advantages of this approach.

An instrumental development that could have a significant influence on the analysis of solid samples by LA is *distance-of-flight mass spectrometry* (DOF-MS). In this technology, batches of ions are spatially separated across a field-free region according to their m/z -dependent velocities and then directed onto a spatially selective ion detector. Like TOF-MS, DOF-MS is well suited for the analysis of laser-generated aerosols because it offers rapid simultaneous multi-element detection over the whole mass range. Initial results³⁸⁴ from the first coupling of LA to an ICP-DOF-MS instrument equipped with a microchannel plate-based imaging detector provided LODs of $1\text{ }\mu\text{g g}^{-1}$ for steady state LA signals. The system was also capable of performing time-resolved single-pulse LA analysis with a LOD of 200 fg for U. Shot-to-shot reproducibility was 6% RSD and isotope ratios were measured with a precision of 0.3% with a 10 s integration time. It is expected that future developments in high-speed ion-detection arrays will facilitate the growth of DOF-MS for the measurement of transient signals.

Although the majority of U–Pb dating applications are performed by MC-ICP-MS, much useful data can be acquired using *quadrupole instruments*. Columbite-tantalite (Coltan) is an ideal mineral for U–Pb dating of Nb–Ta mineralisation because of its high U and low common Pb contents. To obtain accurate dates from samples of this mineral in pegmatites and granites from China, Che *et al.*³⁸⁵ found that it was necessary to use a coltan standard from Namibia for external standardisation rather than the 91 500 zircon RM as there was a marked difference in ablation characteristics between these two minerals when using a ArF excimer system at 193 nm. This finding raises questions about the use of zircon RMs as external standards in U–Pb age

determinations of baddeleyite (ZrO_2), another mineral that incorporates relatively high amounts of U in its crystal lattice. Wohlgemuth-Ueberwasser *et al.*³⁸⁶ evaluated the use of baddeleyite from the Duluth Gabbro FC-4b as an external standard in the analysis of baddeleyites from South Africa and Finland. This matrix-matched standard made it possible to correct for downhole and laser-induced fractionation and provide dates that were both accurate (within the error of published U–Pb ages obtained by ID-TIMS) and precise (0.3–0.7%, 2σ , on the concordia ages). The lack of zoning, as shown by CL imaging, and the homogeneous age distribution of the FC-4b baddeleyite crystals made it suitable for use as a RM. Another accessory mineral, allanite, can provide reliable chronological information on metamorphic and magmatic events but has rarely been used successfully for dating hydrothermal ore deposits because of high levels of common Pb and the resultant degradation in precision resulting from the corrections required. However, Deng *et al.*³⁸⁷ measured trace elements and U–Th–Pb isotopes by LA-ICP-MS in spot ablations of allanite grains from a Chinese iron skarn deposit. Although the allanite grains exhibited optical and chemical zoning, they had low Th and U contents and did not contain common Pb so were comparable to zircon RMs 91 500 and GJ-1. Consequently, a matrix-matched external standard was not required to obtain a high precision U–Pb age of $136 \pm 1\text{ Ma}$, indistinguishable from a less precise Th–Pb age of $139 \pm 2\text{ Ma}$ and consistent with a U–Pb age of $137.1 \pm 1.5\text{ Ma}$ obtained for a zircon from a nearby ore-related diorite intrusion.

To improve the sensitivity of a MC-ICP-MS instrument for the *measurement of B isotope ratios by LA* of geological materials with low B content, three different combinations of sample and skimmer cones were investigated together with the addition of nitrogen gas to the central channel.³⁸⁸ Compared to the standard arrangement (H skimmer cone and standard sample cone), the use of the new X skimmer cone and Jet sample cone improved the ^{11}B signal intensity by a factor of 3.8. The addition of nitrogen at 4 mL min^{-1} improved the stability of the instrumental mass bias although it had little effect on the B signal intensity. Boron ratios measured in nine different RMs, including reference minerals as well as MPI-DING, NIST and USGS reference glasses, were in good agreement with literature values. Results for DD-1 (an in-house natural tourmaline), GSD-1G and GP-4 (USGS reference glasses) were very consistent, indicating that they would be good candidate RMs for B isotope measurements.

Although TIMS is still regarded as the benchmark method for the *determination of Nd and Sr isotope ratios* because of its inherently high precision, MC-ICP-MS has gained in popularity for these measurements because of its higher sample throughput and, when combined with LA, the ability to perform *in situ* analysis. However, isobaric interferences hamper the precise determination of Nd and Sr isotope ratios by LA-MC-ICP-MS so Yang *et al.*³⁸⁹ assessed 11 apatite RMs commonly used in U–Th–Pb geochronology as potential Nd or Sr isotope RMs. The Nd and Sr isotope ratios they obtained were consistent with values from solution-based methods by MC-ICP-MS or TIMS, indicating the reliability of their analytical and data



reduction protocol. It proved impossible to obtain reliable $^{87}\text{Sr}/^{86}\text{Sr}$ data by LA-MC-ICP-MS for samples with both Er/Sr or Yb/Sr ratios greater than 0.1 and low Sr contents. Eight of the apatites tested were relatively homogeneous in terms of their Sr isotopic compositions while six were relatively uniform in terms of their Sm–Nd isotopic compositions. However, the UWA-1 sample, a fluorapatite from Bancroft Ontario, was suitable for neither Nd nor Sr isotopic analyses and Durango apatite was unsuitable for Sm–Nd determinations despite yielding homogeneous $^{143}\text{Nd}/^{144}\text{Nd}$ data. To minimise the isobaric interference of CaPO^+ on $^{87}\text{Sr}^+$ in the determination of $^{87}\text{Sr}/^{86}\text{Sr}$ in biopapatites by LA-MC-ICP-MS, Lewis *et al.*³⁹⁰ developed a customised plasma interface through which they could introduce helium gas. By adopting this interface and tuning the mass spectrometer for low oxide production, this oxide interference was reduced to such an extent that the accuracy of the $^{87}\text{Sr}/^{86}\text{Sr}$ measurements was within the measured precision of ± 50 ppm (2σ) without any need for further mathematical correction. In a system devised by Huang *et al.*³⁹¹ to measure simultaneously all the relevant isotopes in studies of Rb–Sr and Sm–Nd systematics in natural minerals, a 193 nm excimer LA system was connected to two MC-ICP-MS instruments. The aerosol from the ablation cell was split into two gas streams; one was introduced into a Neptune instrument for Sr determinations and the other into a Neptune Plus instrument for Nd measurements. Varying the proportions of the ablated material received by each instrument did not introduce any bias for the Sr–Nd isotopes measured on apatite and loparite, indicating that no fractionation occurred during aerosol transport. This system was also used to measure Sm–Nd and Lu–Hf isotopes simultaneously from a single sampling site. The data obtained for five natural minerals were identical to the reference values within analytical errors.

In an excellent review of techniques for U–Pb dating of accessory minerals Schaltegger *et al.*³⁹² (164 references) detailed the current status, advantages and limitations of CA-ID-TIMS, LA-ICP-MS and SIMS and the interpretational differences that still need to be resolved. They argued that the choice of technique should be governed by the scientific question posed and demonstrated that comprehensive sample characterisation using a full range of textural and compositional analyses was necessary for the highest quality geochronological data. Inter-laboratory and methodological differences limited the accuracy of LA-ICP-MS data to $\sim 2\%$ (2σ) for $^{206}\text{Pb}/^{238}\text{U}$ and approximately 1% (2σ) for $^{207}\text{Pb}/^{206}\text{Pb}$ but recently recommendations for better practice have been developed (see <http://www.Plasmage.org>). It was recognised that more consistent and better documented practices were required and that any paper submitted for review should contain full information on the parameters affecting data acquisition and manipulation as well as proof of accuracy and laboratory reproducibility. A growth in studies employing detrital zircon geochronology has been stimulated by technical advances in LA-ICP-MS that make it possible to obtain U–Pb ages from individual crystals both rapidly and reliably. The analytical methodology, a range of applications and future directions of this technique were critically assessed in an authoritative review³⁹³ (128 references). It was noted that many

of the applications would benefit from improvements in the precision and accuracy of the measured data. The latter depended on the availability of better RMs used for sample-standard bracketing. One of the most critical areas for future development was software for manipulating, displaying and archiving detrital zircon geochronological data so that researchers fully understood the strengths and weaknesses of the data being generated.

Chemical abrasion, which involves thermal annealing followed by relatively low-temperature partial dissolution in HF, was specifically developed to minimise or eliminate loss of Pb from zircons prior to analysis by TIMS for U–Pb dating and thereby improve precision. Crowley *et al.*³⁹⁴ evaluated the application of CA to LA-ICP-MS by analysing untreated and chemically abraded zircon RMs. The extent to which a zircon was visibly affected by CA seemed to depend primarily on its U concentration and the presence of physical defects, but all U–Pb data from treated zircons showed a substantial improvement in concordance compared with data from untreated samples. Comparison of downhole fractionation of $^{206}\text{Pb}/^{238}\text{U}$ in untreated and abraded portions of the 91 500 zircon RM showed that it was important to expose both RMs and unknown samples to CA in the same way. In a similar study by von Quadt *et al.*,³⁹⁵ the precision of U–Pb age determinations of CA-treated grains was 0.1–0.2% for ID-TIMS analysis but only $\sim 1.5\%$ by LA-ICP-MS. The U–Pb ages determined by the two analytical techniques overlapped within analytical uncertainty. Differences of between 4 and 6% were found between U–Pb ages obtained from untreated and CA-treated zircons. However, both studies cautioned that results from the CA technique may need careful interpretation in some cases, particularly for very young samples (<1 Ma) for which Pb-loss in the radiation-damaged area is unimportant and for very old zircons (Archean) with elevated U concentrations.

A logical development in U–Pb dating of zircon and monazite has been the use of fs LA combined with MC-ICP-MS instruments equipped with high gain amplifiers for increased sensitivity.³⁹⁶ By this technique, it was possible to achieve accurate U–Pb dating with an internal precision comparable to that obtainable by SHRIMP, although the sample volume required for a single spot by LA-MC-ICP-MS was ten times greater. In a study of zircons with high U content from granite-hosted uranium ore deposits in South China,³⁹⁷ SHRIMP analyses were unreliable due to a matrix-effect from the high U concentrations, whereas by LA-ICP-MS matrix effects were insignificant even in rims with U concentrations of up to 26 000 ppm. However, to achieve accurate data it was important to check the cross-calibration between the different modes of ion collection on the quadrupole ICP-MS pulse-analogue detector. Accurate U–Pb dating of very young zircons (<1 Ma) is challenging partly because of the very small amount of radiogenic Pb formed they contain. In a new method³⁹⁸ of Th–U dating such zircons by LA-MC-ICP-MS, the formation of previously unreported complex polyatomic species during ablation of different zircons was minimised by increasing the plasma temperature and thus the residence time of ions in the ICP. Careful instrumental optimisation was a compromise between maximum sensitivity and



minimum U–Th fractionation and was fundamental to precise and accurate *in situ* dating. As might be expected for these old zircons, repeat analyses of $^{230}\text{Th}/^{238}\text{U}$ in the 91 500 zircon RM and an in-house zircon RM over eight months were indistinguishable from secular equilibrium. The calculated ages were in agreement with other quaternary dating methods such as ^{14}C , $^{40}\text{Ar}/^{39}\text{Ar}$ and ^{36}Cl .

Another area where LA-ICP-MS has had a significant impact is in the *imaging of mineral crystals*, of particular value to the mineral exploration industry. However, the analysis of multiple mineral phases presents many difficulties, not least in the choice of internal standard and RMs. Paul *et al.*³⁹⁹ devised a method of extending single grain mapping to multi-phase materials by adapting some of the concepts behind automated mineralogy to LA. The sample was prepared as a standard 30 μm polished petrographic thin-section and elemental images obtained by quadrupole ICP-MS using a 193 nm ArF excimer laser with a spot size of 33 μm , repetition rate of 10 Hz and stage translation rate of 60 $\mu\text{m s}^{-1}$. Successive rasters were spaced 32 μm from their neighbours and it took about 5 h to cover an area of 2.8×5.3 mm. Initial images were created using the CellSpace module within the Iolite software. The use of PCA greatly improved the sensitivity of identifying the mineral phases. Once the individual phases were identified, it was a relatively simple but computationally intensive task to perform IS and RM normalisation. The image was then processed pixel-by-pixel and phase-by-phase to build up maps for each element. A fruitful area of future study could be the integration of SEM elemental maps to provide IS values for subsequent deconvolution of LA maps. Hennekam *et al.*⁴⁰⁰ investigated the accuracy and precision of LA-ICP-MS for line-scan measurements of varved (laminated) sediments for the purpose of accessing high resolution paleoclimatic records within the sediments. Fluid-displacement resin-embedding was used to preserve the laminated structure of these sediments, which are often unconsolidated and difficult to sample. A series of resin-embedded homogenised pellet standards with matrices of calcite, quartz and clay spiked with powdered oxides of Al, Ba, Mo and V were prepared. In addition, two synthetic laminated sediment standards in resin were made, the first with a sequence of laminations with the same matrix (calcite) but different spike concentrations and the second with a sequence of calcite and quartz laminations with similar spike concentrations. Deviations from the reference values were generally <5% and precisions measured as repeated analyses on the same sample <5% RSD. Although the LA-ICP-MS line scanning closely recorded the alternating geochemical profiles of the artificial laminations, the Ca signal showed a clear tailing at the transition from a calcite layer to a quartz layer. Potential artefacts introduced from the use of the non-matrix-matched calibration standard NIST SRM 610 glass were overcome by calibrating the LA-ICP-MS data against calibrations constructed from a parallel series of discrete sample analyses by conventional techniques such as solution ICP-AES, solution ICP-MS and XRF spectrometry.

Kelly *et al.*⁴⁰¹ investigated the effectiveness of *depth profiling using laser ablation* as an alternative to SIMS for measuring changes in mineral chemistry or age as a function of depth. Use

of a single-pulse approach rather than continuous ablation made it possible to reduce the volume of material analysed by LA-ICP-MS to levels required for SIMS analysis. Profiles of U–Pb ages in unpolished, naturally zoned zircon grains from a Neo-archaeon metasediment were obtained by ablation with a 193 nm laser using a 48 μm beam diameter at a repetition rate of 2.5 Hz, the slowest rate capable of being smoothed into a steady signal by the “SQUID” smoothing device employed. Rare earth element profiles were also acquired but with a smaller spot size of 17 μm at a repetition rate of 3 Hz. It was possible to identify isotopically distinct rims <3 μm thick and to demonstrate that REE alteration had penetrated no more than 10 μm into the crystal. Ages provided by LA-ICP-MS analysis fell within the 2s uncertainties of $^{207}\text{Pb}/^{206}\text{Pb}$ ages measured by SIMS on the same zircon population. Although the smaller SIMS spot size was less subject to lateral mixing, the LA-ICP-MS analysis was much more rapid. It was possible to identify rock-fluid alterations of significance in studies on the timing of metamorphic or hydrothermal fluid events in relation to metallic ore deposits.

4.2.2 Laser induced breakdown spectroscopy. The increasing popularity of LIBS for the analysis of geological materials was highlighted in several *recent reviews*. A treatise (215 references) by Senesi⁴⁰² covered basic theory and practice, conventional laboratory and portable configurations, the main methodologies of LIBS measurements together with the advantages and limitations of the technique. The review also provided a comprehensive overview of the application of LIBS to the analysis of minerals and rocks, including the remarkable progress made in the last decade on the use of LIBS on robotic vehicles for extra-terrestrial studies. A shorter review (123 references) by Qiao *et al.*⁴⁰³ concentrated on the qualitative and quantitative aspects of the analysis of geological materials by LIBS. Recent developments were illustrated by examples from the analysis of ores, extra-terrestrial materials, speleothems, marine sediments and fluid inclusions. Currently most studies remain laboratory-based but improved field-portable systems, together with better data processing methods make LIBS a potentially significant tool in geological applications. McMillan *et al.*⁴⁰⁴ discussed three case studies to illustrate different ways in which LIBS can be employed in a geological context: (i) to screen samples in the field for small changes in composition prior to sampling for conventional chemical analysis; (ii) provenancing and correlation studies, such as identifying the origin of gemstones from different deposits; and (iii) geochemical mapping, using a sample of copper ore as an example.

The ability of LIBS to differentiate ores rapidly *in situ* with minimum sample preparation makes it a suitable tool in the *mineral industry* for QC purposes. Applications included combination with PLSR in the determination Al_2O_3 , CaO, MgO and SiO_2 in iron ores⁴⁰⁵ to derive the sample acidity from a ratio involving these four oxides. Different grades of iron ore were classified⁴⁰⁶ using LIBS combined with Random Forest, a new classification algorithm based on multiple classifiers. A method⁴⁰⁷ for the determination of fluorite (CaF_2) in powdered ore samples was based on the measurement of the emission from CaF molecular bands as an alternative to the use of atomic F emission lines. In the determination of Cu in mineral ores,⁴⁰⁸



the samples were first classified by rock type using PCA of their LIBS spectra. This division into individual classes allowed matrix-specific calibrations for each rock type to be used and resulted in improved accuracy and precision. A fast classification of bricks,⁴⁰⁹ based on their LIBS spectra and a combination of PCA and linear discriminant analysis, was demonstrated by analysis of 29 samples from seven different locations.

The utility of LIBS for *geochemical prospecting* was assessed²⁸⁶ through the direct determination of Ag, Cu, Mo and Pb present at concentrations close to their crustal abundance in ores and soils from four different types of mineralisation. Prior to measurement, the powdered samples were pressed into 12 mm diameter pellets under a pressure of 750 MPa. Selection of an appropriate IS compensated for the large matrix effects observed for Mo but no matrix effects were observed for the other elements. Although the LODs for Cu, Mo and Pb (0.6, 0.3 and 8 ppm, respectively) were sufficient to determine these elements at their crustal abundances, that for Ag (0.3 ppm) was insufficient. One drawback to the technique was the relatively narrow linear range of 1–100 ppm for the resonance lines selected. With the increased use of pXRF equipment for mineral prospecting, it will be interesting to see whether LIBS makes a significant impact in this field. Although currently LIBS could probably provide better LODs, a comparison of the figures of merit for LIBS and pXRF on the same samples would be informative.

The LIBS technique has been used to detect *subtle differences in rock compositions*. In a novel method⁴¹⁰ for analysing individual carbonate grains, sand grains were mounted on a slide with acrylic adhesive, stained and viewed with a high magnification camera. Mounting of 125–150 grains on each slide provided >100 carbonate grains, sufficient to identify groups of carbonate populations. Non-carbonate grains were excluded from the dataset using hierarchical cluster analysis and sets of training data constructed using PCA. Final modelling was carried out using a Soft Independent Modelling of Class Analogy method, a supervised classification method of pattern recognition based on PCA. It was acknowledged that sourcing matrix-matched standards for LIBS calibration remained a challenge and that, when applied to individual sand grains, the technique was best suited to pattern recognition and classification. It revealed that carbonate grains from sand dunes in Oman were comprised of several sub-populations and originated from multiple sources. Roux *et al.*⁴¹¹ determined 12 major and minor elements *in situ* to evaluate a homemade portable LIBS system for classification of volcanic rocks into various magmatic series. A LIBS classification model, based on ICP-AES analyses of these rocks, was constructed and used to discriminate rocks in the field with 90–100% success.

The recent explosion of interest in the use of LIBS instruments has been stimulated in part by development of instruments for *planetary exploration missions*. In the year after the Mars Curiosity rover landed in August 2012, the ChemCam instrument generated more than 75 000 LIBS spectra and some data interpretation is now available. Specially designed calibration targets⁴¹² on board the Curiosity rover included homogeneous glass and fine-grained glass-ceramics used to construct

calibrations for each element of interest prior to LIBS measurements of Martian samples. The *in situ* univariate calibrations involved identifying the most stable emission lines and optimising the auto-focussing system and laser energy. Comparisons with APXS data for selected targets showed good agreement for most major elements, although estimates of SiO₂ were not possible using univariate calibration and the K₂O and Na₂O contents were probably underestimated because of the compositions of the on-board calibration targets. Trace element calibration curves for Li, Mn and Sr down to several ppm were used for rapid identification of noteworthy rocks and soils along the traverse.

Work has already started on the *next generation of instruments* for the analysis of solids on planetary bodies. Following the success of the ChemCam instrument, Gasda *et al.*⁴¹³ reported a prototype design based on a combination of remote LIBS and Raman spectroscopy. The Q-switched laser-induced time-resolved spectroscopy used was approximately 70 000 times more efficient at recording signals than a commercially-available LIBS instrument, due to the development of a directly coupled system, the use of an intensified CCD image detector and a pulsed laser that allowed time-resolved measurements. With an improved S/N of at least an order of magnitude, the dual instrument provided enhanced quantitative analysis of the LIBS spectrum with a spatial resolution of 200–300 µm when data were collected 7 m from the target. The Raman instrument was capable of 1 mm spatial resolution at a distance of 3 m from the target and bioorganic fluorescence detection at greater distances. This performance fulfilled all of NASA's expectations for such instruments. Other laboratory prototype instruments designed for space research included a microscope camera system for high resolution optical imagery and a miniature LA ionisation mass spectrometer⁴¹⁴ to improve the sensitivity and spatial resolution of *in situ* chemical analysis of extra-terrestrial materials. These instruments formed part of a miniature analytical suite proposed for ESA's MarcoPolo-R mission to an asteroid. The mass spectrometer had an effective dynamic range of at least eight orders of magnitude and, in addition to major element compositions, trace elements at concentrations below 1 ppm could be measured. Isotope ratio analysis was performed with accuracies at the ‰ level.

The relatively new technique of determining *K–Ar ages in rocks and minerals by LIBS* is based on the simultaneous extraction of Ar and K by LA with detection of K by LIBS, using the light emitted in the ablation plume, and Ar measurement by noble gas MS. The methodology, first proposed in 2008, relied on the fact that the only quantity required to calculate a K–Ar age, the ⁴⁰Ar*/⁴⁰K ratio (where ⁴⁰Ar* is radiogenic argon), was preserved in the ablated aerosol. Solé⁴¹⁵ described a fully developed *in situ* protocol, known as micro-K–Ar, in which each analysis consisted of 1 to 12 laser runs on the same crater and each run was a burst of 30–50 laser pulses. The number of pulses was optimised to obtain an adequate LIBS signal for K and the total volume ablated chosen to obtain sufficient Ar signal. If an uncertainty of ≤5% could be tolerated for a particular application, this method had the advantages of very fast analytical times and analysis of unirradiated samples when



compared with the classical K–Ar and the laser microprobe Ar–Ar dating techniques. In addition, LIBS provided chemical information. Similar methods were proposed for the remote exploration of Mars (e.g. Cho *et al.*,⁴¹⁶ Cohen *et al.*⁴¹⁷) but, unlike the APXS instrumentation used on the Curiosity rover to measure whole-rock K–Ar ages, the LIBS measurements needed to be conducted in a vacuum chamber to allow for simultaneous Ar determinations. In a detailed assessment of figures of merit for K measurements under high vacuum conditions ($<10^{-2}$ Pa), Cho *et al.*⁴¹⁶ used a Nd:YAG laser and a compact Czerny–Turner type spectrometer equipped with a CCD detector to measure 23 geological RMs by LIBS. The LOD was estimated to be 300 ppm and the relative uncertainty (1σ) of the K calibration was 20% for 1 wt% K₂O. They calculated that if the Ar content was measured with a 15% error for 3500 Ma year-old rocks containing 1 and 0.3 wt% K₂O, then the K–Ar ages would be determined with 10% and 20% (1σ) errors, a considerable improvement on current Martian chronology, in which the uncertainty is a factor of 2 to 4. The K–Ar laser experiment⁴¹⁷ (KARLE) at NASA, destined to make *in situ* noble gas geochronology measurements aboard planetary robotic missions, reported a measurement uncertainty of 10% or better for the determination of whole-rock K–Ar ages for rocks older than 2600 Ma. In this experiment the relative K contents determined using LIBS were related to the absolute Ar abundance by sample masses (determined by optical measurement of the ablated volume) and bulk densities (using sample mineralogy). All the analytical components had been flight-proven and did not require further technical development.

A significant development in *underwater LIBS* was a device called ChemiCam⁴¹⁸ capable of performing *in situ* multi-element chemical analysis of liquids and mineral deposits in the ocean at depths of up to 3 km. This system, which consisted of a long-pulse (~ 150 ns) laser, a spectrometer and a high-speed camera, was successfully deployed from a remotely operated vehicle which provided the power supply, instrument control and signal telemetry through a tether. The construction of a compact and reliable long-pulse laser was considered as key for the success of this project. The sensitivity was sufficient to detect Ca, K, Li, Mg and Na simultaneously over a range of concentrations appropriate for seawater analysis. The lowest LOD achieved was $25 \mu\text{mol kg}^{-1}$ for Li. For mineral deposits, reliable detection of elements at >1.0 wt% was possible and methods to determine the relative abundance of Cu, Pb and Zn in hydrothermal deposits were developed.

Calibrations that relate laboratory standards to unknown samples are key to interpreting any type of LIBS data. Boucher *et al.*⁴¹⁹ examined ten *linear and non-linear regression methods* for modelling and interpreting the chemical abundances from LIBS spectra of geological samples. Although model performances differed, all techniques except *k*-nearest neighbour produced statistically-indistinguishable results when the probability function (p) was set at 0.05.

4.3 Sample dissolution, separation and preconcentration

Although there is no shortage of methods for the *extraction and determination of gold*, there is continuing demand for a rapid

and accurate procedure with low LODs particularly for the mining industry. Apart from the difficulty of complete extraction of Au from the host rock, a strategy is required to overcome memory effects in the glass sample introduction systems used in AAS, ICP-AES or ICP-MS. To overcome these problems Wang and Brindle⁴²⁰ treated milled powders with HNO₃–HBr acids in a digestion device known as the ColdBlock™, in which samples were heated by IR radiation. A solution of 1% (*m/v*) L-cysteine and 1% (*v/v*) HCl was effective in stabilising solutions containing Au and eliminating the Au memory effect in ICP-MS. The procedure was validated by analysing six CRMs certified for Au, including one sulfide-rich copper concentrate. Taking 0.5–2.0 g of sample and digestion times of 10–12 minutes, 94–100% recoveries of Au were achieved using a total acid volume of 6–9 mL with a between-run precision of 2–4%.

Dedicated instruments based on thermal decomposition, catalytic conversion, amalgamation and AAS are commonly used to determine the *Hg content of geological materials*. To improve low Hg recoveries from phosphate and apatite rocks, D'Agostino *et al.*⁴²¹ performed an alkaline fusion directly inside the furnace of the instrument. The flux consisted of a mixture of Na₂CO₃, K₂CO₃ and Li₂CO₃, which melted at about 400 °C and decomposed phosphorite matrices at 700 °C by transforming the crystal lattice into a carbonate form. Recovery of Hg from IRMM CRM BCR 32 (Moroccan phosphate rock) was close to 100%, far superior to the 40% recovery achievable when alkaline fusion was not used. Analysis of a range of geological CRMs and RMs demonstrated that Hg recoveries for apatite and phosphate rocks were greatly improved with the alkaline fusion while recoveries for other rock types were unaffected.

Geological materials with high iron contents may require special conditions for their dissolution. Sampaio and Enzweiler⁴²² assessed three procedures for complete dissolution of five iron formation RMs. Two of the methods employed either open-vessel or closed-bomb digestions involving HF and the third sintering with Na₂O₂. Unusually, full digestion of the RMs with the bomb procedure required the addition of a small amount of water to the acids. In general the REE recoveries from the hot plate digestion were slightly higher than those from the bomb digestion but those for the heavy REEs in two of the RMs were up to 30% lower than the published values. The results from sintering tended to be lower than those obtained from the bomb digestion, which was considered to provide the most accurate data. In a study⁴²³ of REEs at ng g^{-1} concentrations in magnetite samples from banded iron formations both cation- and anion-exchange chromatographic procedures were evaluated. Samples were dissolved in HF–HBr acids in a Teflon capsule by heating at 130 °C on a hot plate for 48 h and the digests cleaned up using either AG50W-X12 or AG1-X8 resin prior to HR-ICP-MS analysis. Although the results for both methods were in agreement within experimental limits, the anion method was considered to be more suitable because it was more rapid and consumed smaller volumes of reagents, resulting in lower blanks. Unfortunately, some of the iron formation RMs used in these studies are no longer commercially available, highlighting the paucity of well-characterised iron formation RMs.



Digestion procedures for the measurement of PGE concentrations and Os and Re isotope ratios in geological materials have been reassessed. After intensive tests, Ishikawa *et al.*⁴²⁴ recommended inverse aqua regia attack of 1–2 g of sample in Carius tubes heated to 240 °C for 72 h, CCl₄ solvent extraction of Os and desilicification with HF. Whereas the method resulted in significantly improved recoveries from basaltic RMs, particularly for Ru, mainly due to the use of HF in the desilicification step, for ultramafic and sedimentary RMs the recoveries were largely independent of the use of HF. Sample heterogeneity revealed in CANMET CRM TDB-1 (diabase) was thought to relate to minor minerals – probably sulfides – enriched in Ir, Os, Pt and Ru. In contrast, the ID-ICP-MS analysis of USGS RM BIR-1 (basalt) gave excellent reproducibilities (RSDs, $n = 9$) of 5.1, 1.5, 5.1, 0.7 and 2.0% for Ir, Pd, Pt, Re and Ru, respectively. The NTIMS determination of Os in the same sample had reproducibilities (RSD, $n = 9$) of 6.9% for the Os concentration and 0.6% for the ¹⁸⁷Os/¹⁸⁸Os ratio. Li *et al.*⁴²⁵ improved the extraction of Os and Re from basaltic and andesitic rocks by employing HF desilicification prior to Carius tube digestion. Both these studies indicated that the addition of HF in the analytical scheme can be beneficial when some of the elements of interest are structurally bound or occur as inclusions in the silicate minerals. In a modification of established protocols for the chemical separation of the PGEs and Re from matrix elements in geological materials, necessary to avoid complex interferences on the PGEs, Chu *et al.*⁴²⁶ first separated Ir, Pd, Pt, Re and Ru by anion-exchange chromatography into Re–Ru, Ir–Pt and Pd subgroups, each of which were then further purified. The secondary purification of Pd and Ir–Pt on Eichrom®-LN columns was deemed particularly important to minimise any interferences from ZrO and HfO in the determination of Ir, Pd and Pt by ID-MC-ICP-MS. The procedural blanks were generally comparable to recently published blank data. The accuracy of the procedure was confirmed using a peridotite and several mafic rock RMs. Results for USGS RM BIR-1a (basalt), in particular, confirmed its suitability as a mafic RM for the measurement of Re–Os isotopes and the PGEs.

4.4 Instrumental analysis

4.4.1 Atomic absorption and atomic emission spectrometry. Although analytical techniques based on detection by AAS and ICP-AES are routinely employed in geoanalytical laboratories, there are increasingly few novel developments to report. After assessing a variety of digestion procedures, Evdokimova *et al.*⁴²⁷ opted for one based on sintering with MgO in the presence of NaNO₃ (or K₂S₂O₇) for the determination of Re in copper and molybdenum ores and concentrates by ICP-AES. Rhenium measurements were made at 197.248 nm using Gd as an internal standard. Sodium and potassium were added to the calibration solutions to compensate for non-spectroscopic matrix effects. Recoveries were 100–111% with precisions of 1.1–3.2% RSD ($n = 5$) for four relevant RMs. A simple method for the separation of the REEs, Th and Y from uranium, niobium and tantalum-rich mineral samples prior to their measurement by ICP-AES was reported by Krishnakumar

*et al.*⁴²⁸ After fusion with KHSO₄, the elements of interest were precipitated as their oxalates, thereby separating them from matrix elements like Nb and Ta which remained in solution at pH 2 or less. The presence of KHSO₄ enhanced the precipitation of the HREE oxalates and resulted in virtually complete recoveries and separation from interfering elements. The method precision was 1–3% RSD at typical analyte concentrations. The quest for a fast multi-element analytical method with simplified sample preparation prompted development of an ETV-ICP-AES procedure⁴²⁹ for the determination of trace elements in coal. The procedure had precisions of <10% and LODs in the sub-ppm range and was validated against a range of coal RMs. It was amenable to automation and considered to be a suitable alternative to traditional more labour intensive methods.

4.4.2 Inductively coupled plasma mass spectrometry. Instrumental developments in ICP-MS are covered in our sister update³ on advances in atomic spectrometry and related techniques. The robustness of a Ar–N₂–H₂ mixed-gas plasma⁴³⁰ was assessed through the quadrupole ICP-MS analysis of seawater CRMs and in-house Pd–Pt ore RMs using only a simple external calibration. The addition of 23% (v/v) N₂ to the outer plasma gas and 0.50% (v/v) H₂ to the central channel as a sheath around the nebuliser gas flow resulted in a dramatic reduction (by over an order of magnitude) in oxide levels and background signals from ArO⁺ and Ar⁺, although background signals from NO⁺ and ArN⁺ increased by a similar amount. Levels of doubly-charged ions also increased and LODs were generally 5–15 fold poorer than for an argon plasma for a matrix-free solution. The LODs for some elements were improved in a 0.1 M sodium matrix. Nevertheless, the inherent robustness of the Ar–N₂–H₂ mixed-gas plasma was demonstrated through quantitative multi-element analysis of ore RMs and the determination of Cd and Mo in seawater without matrix-matching or IS. Chen *et al.*⁴³¹ assessed the effect of the addition of ethanol on the performance of a shielded torch in the analysis of geological RMs. Although the shielded torch increased the sensitivity by a factor of 17–58 for 39 elements, it also increased levels of oxide formation. The addition of 4% ethanol enhanced the signal intensities for As, Au, Sb, Se and Te but suppressed intensities for other elements. In addition, the formation of CeO⁺ and Ce²⁺, as well as Kr and Xe background signals, were suppressed. The combination of a shielded torch and introduction of ethanol allowed the direct determination of ng levels of Te with a LOD of ca. 0.5 ng kg^{−1}. Liezers *et al.*⁴³² demonstrated for the first time that quadrupole ICP-MS instruments could be modified to generate ng–μg quantities of a single isotope of an element with extremely high purity (>99.99%). A standard instrument detector was replaced with a modified collector assembly machined from PEEK with a copper foil target attached to the end. This arrangement allowed collection of ¹⁵¹Eu from a Eu standard solution while monitoring the incident ion current. Potential applications of this development could be considerable and included the preparation of highly-enriched isotope spikes using widely available equipment.

The precision and accuracy of isotope ratio data are heavily dependent on various corrections applied to measured ion signals. A review⁷⁶ (70 references) of Pb isotope measurements by MC-



ICP-MS and TIMS explored how measurement precisions had improved by an order of magnitude over the last 20 years. Much of this improvement lay in the techniques used for correcting for mass fractionation. A statistical comparison of the analytical uncertainty of each technique based on data acquired in the analysis of rocks, soils and metals was used to choose the most appropriate correction method. On a related topic, a simple procedure⁴³³ was proposed to assist analysts in selecting the most appropriate model for mass discrimination correction in ID-ICP-MS. Doherty⁴³⁴ investigated the origins of drift and proportional errors in Pb isotope ratio data corrected for mass bias using Tl as the IS. Comparison of results obtained using a model developed in this study with measured drift trends confirmed that multiple correction factors should be applied to isotope measurements obtained by MC-ICP-MS in the order mass bias correction, drift correction and a proportional error correction. In a companion paper, Doherty *et al.*⁴³⁵ demonstrated that neither of the two general methods of isotope ratio drift correction, polynomial interpolation and internal standardisation, was always reliable. They advocated the use of the range-based merit function ω_m to identify the optimal correction factor for isotope measurements by MC-ICP-MS on a run-by-run basis. The ω_m test could be applied to a variety of isotopic systems provided enough reference signals were measured to perform the calculations. The time lag⁴³⁶ between signals from different Faraday detectors was found to be a major source of drift in isotope ratios during acquisitions from transient signals, such as those generated by chromatography coupled to MC-ICP-MS. A strategy was proposed to correct for this observed drift based on synchronisation of the raw isotope signals and the precise calculation of the time lag between different amplifier responses. Application of this drift correction to Pb isotope ratios from transient signals generated by flow injection and GC introduction systems resulted in a 14 to 20-fold improvement in measurement uncertainty.

A summary of newly published methods for the *determination of isotope ratios by MC-ICP-MS* is given in Table 6.

There is much interest in the *determination of B isotopes*, particularly in marine biocarbonates for paleoclimatic reconstructions such as past seawater pH. A comparison⁴³⁷ of ion-exchange chromatography and microsublimation for isolation of B from a range of matrices concluded that the latter offered more efficient matrix removal, lower blanks and better $\delta^{11}\text{B}$ precisions and was also more rapid and economical. An automated sample introduction system⁴³⁸ for B isotope measurements by MC-ICP-MS employing a demountable DIHEN not only increased throughput but also promoted greater stability as a result of the rapid washout. Precisions were sub-0.1‰ for $\delta^{11}\text{B}$ in pure boric acid. Even though the main limitation to achieving this precision for natural samples, including silicate rocks and carbonates, was the chemical separation, the achievable precisions of 0.2–0.4‰ (2SD) were sufficient for most geochemical applications. The B isotope analysis of marine biocarbonates is challenging because of the low B contents present. Misra *et al.*⁴³⁹ summarised $\delta^{11}\text{B}$ methods and their precisions for the analysis of mainly carbonates and waters by MC-ICP-MS or TIMS. They reported a new method based on

microsublimation prior to analysis by HR-ICP-MS in an HF matrix to improve the wash out characteristics. A jet interface increased instrumental sensitivity 5-fold. Precisions of $\leq 0.5\%$ (2 σ) for $\delta^{11}\text{B}$ measurements were achieved with low B mass consumption (<3.0 ng B for quintuplicate analysis). Replicate separations indicated that laboratory contamination of samples was still the biggest challenge in $\delta^{11}\text{B}$ determination procedures, especially for small sample masses. This problem may be minimised in a novel LA approach⁴⁴⁰ involving the simultaneous measurement of B isotopic composition and B/Ca ratio on ng masses of foraminifera and corals. In this technique, an optical fibre connected the torch of the MC-ICP-MS system to an optical spectrometer, so that an aerosol generated by ablating single foraminiferal shells could be analysed by both instruments. Data on the B : Ca ratio was used to correct for different ablation rates. The $\delta^{11}\text{B}$ of foraminifera within a size range of 380 to 520 μm and a mean B concentration of 53 $\mu\text{g g}^{-1}$ were measured with an internal precision of 0.52‰.

Reviews of isotope systems and their geological applications can provide valuable perspectives. Chakrabarti⁴⁴¹ (112 references) compared current analytical capabilities with the observed variation in Si isotope compositions in wide range of natural materials including bulk meteorites and lunar rocks, terrestrial igneous rocks, waters and biota. A review⁴⁴² (84 references) of protocols for the determination of Mg isotope ratios by MC-ICP-MS provided a detailed description of the measurement process and the pitfalls in high precision isotope analysis as well as the behaviour of Mg during geological processes. Tungsten isotope ratios are useful in understanding the first stages in the history of the solar system and planetary formation but their measurement requires the high precision achieved by Breton and Quitté.⁴⁴³ With a long term reproducibility of 80 ppm for $^{183}\text{W}/^{184}\text{W}$, they were able to resolve W-isotope variations in terrestrial and extraterrestrial materials from –0.05 to +0.36‰ per mass unit.

A practical guide⁴⁴⁴ to the design and implementation of the double-spike technique for precise *determinations of Mo isotope composition* may also be applicable to double-spike procedures for other elements. In a related paper, Malinovsky *et al.*⁴⁴⁵ presented a methodology for determining Mo isotope ratios by MC-ICP-MS using calibration with synthetic isotope mixtures.

Although the *double-spike approach* for the correction of instrumental mass bias in mass spectrometry is well established, more consistency in the data reduction of such data is desirable. With this in mind, Creech and Paul⁴⁴⁶ produced IsoSpike, a generalised computer procedure designed to process double-spike mass spectrometry data and constructed as an add-on for the Iolite data reduction package. The integration-by-integration approach was faster and more consistent than commonly employed methods. In addition, data could be visualised and exported. The procedure was applicable to any double-spike system and is freely available (<http://www.isospike.org>).

4.4.3 Other mass spectrometric techniques

4.4.3.1 Thermal ionisation mass spectrometry. The *improvement of detector systems* has been a fruitful area of research in addressing the challenge of producing more precise isotope



Table 6 Methods used in the determination of isotope ratios in geological materials by ICP-MS and TIMS

Element	Matrix	Sample treatment	Technique	Comments	Reference
B	Silicate glass, Ca-rich water, seawater, spinach	(i) Chromatographic separation of 0.1 mL sample digest on AG 50W-X8 cation-exchange resin. Eluted B fraction spiked with HF and loaded onto an Eichrom® strong anion-exchange resin, matrix removed with 0.5 M HF + 2 M HCl and B eluted with 6 M HCl; or (ii) sublimation of 50 µL sample digest in 1.4 M HNO ₃ at 110 °C for 24 h	MC-ICP-MS	Comparison of 2 separation methods: ion chromatography and microsublimation. The latter better in terms of efficiency of matrix removal, lower procedural blank, precision of $\delta^{11}\text{B}$ values, time and consumable costs (exception was spinach where fractionation occurred during sublimation)	437
B	Silicate rocks	Alkali fusion followed by purification on Amberlite™ IRA 743 B-specific resin, B absorbed on resin at pH > 8 and eluted with 0.1 M HNO ₃ or HCl (pH ~1)	MC-ICP-MS	Observed bias in $\delta^{11}\text{B}$ values attributed to selective adsorption of metasilicate species to Amberlite IRA 743 resin under different pH conditions	455
B	Silicate rock, carbonates, waters	Silicate samples digested by K ₂ CO ₃ fusion, cations removed using Dowex™ AG 50W-X8 cation-exchange resin and then B purified on Amberlite™ IRA 743 columns	MC-ICP-MS	An automated direct injection nebuliser employed. Precision of $\delta^{11}\text{B}$ in pure boric acid solutions 0.1‰ but 0.02–0.5‰ for natural samples after chemical separation. $\delta^{11}\text{B}$ of $7.25 \pm 0.47\text{‰}$ (2SD, $n = 8$) in GSJ CRM JB2 (basalt)	438
B	Marine carbonates, waters	Sublimation (micro-distillation) of 50 µL sample digest (<pH 2) at 95 °C for 15–18 h before addition of 0.5 mL of 0.3 M HF	HR-ICP-MS	Precision of $\delta^{11}\text{B}$ measurements $\leq 0.5\text{‰}$ (2σ) with low B mass consumption (<3.0 ng B for quintuplicate analysis). HF-based matrix and platinum injector for improved washout; jet interface improved instrument sensitivity 5-fold	439
B	Marine carbonates	Samples dissolved in dilute HNO ₃ , major cations removed by cation-exchange, then B fraction passed through anion-exchange column	MC-ICP-MS	Analysed solutions contained 50–500 ppb B, equivalent to 2–10 mg coral samples. $\delta^{11}\text{B}$ of $24.3 \pm 0.34\text{‰}$ (2SD) in carbonate RM JCp-1	456
B	Marine carbonates	None	LA-MC-ICP-MS, ICP-AES	Simultaneous measurement of B isotopic composition and B/Ca ratio on ng masses. Light transmitted to ICP-AES instrument via optical fibre from MC-ICP-MS torch. For foraminifers $\delta^{11}\text{B}$ was measured with a precision of 0.52‰ for a mean B content of $53 \pm 7 \mu\text{g g}^{-1}$	440
Cr	Silicate rocks	4-step chromatographic procedure for Cr purification: (i) AEC on AG1-X4 resin using 6 M HCl to remove Fe; Cr converted to Cr ^{III} before (ii) matrix removal on AG50W-X8 resin; (iii) separation from Ti on Eichrom® TODGA resin in conc. HNO ₃ ; (iv) separation from V on TODGA resin in 8 M HCl	MC-ICP-MS	Total blank few ng Cr (insignificant). Nitride and oxide interferences minimised. Precisions better than 2.5 ppm for ⁵³ Cr and 5.8 ppm ⁵⁴ Cr (2SD), which represents a 2-fold improvement on previous studies with higher throughput than TIMS	458
Cs	Marine sediments	Lithium borate fusion, followed by column separation using ammonium molybdophosphate and cation-exchange chromatography on AG 50W-X8 resin, with a final clean up on Eichrom® Sr resin to separate Ba from Cs	SF-ICP-MS	LOD of 0.05 ng kg ⁻¹ achieved for ¹³⁵ Cs and ¹³⁷ Cs in sediments. Main issue is removal of barium to eliminate isobaric interferences arising from ¹³⁵ Ba and ¹³⁷ Ba. ¹³⁵ Cs/ ¹³⁷ Cs can be used in nuclear forensic work	269
Cu	Geological samples	After dissolution in HF-based acid mixtures, AEC on AG1-X8 was used to separate Cu, Fe and Zn. After removing matrix elements, Cu was eluted with 6 M HCl, Fe with 0.5 M HCl and Zn with 3 M HNO ₃ . Column yield 100%	MC-ICP-MS	Ni spike used to correct for mass bias. Precisions were $\pm 0.04\text{‰}$ (2s) for $\delta^{65}\text{Cu}$, $\pm 0.03\text{‰}$ for $\delta^{57}\text{Fe}$ and $\pm 0.06\text{‰}$ for $\delta^{66}\text{Zn}$. Data for 15 geological RMs reported	457



Table 6 (Contd.)

Element	Matrix	Sample treatment	Technique	Comments	Reference
Fe	Geological samples	See Cu, ref. 457	MC-ICP-MS	Ni spike used to correct for mass bias	457
Hf	Silicate rocks	See Sr, ref. 459	MC-ICP-MS	Proposed separation scheme to replace the traditional 3-step separation scheme for Sr-Nd-Hf. Blanks 55–65 pg Hf	459
Mg	Rock RMs	HF-HNO ₃ digestion ending up in 1 mL 2 M HNO ₃ . Separation on AG 50W-X12 cation-exchange resin. Inclusion of HNO ₃ -HF step to improve separation from remove matrix elements such as Al, Fe, Li, Na, Ti	MC-ICP-MS	Method designed for rocks with low Mg content (MgO < 1 wt%). Long-term reproducibility for $\delta^{26}\text{Mg}$ better than $\pm 0.05\text{‰}$ (2σ). Mg isotope data reported for a range of 16 rock RMs	460
Mo	Geological samples	A ^{97}Mo – ^{100}Mo double spike added to digested sample before Mo purification by ion-exchange chromatography on BioRad AG MP-1 M resin, with the Mo fraction collected in 8 M HF + 2 M HCl		Validation of ^{97}Mo – ^{100}Mo double spike protocol. Procedural blanks 3–12 ng. Long-term reproducibility of $<0.05\text{‰}$ (2σ) for $\delta^{98}\text{Mo}/^{95}\text{Mo}$ measurements of standards. Spike:sample molar ratios need to be between 0.4 and 0.8 for accurate results. Accuracy confirmed by measurements of USGS CRMs BCR-2 (basalt) and SDO-1 (shale)	444
Mo	Geological samples	A ^{97}Mo – ^{100}Mo double spike was added to 40–70 mg of sample powder before digestion in HF-HNO ₃ -HCl. Chemical separation of matrix and interfering elements performed on a BPHA resin column before Mo eluted with 6 M HF + 1 M HCl, with <i>ca.</i> 100% recovery	MC-ICP-MS	Procedural blanks 0.14–0.21 ng – relatively low due to comparatively small volumes of resin and acids used. A disadvantage is the relatively large volumes of HF required. Measurement reproducibility of $<0.09\text{‰}$ (2σ) for $\delta^{98}\text{Mo}/^{95}\text{Mo}$. Mean value for USGS CRM BHVO-2 (basalt) similar to values reported elsewhere	461
Nd	Silicate rocks	See Sr, ref. 459	TIMS	Proposed separation scheme to replace the traditional 3-step separation scheme for Sr-Nd-Hf. Blanks 70–80 pg Nd	459
Nd	Geological materials	See Sr, ref. 462	TIMS and MC-ICP-MS	Proposed separation scheme for Sr-Nd-Pb. Analyses normalised to $^{146}\text{Nd}/^{144}\text{Nd}$ using an exponential law. Recoveries > 90% Nd; procedure blank < 50 pg Nd. External precision by MC-ICP-MS (12 to 32 ppm) worse by a factor of 3–5 compared to that of TIMS	462
Nd	Uranium ores and concentrates	After digestion, the lanthanide content of the sample was separated by selective retention on Eichrom® TRU resin and eluted in 4 M HCl. In a second step, Eichrom® Ln resin was used to separate Nd from the rest of the lanthanides. After separation the Nd : Sm ratio was <0.01	MC-ICP-MS	As no certified Nd isotope standard with uranium matrix available, method was validated by measuring $^{143}\text{Nd}/^{144}\text{Nd}$ in USGS CRM BCR-2 (basalt) and GJS CRM JB-2 (basalt). Nd isotopes considered a promising diagnostic for the source of uranium ores	463
Nd	Geological materials	Sample digested with HF-HNO ₃ -HClO ₄ and Nd separated in 3 steps; (i) cation-exchange chromatography on AG 50W-X12 to separate REEs from matrix elements; (ii) Ce in eluate oxidised to Ce ^{IV} and then removed by SPME using mini HEHEHP tandem column; (iii) Sm and Nd separation on HEHEHP column	TIMS	Total procedure blanks 65–90 pg Nd; yield > 92%. Virtually all Ce removed as well as elimination of Na and Sm but corrections still performed for isobaric interferences from Ce and Sm on Nd isobars. Proposed protocol validated by measurements of nine USGS and GSJ RMs	464
Nd	Melt inclusions	See Sr, ref. 447	TIMS	See Sr, ref. 447	447



Table 6 (Contd.)

Element	Matrix	Sample treatment	Technique	Comments	Reference
Os	Geological materials	Carius tube digestion with inverse <i>aqua regia</i> (3 + 1 HNO ₃ /HCl) followed by sparging with argon gas and transfer to the ICP-MS instrument fitted with enhanced-sensitivity ICP interface and 10 ¹² Ω high-gain amplifiers on the Faraday collectors	MC-ICP-MS	Precision of 0.02% (2SD) obtained on 2 ng Os was comparable with those by other methods including NTIMS. Method applicable to most rock samples containing 15–4000 pg Os	465
Pb	Geological materials	See Sr, ref. 462	MC-ICP-MS	Proposed separation scheme for Sr-Nd-Pb. Pb content determined independently to calculate ²⁰³ Tl/ ²⁰⁵ Tl spike required. After Tl-normalisation and an exponential function, data renormalised to recommended values of NIST SRM 981 (common Pb isotopic standard). Recoveries > 90%; procedure blank < 10 pg Pb	462
S	Marine sediments	2–5 g frozen sediment dried under vacuum, free lipids obtained by microwave extraction at 100 °C for 15 min in 9 + 1 (v/v) dichloromethane–MeOH. Organosulfur compounds separated on a silica gel column by sequential elution	GC-MC-ICP-MS	$\delta^{34}\text{S}$ measurements of organosulfur compounds from marine sediments ranged from –43.6‰ to –18.7‰, similar to coexisting pyrite but more ³⁴ S-depleted than total extractable and residual organic S	466
Se	Black shales	Samples digested in HF–HNO ₃ –H ₂ O ₂ at <80 °C to avoid Se loss. Double spike (⁷⁴ Se– ⁷⁸ Se or ⁷⁸ Se– ⁸² Se) added, reduced in 4 M HCl and Se purified on thioglycolic cotton fibre. Solutions doped with high purity Mg before desolvation nebulisation	MC-ICP-MS	Two different Se double spikes trialled in this study. Aluminium cones used to reduce NiO contribution. Mg-doping and desolvation enhanced Se sensitivity 2-fold compared to HG introduction to ICP. Data for Se isotope ratios in two USGS CRM shales (SGR-1 and SCo-1)	467
Sr	Geological materials	After digestion with HF–HNO ₃ , ascorbic acid added to reduce Fe ^{III} to Fe ^{II} . Sample passed through two columns in series. The upper Eichrom® Sr column extracted Sr and Pb while the lower Eichrom® TRU column extracted the LREEs. Sr eluted from Sr column in 0.05 M HNO ₃ and then Pb eluted with 6 M HCl. The LREEs were eluted directly onto Ln Spec resin to obtain Nd fraction by sequential elution with 0.25 M HCl	TIMS	Proposed separation scheme for Sr-Nd-Pb, which has low acid consumption and can be completed in 6 h. TIMS used for Sr measurements as MC-ICP-MS did not offer any advantage. Analyses normalised to ⁸⁶ Sr/ ⁸⁸ Sr using an exponential law. Procedure blank < 100 pg Sr	462
Sr	Silicate rocks	Sample digests from a HF–HNO ₃ –HClO ₄ attack passed through a two-layered mixed-resin column: upper layer contained AG 50W-X12 resin and bottom layer Eichrom® Ln resin. Most matrix elements eluted first followed by Sr, Nd and Hf in turn	TIMS and MC-ICP-MS	Proposed separation scheme to replace the traditional 3-step separation scheme for Sr-Nd-Hf. Blanks 170–200 pg Sr. The method was validated using USGS CRMs BCR-2 (basalt), W-2 (diabase), BHVO-2 (basalt) and GSJ andesite CRMs JA-1 and JA-3	459
Sr	Melt inclusions	Samples digested in HF–HNO ₃ before separation on two columns in series, the upper containing Eichrom® Sr resin and the lower TRU resin. After loading, column separated to retrieve Sr from Sr resin and LREEs eluted from TRU resin onto Ln Spec resin to obtain Nd fraction by sequential elution with HCl	TIMS	Sr isotopes measured using default 10 ¹¹ amplifiers whereas Nd determined using new 10 ¹³ amplifiers. Method validated using USGS CRMs AGV-1 (andesite) and BHVO-2 (basalt) and samples as small as 2 ng Sr and 30 pg Nd successfully analysed. Advantage over LA-ICP-MS is that method not limited by amount of Rb in sample	447



Table 6 (Contd.)

Element	Matrix	Sample treatment	Technique	Comments	Reference
Ti	Basalts	50–100 mg sample digested with HF–HNO ₃ –HClO ₄ . A ⁴⁷ Ti– ⁴⁹ Ti double spike (50% of each isotope) added to an aliquot and Ti separated from matrix using an Eichrom® TODGA column. Ti purified further on AG1-X8 resin, particularly to remove Mo, and collected in 5 mL of 9 M HCl + 0.01 M HF	MC-ICP-MS	Insignificant procedural blank of 10–15 ng. External precision of ca. 0.020‰ (2SD). New data for $\delta^{49}\text{Ti}$ for 5 basalt RMs. All data reported relative to newly created RM prepared from very pure Ti metal rod	468
W	Geological samples	After dissolution in HF–HNO ₃ –HCl, sample digests in 6 M HCl were treated with more HF and W washed from any fluoride precipitates. AEC on AG1-X8 resin to separate W from matrix elements, with W eluted in 4 M HNO ₃ + 0.5 M HF in the final cut. 100% W recovery was achieved with Mo : W ratios < 10 ^{–3}	MC-ICP-MS	Procedure blank 50–100 pg W. Long-term reproducibility for ¹⁸³ W/ ¹⁸⁴ W was 80 ppm (2σ). ¹⁷⁸ Hf/ ¹⁷⁹ Hf ratio used to correct for instrumental mass bias. Protocol demonstrated to be suitable for a range of geological matrices	443
W	Iron meteorites	W in sample digest purified in a two-step AEC procedure. An aliquot of the resulting solution loaded onto a rhenium filament, dried at 100–120 °C and then inserted into the ETV chamber and W evaporated at a filament temperature of >1000 °C in a stream of helium	ETV-MC-ICP-MS	Mass fractionation during evaporation of W from the filament was corrected using the Rayleigh fractionation law. Precision of ¹⁸² W/ ¹⁸³ W and ¹⁸³ W/ ¹⁸⁴ W ratios on 6 ng W was comparable to those from 30–50 ng W by conventional solution nebulisation	469
Zn	Geochemical and cosmochemical rocks	⁶⁷ Zn spike added to sample powders before digestion in mixture of HF–HNO ₃ –HClO ₄ . Two-step chemical separation on aliquot of digest using solvent extraction in diisopropyl ether (to remove Fe) and AEC to separate Zn from matrix elements including Ba. Either ⁶⁶ Zn/ ⁶⁷ Zn or ⁶⁸ Zn/ ⁶⁷ Zn ratio could be used for ID calculation	ID-ICP-MS	High procedural blank due to impurities in the reagents resulted in a Zn LOQ after matrix separation of 3.6 μg g ^{–1} compared to 0.087 μg g ^{–1} with no separation. However, separation gave best accuracy and precision for range of geological RMs	470
Zn	Geological samples	See Cu, ref. 457	MC-ICP-MS	Cu spike used to correct for mass bias	457

ratio measurements on smaller sample masses by TIMS. Mounting prototype 10¹³ Ω resistors in the feedback loop of Faraday cup amplifiers resulted⁴⁴⁷ in a 10-fold improvement of S/N and more precise Nd and Sr isotope data when analysing small ion beams (<20 mV). Sarkar *et al.*⁴⁴⁸ compared the performances of Faraday collector amplifiers fitted with 10¹² Ω resistors and MICs for Pb isotope determinations of pg-size samples. The Faraday array performed better for sample sizes down to 10 pg Pb, producing data 4–5 times more precise than static MICs (0.05%, 2SD, vs. 0.18–0.23% for ²⁰⁷Pb/²⁰⁶Pb). Sample sizes <10 pg were only measured in MIC mode as the ²⁰⁴Pb signal was below the LOD in Faraday mode. Thus, the MIC system offered considerable promise for tracer work in the <10 pg Pb range where data with an accuracy and precision of a few percent are useful, provided blank contributions were kept below 0.1 pg. An overview of advances in TIMS ion detection over the last few years can be found in Wiedenbeck *et al.*⁴⁴⁹

Sources of *NTIMS systematic bias and random error* associated with high precision ¹⁸⁶Os/¹⁸⁸Os measurements were examined in detail.⁴⁵⁰ The largest contribution to random error, total amplifier noise on baseline integrations, was reduced by

increasing the acquisition time for baseline measurements. Although it was important to determine the in-run oxygen isotopic composition to correct for isobaric interferences involving ¹⁷O and ¹⁸O, it was considered sufficient to take oxygen isotope measurements before and after the run and not waste time making line-by-line O isotope measurements within the run. The importance of monitoring and correcting for PtO₂[–] interferences was emphasised as these could mask other potential interferences on ¹⁸⁶Os/¹⁸⁸Os measurements. Within-run measurement of oxygen isotope composition for oxide corrections was however recommended by Chu *et al.*⁴⁵¹ to obtain high precision Nd isotope data by NTIMS. Small ion signals of ¹⁵⁰Nd¹⁷O⁺ and ¹⁵⁰Nd¹⁸O⁺ were measured with amplifiers equipped with 10¹² Ω resistors and the Nd¹⁶O⁺ beams with 10¹¹ Ω amplifiers. The ¹⁴³Nd/¹⁴⁴Nd ratios of several geological RMs determined on 4 ng Nd loads were consistent within analytical error with previously reported values and had an external precision of better than 30 ppm (2RSD).

To improve the accuracy and precision of U–Pb geochronology and facilitate better inter-laboratory comparisons within the U–Pb community generally, two *mixed U–Pb tracers* were



prepared and calibrated.⁴⁵² The U/Pb ratio of the tracer had an uncertainty of <0.05% (95% CL) and was fully traceable to SI units. Thus comparison of data generated in different laboratories using this tracer solution would not require propagation of uncertainty in the U/Pb ratio of the tracer, effectively eliminating a major source of inter-laboratory bias. A companion paper⁴⁵³ outlined the algorithms required for the transformation of the tracer calibration inputs and their associated uncertainties into the parameters required for U–Pb ID-TIMS data reduction.

In an investigation⁴⁵⁴ of the whole-grain evaporation technique for the determination of *Pb isotopes in zircon grains*, hand-picked grains were initially heated to 1450 °C to remove common Pb and then two approaches for the evaporation and condensation of Pb assessed. Grains loaded onto an evaporation filament were heated at 1600–1700 °C for 1–2 h and radiogenic Pb, together with a small amount of silica, condensed either onto an extra wide rhenium filament placed 1–2 mm away (the filament condensation approach) or onto the interior surfaces of a 3 mL Savillex FEP vial (the vial condensation approach). The condensed Pb was subsequently recovered in HF and, following addition of a ²⁰²Pb–²⁰⁵Pb double spike, dried down for loading onto a conventional rhenium filament. Both methods achieved good accuracy and precision because of the ability to add the Pb double spike, and allowed Precambrian rocks containing <200 ppm U to be dated with a precision of ±0.5 Ma or better. Although blank levels were higher and more erratic for the vial condensation method, this procedure was more efficient and easier to apply and possible improvements were suggested.

Other newly published methods for the *determination of isotope ratios by TIMS* are included in Table 6.

4.4.3.2 Secondary ion mass spectrometry. A review⁴⁴⁹ of recent advances in SIMS as applied to geochemical applications noted that state-of-the-art instrumentation can routinely produce data sets for isotopic studies with precisions of better than ±0.2‰ (1s) for major elements on a few 100 pg of material. It was concluded that the quality of available RMs rather than SIMS instrument technology was the limiting factor in defining analytical uncertainty and that any direct comparison between SIMS laboratories would only be meaningful if the same calibrant was used or the chain of traceability was kept very short. In a novel method⁴⁷¹ for synthesising homogeneous RMs, nanocrystals of calcite (20–40 µm) were sintered at 1000 °C and 1 GPa for 24 h to produce coarse-grained crystals (100–500 µm). *In situ* determination of ¹⁸O/¹⁶O ratios by SIMS showed no detectable variation in the synthetic calcite within an analytical uncertainty of 0.1‰ (1SD). Trace elements P and Sr were also homogeneously distributed. Modification⁴⁷² of the optical microscope system in a Cameca IMS 1280 instrument to incorporate a UV light source improved the optical resolution from 3.5 to 1.3 µm, making it easier to view samples at the analytical scale of 1–10 µm. New software for sample imaging also enhanced the accuracy of positioning and efficiency of instrument operation.

The use of SIMS to determine water contents in minerals is gaining in popularity because it has the advantage of being able

to measure *hydrogen isotope ratios* as well. The water content and D/H ratio in apatite and silicate glasses were measured⁴⁷³ by nanoSIMS using three different detector configurations. An LOD of <10 ppm water content was achieved by improving the vacuum in the analysis chamber, using a high primary beam current and applying a blanking technique to reduce the H background. The three configurations had different applications. The peak jump isotope mode was preferred for determining F, S and ³⁵Cl/³⁷Cl but the multicollection isotope mode gave comparable precisions more quickly in the determination of water contents and H isotopes. The multicollection element mode had higher sensitivity than the two isotope modes but could not be used for the measurement of water content because of matrix effects. A procedure⁴⁷⁴ for measuring Cu and H isotopes in turquoise by SIMS was developed as a tool for the provenancing of turquoise and other Cu-bearing gem minerals. Variations in instrumental mass fractionation were correlated with the water and iron content of the samples. The correction models proposed relied on the availability of suitably characterised standards so turquoise samples with a range of compositions were selected as standards and analysed independently by gas source MS (D/H) and MC-ICP-MS (⁶³Cu/⁶⁵Cu). When two or three of these turquoise standards were included in every SIMS analytical session to bracket the unknown samples, accuracies of ±5‰ for D/H and ±0.5‰ for ⁶³Cu/⁶⁵Cu were obtained.

Current capabilities⁴⁷⁵ of SIMS for the *determination of B isotopes* in natural volcanic glasses were assessed using three MPI-DING glasses (GOR128-G, GOR132-G and StHs6/80-G) and RM B6, a natural obsidian glass that was characterised in a B isotope inter-laboratory study in the early 2000s and distributed by the IAEA. The enhanced transmission and stability of the instrumental setup resulted in an improvement in analytical uncertainty by a factor of 2–4 and a reduction in analysis time by a factor of three compared to previous studies. Although the measurement repeatability was 0.5‰ (2RSE) when B concentrations were >20 µg g^{−1}, five analyses of homogenous basaltic glass containing only 1 µg g^{−1} B were required to achieve a precision of better than ±1.5‰ (2RSE). No significant differences in instrumental mass fractionation were observed for the range of glass compositions investigated and drift during a day was <1.8‰. Single analyses with a spatial resolution of 30 µm × 30 µm were completed within 32 minutes. Similar issues were investigated in a SIMS study⁴⁷⁶ of B isotopes in palagonite, a basalt glass that has undergone hydrolytic alteration. Illite IMt-1 from Silver Hill, Montana was a suitable calibration material for this purpose as it had a similar, relatively high, B content and was easy to mount for SIMS analysis. Measurements made before and after treatment of the samples with NH₄Cl to remove exchangeable B provided information on the structure of the palagonite samples.

An overview⁴⁷⁷ of the protocols and pitfalls in the *in situ* measurement of *oxygen isotope ratios* in monazite by SHRIMP identified the sourcing of suitable RMs as a common problem in many applications of SIMS to geological samples. Three monazites, two of which are recognised U–Th–Pb standards, were characterised and analysed independently for O isotopes



by laser fluorination techniques. Two of these, USGS-44069 and Itambé monazite, were proposed as O isotope standards with $\delta^{18}\text{O}$ reference values of $7.67 \pm 0.26\text{‰}$ and $0.46 \pm 0.20\text{‰}$, respectively. The reproducibility of $0.4\text{--}0.6\text{‰}$ (95% CL) obtained at a standard spatial resolution of $20\text{--}25\text{ }\mu\text{m}$ was similar to that obtained for homogeneous glasses by SHRIMP. Additional corrections were required for matrix effects, particularly when the Th content of the sample was significantly different from that of the standards ($2.1\text{--}6.4\text{ wt\% Th}$). To evaluate the influence of surface relief, analyses of zircon crystal rims were compared⁴⁷⁸ with those made close to the centre of the crystal. Within a single grain, the topographical effect was more prominent in the horizontal direction of the stage than in the vertical direction. The poorer precision, attributed to lateral dispersion of the secondary ions caused by the surface topography changing the ion position in the plane of the entrance slit, could be significantly improved by increasing the magnification of the transfer optics.

Ways of improving the precision and spatial resolution of sulfur isotope analysis by nanoSIMS was explored⁴⁷⁹ using three different arrays of Faraday cup (FC) and electron multiplier (EM) detectors. Corrections for the effects of EM aging and quasi-simultaneous arrival of the ion beam at the detector were applied before instrumental mass fractionation corrections from standard-sample bracketing. A lateral resolution of *ca.* $5\text{ }\mu\text{m}$ in samples of pyrite and sphalerite gave an analytical precision of better than 0.3 , 0.3 and 0.7‰ (1SD) for $\delta^{33}\text{S}$, $\delta^{34}\text{S}$ and $\delta^{36}\text{S}$, respectively, when the ^{32}S , ^{33}S and ^{34}S beams were measured with FCs and the ^{36}S beam with the EM. The best lateral resolution of $0.5\text{ }\mu\text{m}$ was obtained when the ^{32}S , ^{33}S and ^{34}S beams were all counted with EMs, in which case the analytical uncertainty was $<1.5\text{‰}$ (1SD) for both $\delta^{33}\text{S}$ and $\delta^{34}\text{S}$. On the other hand, Ushikubo *et al.*⁴⁸⁰ employed a FC detector to measure the ^{36}S beam because the relative efficiency between two FC detectors (compared to that between FC and EM detectors, as used in the previous study) was more stable. The restricted count rate for an EM prevented the use of a strong primary beam current, thus reducing the analytical precision attainable for the other S isotopes. The pyrite standard UWPY-1, whose S isotopes ratios were determined independently by gas source MS, was used as a running standard during SIMS analysis. Typical reproducibilities of spot-to-spot analyses of UWPY-1 with a primary beam diameter of $20\text{ }\mu\text{m}$ were 0.23 , 0.05 and 0.86‰ (2SD) for $\delta^{34}\text{S}$, $\Delta^{33}\text{S}$ and $\Delta^{36}\text{S}$, respectively.

The U–Th–Pb dating of geological materials, especially zircons, continues to be a major activity in SIMS laboratories.⁴⁴⁹ Liu *et al.*⁴⁸¹ proposed a hybrid method of acquiring data in the dating of zircons in which the $^{207}\text{Pb}/^{206}\text{Pb}$ ratio was measured with high precision in the static multi-collector mode without compromising the precision of the $^{238}\text{U}/^{206}\text{Pb}$ ratio measurement made in the peak hopping single collector mode. Four zircon RMs (91 500, M257, Temora and Plešovice) were analysed to demonstrate that this new analytical protocol could simultaneously obtain $^{207}\text{Pb}/^{206}\text{Pb}$ and $^{238}\text{U}/^{206}\text{Pb}$ ages with comparable quality and thus effectively evaluate the concordance of the U–Pb system on zircons as young as 500 Ma .

4.4.3.3 Accelerator mass spectrometry. This technique is mainly used to detect long-lived radionuclides and provides the lowest LODs of all MS methods, reaching atomic abundances as low as 10^{-16} . *Recent advances in accelerator-based methods* and the wide range of geochemical applications employing AMS were covered in the biennial review⁴⁴⁹ (188 references) of geo-analytical techniques published in *Geostandards and Geo-analytical Research*. Not only is ^{129}I the focus of much research as a result of the Fukushima incident but also in environmental and geological applications involving the measurement of naturally produced ^{129}I . Liu *et al.*⁴⁸² separated I by co-precipitation of AgI with AgCl in the measurement of very low levels of ^{129}I in carrier-free AgI–AgCl sputter targets. Copper sample holders were preferred over aluminium ones because the latter reacted with the sputter targets. A conducting matrix of niobium powder was mixed with the AgI–AgCl powder in the proportion of $5 + 1\text{ (m/m)}$ to obtain a stable and high I ion current intensity and to reduce memory effects. A typical current of $5\text{--}100\text{ nA }^{127}\text{I}^{+}$ was obtained using AgI–AgCl targets containing $5\text{--}80\text{ }\mu\text{m I}$. Although the method appears to be promising, data from the analysis of real samples have yet to be presented.

4.4.3.4 Isotope ratio mass spectrometry. The carbon and oxygen isotope compositions of carbonate minerals are typically measured using automated systems to digest and purify the evolved CO_2 prior to measurement by IRMS because of their efficiency in handling small sample sizes. However, a note of caution was sounded⁴⁸³ when three different instruments (Kiel IV, GasBench II and a dual inlet IRMS) were used to analyse loess and lake sediments because large variations occurred in the $\delta^{13}\text{C}$ and $\delta^{18}\text{O}$ values obtained. The observed maximum differences of between -0.4‰ to 0.3‰ for $\delta^{13}\text{C}$ and -0.5‰ to $+0.6\text{‰}$ for $\delta^{18}\text{O}$, relative to the mean values of the three methods, may have been related to the organic matter in the samples. However, vacuum roasting of the samples prior to measurement only increased the variability of the data in some cases. Data from one of the automated methods were generally lower than those from the other two. The use of clumped isotope compositions of carbonate, *i.e.* isotopologues such as $^{13}\text{C}^{18}\text{O}^{16}\text{O}$, to elucidate paleotemperatures is a relatively new field of research and requires the determination of Δ_{47} , defined as the excess abundance of CO_2 of mass 47 relative to the theoretical random distribution. However, comparison of Δ_{47} data generated by different laboratories using IRMS methods remains a problem, as exemplified by a recent inter-laboratory calibration exercise⁴⁸⁴ in which differences of up to 0.07‰ (equivalent to a temperature difference of $15\text{ }^\circ\text{C}$) were reported. The extraction potential of the IRMS ion source was an important factor influencing the accuracy and precision of CO_2 clumped isotope measurements. At an optimum extraction potential of 90% , reproducible and accurate Δ_{47} values for IAEA CRM NBS-19 (TS-limestone) were maintained for over one year.

A recognised method for determining stable sulfur isotopes $^{32}\text{S}/^{34}\text{S}$ alongside $^{13}\text{C}/^{12}\text{C}$ and $^{15}\text{N}/^{14}\text{N}$ is the coupling of an EA to an IRMS instrument. A new purge and trap EA system⁹⁶ generated high quality SO_2 peaks even for samples with low S



concentrations (<1% m/m). The CO₂ and SO₂ generated by the conventional EA were trapped separately and desorbed at 220 and 850 °C, respectively. The N₂ passed straight through the trap assembly. Although the measurement of ³²S/³⁴S ratios in CRMs BCR 32 (Moroccan phosphate) and NIST 120c (Florida phosphate rock) containing 0.4–0.7% S m/m were accurate,⁴⁸⁵ relatively large aliquots (5–8 mg) had to be analysed to ensure satisfactory precision (0.4‰, 1SE). These materials were proposed as potential isotope RMs for future studies of S isotopes in biogenic apatites.

4.4.4 X-ray spectrometry. For a comprehensive review of recent advances in XRF instrumentation and geological applications, the reader is advised to consult the update on XRF spectrometry⁵ (426 references).

Although *portable XRF instrumentation* has been commercially available for well over a decade, it has only had a major impact since the introduction of silicon drift detectors, which are capable of better resolution than previous detectors. The acceptance of pXRF technology has not been assisted by the fact that the accuracy and precision of these instruments has not lived up to manufacturers' claims when applied to geological materials.²⁹⁰ In 2012 Hall *et al.* (<http://www.appliedgeochemists.org>) undertook a detailed examination of the performance of portable XRF technology on behalf of the Canadian Mining Industry Research Organisation. Their report was a salutary assessment of the state-of-the-art, demonstrating inconsistent results between instruments even from the same manufacturer and their inability to handle spectral interferences. They concluded that no instrument of the five tested (three handheld and two portable benchtop instruments) stood out as being superior as their performance depended on the element and matrix.

A resurgence of interest in pXRF was marked by a recent issue of *Geochemistry: Exploration Environment Analysis* (August 2014, vol 14) devoted to this technique. A number of instrumental *comparative studies within geological applications* supplemented the observations of Hall *et al.*²⁹⁰ Brand and Brand²⁸⁹ tested multiple units of the same model of handheld equipment from two manufacturers under standardised conditions in periods of five hours of continuous operation. Data were generally precise (<5% RSD) but very inaccurate and performance varied significantly between individual instruments from the same manufacturer. Instrument performance deteriorated measurably over two to three months and operators were advised to record the battery serial numbers, as replacing the lithium-ion battery pack during a run was seen to have a measurable effect on the precision and accuracy of some data. This deterioration together with inconsistent factory calibrations and variable battery power meant that every pXRF instrument should be considered unique and that raw data from several instruments should not be combined without appropriate post-processing or recalibration. Ross *et al.*⁴⁸⁶ confirmed that pXRF instruments produce precise (<5% RSD) but not particularly accurate data in a test of three Olympus machines for analysing unprepared exploration drill cores using factory calibrations. Empirical correction factors unique to each instrument and each project were required to account for systematic biases. Within 20 cm long cores, the effect of

mineralogical heterogeneity was much greater than the instrument precision.

*Measurements of whole-rock powders*⁴⁸⁷ with a benchtop Olympus Innov-X X5000 pXRF spectrometer were within ±20% of values previously obtained by conventional laboratory-based methods for many major and minor elements except when at concentrations approaching the LOD. The data for Cr, Ni, V, MgO and P₂O₅ were poorer and more variable. A single-point external calibration using a RM with a similar matrix and composition was applied to the raw values. It was concluded that pXRF spectrometry was fit-for-purpose as a preliminary screening tool to discriminate lithogeochemical variations prior to sample selection but was not a substitute for conventional laboratory-based chemical analysis, particularly when important economic decisions were to be made.

Portable XRF instrumentation has been widely adopted by the *mining industry* to collect large amounts of multi-element data rapidly in the field at relatively low cost and is now regarded by some exploration geologists as the modern equivalent of the geological hammer. The capability to make *in situ* measurements of exploration drill cores at high resolution, down to centimetres if necessary, resulted in improved geological logs and maps on which to base decisions. Thus, pXRF data from half-cut diamond drill core surfaces were used to characterise dolerite dykes intruded into an area of gold mineralisation in Western Australia.⁴⁸⁸ Plots of Ti *versus* Zr combined with PCA revealed four distinct geochemical groupings of dolerite dykes. This new geological interpretation resulted in a significant amount of rock previously modelled as dolerite being reclassified as potential host rock for gold exploration. Similarly, Ross *et al.*⁴⁸⁹ distinguished between two visually similar and variably altered rhyolites in a Canadian massive sulfide deposit on the basis of plots of Ti/Zr against Al/Zr obtained by pXRF analysis of core surfaces, thereby confirming that the correct stratigraphic target had been reached.

However, not all operators of pXRF equipment appreciate the principles behind the acquisition of *quality assured data* and the lack of a standardised approach for pXRF data collection often makes it difficult to compare datasets collected by different users at different times, particularly when used on uncrushed rock. Fisher *et al.*⁴⁹⁰ stressed the need for quality assurance and control systems as robust as those employed in conventional assaying. Key considerations when establishing a workflow for the acquisition of pXRF data for exploration and mining applications included the development and documentation of sampling protocols, instrument set-up, QA/QC checks, calibration to standards of known concentration, drift monitoring, collection of blanks and data management. The crucial steps in a rapid pXRF assessment of komatiite-hosted nickel sulfide deposits⁴⁹¹ in Western Australia were the development of a strict calibration process as well as numerous data quality checks. Comparison of pXRF data determined on manually sawn half-cores with those obtained by conventional laboratory XRF spectrometry demonstrated that for typical abundances of Cr, Ni, Ti and Zr in komatiites the quality of the analytical data was good enough to evaluate sulfide segregation and to define the nickel sulfide prospectivity of the komatiitic units.



Several Canadian studies examined the suitability of pXRF spectrometry for *assessment of REE-enriched deposits*. Simandl *et al.*⁴⁹² evaluated the technical merits and limitations of portable XRF technology for mineral exploration of rare metals such as Nb, Ta and REEs by using data acquired over nearly two years from the analysis of three powdered geochemical standards and a silica blank. Under relatively ideal conditions, data with precisions of <4% RSD and accuracies of better than $\pm 17\%$ were obtained for Ce, La, Nd, Pr and Y at concentrations >0.1%. Although it was not possible to detect any of the HREEs, the elements Ce, La and Y were considered to be good pathfinder elements in the search for REE deposits. In particular, Y was suitable because of its lower LOD and similar chemical characteristics to the HREEs. The same model of pXRF instrument was assessed for its suitability for the exploration⁴⁹³ of carbonatite-related deposits for Nb and REEs. From an exploration geologist's point of view, in most cases useful field determinations of Al, Ba, Ce, K, La, P, Sr, Zn, Zr and Y could be made on crushed samples after recalibration to correct for bias. Spot analyses performed directly on 10–15 cm core sections were severely affected by the coarse nature of some carbonatite units. Although taking an average of several spot measurements improved the precision to a level where potentially economically significant zones could be identified, manual scanning of core sections could rapidly distinguish between areas of Nb mineralisation and barren zones and so provide useful information for immediate decision making when drilling exploration cores. Sedimentary phosphate rocks can also be potential sources of F and REEs as well as fertiliser. An orientation survey⁴⁹⁴ of sedimentary phosphate rocks in SE British Columbia concluded that pXRF spectrometry could be used to identify zones enriched in REEs if the determinations were performed on finely ground and homogenised material and biases observed using the factory-set calibrations were corrected by recalibrating the instrument using ICP-MS data. The particular instrument tested operated on four different beams in order to obtain measurements on a wide range of elements (33 were evaluated) and was one of the first capable of determining Nd and Pr without using a radioactive source.

In conclusion, it is evident that the demand for *in situ* geochemical analysis from regional surveys to mapping of individual mineral grains will continue to be a driver for many of the current developments in analytical geochemistry generally, and issues such as appropriate calibration regimes and data processing protocols will still need to be addressed.

5 Glossary of terms

2D	Two-dimensional
A4F	Asymmetrical flow field flow fractionation
AAS	Atomic absorption spectrometry
AEC	Anion exchange chromatography
AES	Atomic emission spectrometry
AFM	Atomic force microscopy
AFS	Atomic fluorescence spectrometry
AGAL	Australian Government Analytical Laboratories

AMS	Accelerator mass spectrometry
ANN	Artificial neural network
APDC	Ammonium pyrrolidine dithiocarbamate
APXS	Alpha particle X-ray spectrometry
ASU	Atomic spectrometry update
AUC	Analytical ultracentrifugation
BCR	Community Bureau of Reference (<i>of the European Community</i>) now IRMM
BPHA	<i>N</i> -Benzoyl- <i>N</i> -phenylhydroxylamine
C ₁₈	Octadecyl bonded silica
CA	Chemical abrasion
CANMET	Canadian Certified Reference Materials Project (of National Resources Canada)
CCD	Charge coupled detector
CCP	Capacitively coupled plasma
CCT	Collision cell technology
CE	Capillary electrophoresis
CI	Confidence interval
CL	Cathode luminescence
CNT	Carbon nanotube
CPE	Cloud point extraction
CRM	Certified reference material
CS	Continuum source
CV	Cold vapour
CVAAS	Cold vapour atomic absorption spectrometry
CVAFS	Cold vapour atomic fluorescence spectrometry
CVG	Chemical vapour generation
DBT	Dibutyl tin
DCM	Dichloromethane
DGT	Diffusion gradient in thin films
DIHEN	Direct injection high efficiency nebuliser
DLLME	Dispersive liquid liquid microextraction
DLS	Dynamic light scattering
DMA	Dimethylarsenic acid
DMDS	Dimethyl disulfide
DMDS _e	Dimethyl diselenide
DMME	Dual magnetic microextraction
DMS	Dimethyl sulfide
DMSe	Dimethyl selenide
DOF	Distance of flight
DOM	Dissolved organic matter
DRC	Dynamic reaction cell
DRS	Diffuse reflectance spectrometry
DTPA	Diethylenetriaminepentaacetic acid
EA	Elemental analyser
ECD	Electrochemical detector
ED	Energy dispersive
EDS	Energy dispersive spectrometry
EDTA	Ethyldiaminetetraacetic acid
EDXRF	Energy dispersive X-ray fluorescence
EGTA	Ethylene glycol tetra-acetic acid
EN	European Committee for Standardisation
EM	Electron multiplier
EPA	Environmental Protection Agency (USA)
EPMA	Electron probe microanalysis
ERM	European reference material
ESA	European Space Agency
ESI-MS	Electrospray ionisation mass spectrometry
ETAAS	Electrothermal atomic absorption spectrometry



EtHg	Ethyl mercury	IUPAC	International Union of Pure and Applied Chemistry
ETV	Electrothermal vaporisation	LA	Laser ablation
FAAS	Flame atomic absorption spectrometry	LC	Liquid chromatography
FC	Faraday cup	LCD	Liquid crystal display
FEP	Fluorinated ethylene propylene	LIBS	Laser induced breakdown spectroscopy
FFF	Field flow fractionation	LLME	Liquid liquid microextraction
FIA	Flow injection analysis	LNEG	National Laboratory of Energy and Geology (Portugal)
FP	Fundamental parameter	LOD	Limit of detection
fs	Femto second	LOQ	Limit of quantification
FT	Fission track	LREE	Light rare earth element
FTIR	Fourier transform infrared	LRM	Laboratory reference material
GBW	CRMs of the National Research Centre for Certified Reference Materials (China)	Ma	Million years
GC	Gas chromatography	MAE	Microwave assisted extraction
GEMOC	The Australian Research Council National Key Centre for Geochemical Evolution and Metallogeny of Continents	MALDI-MS	Matrix assisted laser desorption ionization mass spectrometry
GEOTRACES	An International Study of the Marine Biogeochemical Cycles of Trace Elements and their Isotopes (France)	MAME	Microwave assisted micellar extraction
GOM	Gaseous oxidized mercury	MBT	Monobutyl tin
GSB	CRMs of the Institute for Environmental Reference Materials (of Ministry of Environmental Protection, China)	MC	Multicollector
GSJ	Geological Survey of Japan	ME	Microextraction
HDC	Hydrodynamic chromatography	MeHg	Methyl mercury
HEHEHP	2-Ethylhexyl phosphoric mono-2-ethylhexyl ester	MIBK	Methyl isobutyl ketone
HG	Hydride generation	MIC	Multiple ion counter
Hg _p	Particulate phase mercury	MIP	Microwave induced plasma
HPLC	High performance liquid chromatography	M ₀	Characteristic mass
HPS	High Purity Standards (USA)	MMA	Monomethylarsenic acid
HR	High resolution	MP	Microwave plasma
HREE	Heavy rare earth element	MPI	Max Planck Institute (Germany)
IAEA	International Atomic Energy Agency	MRI	Magnetic resonance imaging
IC	Ion chromatography	MS	Mass spectrometry
ICP	Inductively coupled plasma	MSHA	Mine Safety and Health Administration (USA)
ICP-AES	Inductively coupled plasma atomic emission spectrometry	MWCNT	Multiwalled carbon nanotube
ICP-MS	Inductively coupled plasma mass spectrometry	<i>m/z</i>	Mass to charge ratio
id	Internal diameter	NAA	Neutron activation analysis
ID	Isotope dilution	NASA	National Aeronautics and Space Administration (USA)
IDA	Isotope dilution analysis	NBL	New Brunswick Laboratories (USA)
IEC	Ion exchange chromatography	NBS	National Bureau of Standards (USA) now known as NIST
IERM	Institute for Environmental Reference Materials (of Ministry of Environmental Protection, China)	NCS	CRMs of the China National Analysis Centre for Iron and Steel
IJS	Institut Jozef Stefan (Slovenia)	Nd:YAG	Neodymium doped:yttrium aluminum garnet
IL	Ionic liquid	NEXFAS	Near edge X-ray absorption fine structure
IL-ME	Ionic liquid microextraction	NIES	National Institute for Environmental Studies (Japan)
INAA	Instrumental neutron activation analysis	NIOSH	National Institute of Occupational Safety and Health (USA)
INCT	Institute of Nuclear Chemistry and Technology (Poland)	NIR	Near infrared
IR	Infrared	NIST	National Institute of Standards and Technology (USA)
IRMM	Institute for Reference Materials and Measurements	NP	Nanoparticle
IRMS	Isotope ratio mass spectrometry	NRC	National Resources Canada
IS	Internal standard	NRCC	National Research Council (of Canada)
ISE	Ion selective electrode	NRCCRM	National Research Centre for Certified Reference Materials (China)
ISO	International Organisation for Standardisation	NTIMS	Negative thermal ionisation mass spectrometry
		NWRI	National Water Research Institute (Canada)
		OES	Optical emission spectrometry



PAH	Polyaromatic hydrocarbons	SWAXS	Small and wide angle X-ray scattering
PBET	Physiologically based extraction test	SWCNT	Single wall carbon nanotube
PCA	Principal component analysis	TBT	Tributyl tin
PEEK	Perfluoroalkyl	TD	Thermal desorption
PhHg	Phenyl mercury	TEM	Transmission electron microscopy
PFA	Perfluoroalkyl	TIMS	Thermal ionisation mass spectrometry
PGE	Platinum group element	TMA	Trimethylarsenic acid
PI	Photo ionisation	TOF	Time of flight
PIXE	Particle induced X-ray emission	TRLFS	Time resolved laser fluorescence spectroscopy
PLS	Partial least squares	TS-FF-AAS	Thermospray flame furnace atomic absorption spectrometry
PLS-DA	Partial least squares discriminant analysis	TXRF	Total reflection X-ray fluorescence
PLSR	Partial least squares regression	UADLLME	Ultrasound assisted dispersive liquid liquid microextraction
PM	Particle matter	UAE	Ultrasonic extraction
PM ₁	Particulate matter (with an aerodynamic diameter of up to 1 µm)	UAEME	Ultrasonic extraction microextraction
PM _{2.5}	Particulate matter (with an aerodynamic diameter of up to 2.5 µm)	USGS	United States Geological Survey
PM ₁₀	Particulate matter (with an aerodynamic diameter of up to 10 µm)	USEPA	United States Environmental Protection Agency
PMT	Photomultiplier tube	UV	Ultra violet
ppb	Part per billion	UV-VIS	Ultra violet-visible spectrophotometry
ppm	Part per million	VG	Vapour generation
PTFE	Poly(tetrafluoroethylene)	VIS	Visible
PVG	Photochemical vapour generation	VOC	Volatile organic carbon
pXRF	Portable X-ray fluorescence	WDXRF	Wavelength dispersive X-ray fluorescence
QC	Quality control	XANES	X-ray absorption near edge structure
REE	Rare earth element	XAS	X-ray absorption spectrometry
RM	Reference material	XRD	X-ray diffraction
ROS	Reactive oxygen species	XRF	X-ray fluorescence
RP	Reversed phase		
RSD	Relative standard deviation		
RSE	Relative standard error		
s	Standard deviation of sample		
SARM	South African producers of Metallurgical and Geological Certified Reference Materials		
SAXS	Small angle X-ray scattering		
SD	Standard deviation		
SDS	Sodium dodecyl sulfate		
SE	Standard error		
SEM	Scanning electron microscopy		
SERS	Surface enhanced Raman spectroscopy		
SF	Sector field		
SFOD	Solidification of floating organic drop		
SFODME	Solidification of floating organic drop microextraction		
SHRIMP	Sensitive high resolution ion microprobe		
SI	Le Système International d'Unités (International System of Units)		
SID	Speciated isotope dilution		
SIMS	Secondary ion mass spectrometry		
SMPS	Scanning mobility particle sizer		
S/N	Signal-to-noise ratio		
sp	Single particle		
SPE	Solid phase extraction		
SPME	Solid phase microextraction		
SPS	Spectrapure standards (Norway)		
SRM	Standard reference material		
SS	Solid sampling		
SSID	Species specific isotope dilution		

References

- O. T. Butler, W. R. L. Cairns, J. M. Cook and C. M. Davidson, *J. Anal. At. Spectrom.*, 2015, **30**(1), 21–63.
- A. Taylor, M. P. Day, S. Hill, J. Marshall, M. Patriarca and M. White, *J. Anal. At. Spectrom.*, 2015, **30**(3), 542–579.
- E. H. Evans, J. Pisonero, C. M. M. Smith and R. N. Taylor, *J. Anal. At. Spectrom.*, 2015, **30**(5), 1017–1037.
- C. F. Harrington, R. Clough, S. J. Hill, Y. Madrid and J. F. Tyson, *J. Anal. At. Spectrom.*, 2015, **30**(7), 1427–1468.
- M. West, A. T. Ellis, P. J. Potts, C. Streli, C. Vanhoof and P. Wobrauschek, *J. Anal. At. Spectrom.*, 2015, **30**(9), 1839–1889.
- S. Carter, A. Fisher, R. Garcia, B. Gibson, S. Lancaster, J. Marshall and I. Whiteside, *J. Anal. At. Spectrom.*, 2015, **30**(11), 2249–2294.
- Y. J. Wang, Z. Q. Tu, L. Zhou, Y. J. Chi and Q. Luo, *Spectrosc. Spectral Anal.*, 2015, **35**(4), 1030–1032.
- A. Laskin, J. Laskin and S. A. Nizkorodov, *Chem. Rev.*, 2015, **115**(10), 4335–4382.
- P. Sanderson, J. M. Delgado-Saborit and R. M. Harrison, *Atmos. Environ.*, 2014, **94**, 353–365.
- O. A. Sadik, N. Du, V. Kariuki, V. Okello and V. Bushlyar, *ACS Sustainable Chem. Eng.*, 2014, **2**(7), 1707–1716.
- P. J. Lam, B. S. Twining, C. Jeandel, A. Roychoudhury, J. A. Resing, P. H. Santschi and R. F. Anderson, *Prog. Oceanogr.*, 2015, **133**, 32–42.



- 12 C. Wright, *TrAC, Trends Anal. Chem.*, 2015, **66**, 118–127.
- 13 M. Famele, C. Ferranti, C. Abenavoli, L. Palleschi, R. Mancinelli and R. Draisci, *Nicotine Tob. Res.*, 2015, **17**(3), 271–279.
- 14 A. S. Brown, A. Murugan and R. J. C. Brown, *Accredit. Qual. Assur.*, 2015, **20**(3), 223–227.
- 15 D. M. Cook, D. K. Sleeth, M. S. Thiese and R. R. Larson, *J. Occup. Environ. Hyg.*, 2015, **12**(3), 199–204.
- 16 J. C. Soo, E. G. Lee, L. A. Lee, M. L. Kashon and M. Harper, *Ann. Occup. Hyg.*, 2014, **58**(8), 1006–1017.
- 17 E. G. Lee, W. P. Chisholm, D. A. Burns, J. H. Nelson, M. L. Kashon and M. Harper, *J. Occup. Environ. Hyg.*, 2014, **11**(12), 819–825.
- 18 E. Cauda, M. Sheehan, R. Gussman, L. Kenny and J. Volkwein, *Ann. Occup. Hyg.*, 2014, **58**(8), 995–1005.
- 19 L. G. Cena, M. J. Keane, W. P. Chisholm, S. Stone, M. Harper and B. T. Chen, *J. Occup. Environ. Hyg.*, 2014, **11**(12), 771–780.
- 20 I. Jayawardene, P. E. Rasmussen, M. Chenier and H. D. Gardner, *J. Air Waste Manage. Assoc.*, 2014, **64**(9), 1028–1037.
- 21 D. B. Wang, M. M. Shafer, J. J. Schauer and C. Sioutas, *Aerosol Sci. Technol.*, 2014, **48**(8), 864–874.
- 22 D. B. Wang, M. M. Shafer, J. J. Schauer and C. Sioutas, *Environ. Pollut.*, 2015, **199**, 227–234.
- 23 S. C. Son and S. S. Park, *Environ. Sci.: Processes Impacts*, 2015, **17**(3), 561–569.
- 24 V. Marple, D. Lundgren and B. Olson, *KONA Powder Part. J.*, 2014, **31**, 2–9.
- 25 Q. Huang, Y. L. Liu, J. B. Chen, X. B. Feng, W. L. Huang, S. L. Yuan, H. M. Cai and X. W. Fu, *J. Anal. At. Spectrom.*, 2015, **30**(4), 957–966.
- 26 J. Wittmer, N. Bobrowski, M. Liotta, G. Giuffrida, S. Calabrese and U. Platt, *Geochem., Geophys., Geosyst.*, 2014, **15**(7), 2797–2820.
- 27 B. Vriens, A. A. Ammann, H. Hagendorfer, M. Lenz, M. Berg and L. H. E. Winkel, *PLoS One*, 2014, **9**(7), 9.
- 28 C. D. McClure, D. A. Jaffe and E. S. Edgerton, *Environ. Sci. Technol.*, 2014, **48**(19), 11437–11444.
- 29 V. S. Lin, *Environ. Sci.: Processes Impacts*, 2015, **17**(6), 1137–1140.
- 30 G. Bertolotti and S. Gialanella, *Anal. Methods*, 2014, **6**(16), 6208–6222.
- 31 B. Laurent, R. Losno, S. Chevallier, J. Vincent, P. Rouillet, E. B. Nguyen, N. Ouboulmane, S. Triquet, M. Fornier, P. Raimbault and G. Bergametti, *Atmos. Meas. Tech.*, 2015, **8**(7), 2801–2811.
- 32 B. Shannak, U. Corsmeier, C. Kottmeier and T. Al-Azab, *Atmos. Environ.*, 2014, **98**, 442–453.
- 33 M. Z. Markovic, S. Prokop, R. M. Staebler, J. Liggio and T. Harner, *Atmos. Environ.*, 2015, **112**, 289–293.
- 34 H. L. Guo, H. M. Lin, W. Zhang, C. Y. Deng, H. H. Wang, Q. G. Zhang, Y. T. Shen and X. J. Wang, *Atmos. Environ.*, 2014, **97**, 310–315.
- 35 T. Steiger and R. Pradel, *Accredit. Qual. Assur.*, 2015, **20**(1), 47–52.
- 36 C. Oster, G. Labarraque and P. Fisicaro, *Anal. Bioanal. Chem.*, 2015, **407**(11), 3035–3043.
- 37 O. Butler, D. Musgrove and P. Stacey, *J. Occup. Environ. Hyg.*, 2014, **11**(9), 604–612.
- 38 P. P. Zhao, J. Li, L. F. Zhong, S. L. Sun and J. F. Xu, *Anal. Methods*, 2014, **6**(15), 5537–5545.
- 39 A. Laycock, B. Stolpe, I. Roemer, A. Dybowska, E. Valsami-Jones, J. R. Lead and M. Rehkamper, *Environ. Sci.: Nano*, 2014, **1**(3), 271–283.
- 40 S. Zihlmann, F. Luond and J. K. Spiegel, *J. Aerosol Sci.*, 2014, **75**, 81–93.
- 41 M. Palmi, R. Szalay, D. Bartczak, Z. Varga, L. N. Nagy, C. Gollwitzer, M. Krumrey and H. Goenaga-Infante, *J. Colloid Interface Sci.*, 2015, **445**, 161–165.
- 42 D. Tabersky, N. A. Luechinger, M. Rossier, E. Reusser, K. Hametner, B. Aeschlimann, D. A. Frick, S. C. Halim, J. Thompson, L. Danyushevsky and D. Gunther, *J. Anal. At. Spectrom.*, 2014, **29**(6), 955–962.
- 43 J. Tshilongo, D. Min, J. B. Lee and J. S. Kim, *Bull. Korean Chem. Soc.*, 2015, **36**(2), 591–596.
- 44 B. P. Sweeney, P. G. Quincey, D. Green and G. W. Fuller, *Atmos. Environ.*, 2015, **105**, 169–172.
- 45 J. Vogl, C. Meyer, M. Koenig, D. Becker, J. Noordmann, O. Rienitz, A. Mamakos and F. Riccobono, *J. Anal. At. Spectrom.*, 2015, **30**(2), 479–486.
- 46 P. Grinberg, R. E. Sturgeon, L. D. Diehl, C. A. Bizzi and E. M. M. Flores, *Spectrochim. Acta, Part B*, 2015, **105**, 89–94.
- 47 R. G. Silva, M. N. Nadagouda, C. L. Patterson, S. Panguluri, T. P. Luxton, E. Sahle-Demessie and C. A. Impellitteri, *Environ. Sci.: Nano*, 2014, **1**(3), 284–292.
- 48 P. S. Fedotov, M. S. Ermolin, V. K. Karandashev and D. V. Ladonin, *Talanta*, 2014, **130**, 1–7.
- 49 P. S. Fedotov, M. S. Ermolin and O. N. Katasonova, *J. Chromatogr. A*, 2015, **1381**, 202–209.
- 50 S. Motellier, A. Guiot, S. Legros and B. Fiorentino, *J. Anal. At. Spectrom.*, 2014, **29**(12), 2294–2301.
- 51 S. Wagner, S. Legros, K. Loeschner, J. Liu, J. Navratilova, R. Grombe, T. P. J. Linsinger, E. H. Larsen, F. von der Kammer and T. Hofmann, *J. Anal. At. Spectrom.*, 2015, **30**(6), 1286–1296.
- 52 J. Sysalova, J. Szakova, J. Tremlova, K. Kasparovska, B. Kotlik, P. Tlustos and P. Svoboda, *Biol. Trace Elem. Res.*, 2014, **161**(2), 216–222.
- 53 L. E. Simonella, D. M. Gaiero and M. E. Palomeque, *Talanta*, 2014, **128**, 248–253.
- 54 B. Miljevic, F. Hedayat, S. Stevanovic, K. E. Fairfull-Smith, S. E. Bottle and Z. D. Ristovski, *Aerosol Sci. Technol.*, 2014, **48**(12), 1276–1284.
- 55 K. J. Bein and A. S. Wexler, *Atmos. Environ.*, 2015, **107**, 24–34.
- 56 L. H. Huan, C. H. Yu, P. K. Hopke, P. J. Liyo, B. T. Buckley, J. Y. Shin and Z. Fan, *Aerosol Air Qual. Res.*, 2014, **14**(7), 1939–1949.
- 57 L. H. Huang, C. H. Yu, P. K. Hopke, J. Y. Shin and Z. H. Fan, *J. Air Waste Manage. Assoc.*, 2014, **64**(12), 1439–1445.
- 58 R. S. Picoloto, S. M. Cruz, P. A. Mello, E. I. Muller, P. Smichowski and E. M. M. Flores, *Microchem. J.*, 2014, **116**, 225–229.



- 59 Y. L. Zhang, J. W. Liu, G. A. Salazar, J. Li, P. Zotter, G. Zhang, R. R. Shen, K. Schafer, J. Schnelle-Kreis, A. S. H. Prevot and S. Szidat, *Atmos. Environ.*, 2014, **97**, 1–5.
- 60 M. Resano, M. Aramendia and M. A. Belarra, *J. Anal. At. Spectrom.*, 2014, **29**(12), 2229–2250.
- 61 P. M. Machado, S. Mores, E. R. Pereira, B. Welz, E. Carasek and J. B. de Andrade, *Spectrochim. Acta, Part B*, 2015, **105**, 18–24.
- 62 M. Resano, M. D. Florez, I. Queralt and E. Margui, *Spectrochim. Acta, Part B*, 2015, **105**, 38–46.
- 63 D. Bauer, S. Everhart, J. Remeika, C. T. Ernest and A. J. Hynes, *Atmos. Meas. Tech.*, 2014, **7**(12), 4251–4265.
- 64 K. Nakata, B. Hashimoto, H. Uchihara, Y. Okamoto, S. Ishizaka and T. Fujiwara, *Talanta*, 2015, **138**, 279–284.
- 65 Y. L. Yu, Y. T. Zhuang and J. H. Wang, *Anal. Methods*, 2015, **7**(5), 1660–1666.
- 66 L. H. Shen, P. J. Chen, B. Yan and C. X. Zhang, *Sens. Actuators, B*, 2015, **215**, 9–14.
- 67 J. Jain, D. McIntyre, K. Ayyalasomayajula, V. Dikshit, C. Goueguel, F. Yu-Yueh and J. Singh, *Pramana*, 2014, **83**(2), 179–188.
- 68 S. C. Yao, Y. L. Shen, K. J. Yin, G. Pan and J. D. Lu, *Energy Fuels*, 2015, **29**(2), 1257–1263.
- 69 C. Dutouquet, G. Gallou, O. le Bihan, J. B. Sirven, A. Dermigny, B. Torralba and E. Frejafon, *Talanta*, 2014, **127**, 75–81.
- 70 F. J. Fortes, A. Fernandez-Bravo and J. J. Laserna, *Spectrochim. Acta, Part B*, 2014, **100**, 78–85.
- 71 M. Gaft, L. Nagli, N. Eliezer, Y. Groisman and O. Forni, *Spectrochim. Acta, Part B*, 2014, **98**, 39–47.
- 72 H. L. Yin, Z. Y. Hou, T. B. Yuan, Z. Wang, W. D. Ni and Z. Li, *J. Anal. At. Spectrom.*, 2015, **30**(4), 922–928.
- 73 D. S. Macholdt, K. P. Jochum, B. Stoll, U. Weis and M. O. Andreae, *Chem. Geol.*, 2014, **383**, 123–131.
- 74 K. Nishiguchi, K. Utani, D. Gunther and M. Ohata, *Anal. Chem.*, 2014, **86**(20), 10025–10029.
- 75 N. Pallavicini, E. Engstrom, D. C. Baxter, B. Ohlander, J. Ingri and I. Rodushkin, *J. Anal. At. Spectrom.*, 2014, **29**(9), 1570–1584.
- 76 R. N. Taylor, O. Ishizuka, A. Michalik, J. A. Milton and I. W. Croudace, *J. Anal. At. Spectrom.*, 2015, **30**(1), 198–213.
- 77 A. Bazzano, K. Latruwe, M. Grotti and F. Vanhaecke, *J. Anal. At. Spectrom.*, 2015, **30**(6), 1322–1328.
- 78 Y. Y. Su, W. Wang, Z. M. Li, H. Deng, G. Q. Zhou, J. Xu and X. J. Ren, *J. Anal. At. Spectrom.*, 2015, **30**(5), 1184–1190.
- 79 M. M. Pornwilard and A. Siripinyanond, *J. Anal. At. Spectrom.*, 2014, **29**(10), 1739–1752.
- 80 B. Meermann, *Anal. Bioanal. Chem.*, 2015, **407**(10), 2665–2674.
- 81 O. Borovinskaya, S. Gschwind, B. Hattendorf, M. Tanner and D. Gunther, *Anal. Chem.*, 2014, **86**(16), 8142–8148.
- 82 S. Gschwind, M. D. A. Montes and D. Gunther, *Anal. Bioanal. Chem.*, 2015, **407**(14), 4035–4044.
- 83 D. J. Lewis, *Analyst*, 2015, **140**(5), 1624–1628.
- 84 S. Lee, X. Y. Bi, R. B. Reed, J. F. Ranville, P. Herckes and P. Westerhoff, *Environ. Sci. Technol.*, 2014, **48**(17), 10291–10300.
- 85 X. Y. Bi, S. Lee, J. F. Ranville, P. Sattigeri, A. Spanias, P. Herckes and P. Westerhoff, *J. Anal. At. Spectrom.*, 2014, **29**(9), 1630–1639.
- 86 M. D. Montano, H. R. Badiei, S. Bazargan and J. F. Ranville, *Environ. Sci.: Nano*, 2014, **1**(4), 338–346.
- 87 W. W. Lee and W. T. Chan, *J. Anal. At. Spectrom.*, 2015, **30**(6), 1245–1254.
- 88 R. Peters, Z. Herrera-Rivera, A. Undas, M. van der Lee, H. Marvin, H. Bouwmeester and S. Weigel, *J. Anal. At. Spectrom.*, 2015, **30**(6), 1274–1285.
- 89 A. Kornilova, S. Moukhtar, M. Saccon, L. Huang, W. Zhang and J. Rudolph, *Atmos. Meas. Tech.*, 2015, **8**(6), 2301–2313.
- 90 D. J. Mrozek, C. van der Veen, M. Kliphuis, J. Kaiser, A. A. Wiegel and T. Rockmann, *Atmos. Meas. Tech.*, 2015, **8**(2), 811–822.
- 91 J. Renpenning, K. L. Hitzfeld, T. Gilevska, I. Nijenhuis, M. Gehre and H. H. Richnow, *Anal. Chem.*, 2015, **87**(5), 2832–2839.
- 92 T. K. Bauska, E. J. Brook, A. C. Mix and A. Ross, *Atmos. Meas. Tech.*, 2014, **7**(11), 3825–3837.
- 93 H. R. Keedakkadan and O. Abe, *Rapid Commun. Mass Spectrom.*, 2015, **29**(8), 775–781.
- 94 N. P. Levitt, *Rapid Commun. Mass Spectrom.*, 2014, **28**(21), 2259–2274.
- 95 L. J. Bay, S. H. Chan and T. Walczyk, *J. Anal. At. Spectrom.*, 2015, **30**(1), 310–314.
- 96 F. Fourel, F. Martineau, M. Seris and C. Lecuyer, *Rapid Commun. Mass Spectrom.*, 2014, **28**(23), 2587–2594.
- 97 M. Levy, R. Y. Zhang, J. Zheng, A. L. Zhang, W. Xu, M. Gomez-Hernandez, Y. Wang and E. Olaguer, *Atmos. Environ.*, 2014, **94**, 231–240.
- 98 J. Diab, T. Streibel, F. Cavalli, S. C. Lee, H. Saathoff, A. Mamakos, J. C. Chow, L. W. A. Chen, J. G. Watson, O. Sippula and R. Zimmermann, *Atmos. Meas. Tech.*, 2015, **8**(8), 3337–3353.
- 99 T. Miyakawa, N. Takeda, K. Koizumi, M. Tabaru, Y. Ozawa, N. Hirayama and N. Takegawa, *Aerosol Sci. Technol.*, 2014, **48**(8), 853–863.
- 100 F. Weiland, P. T. Nilsson, H. Wiinikka, R. Gebart, A. Gudmundsson and M. Sanati, *Aerosol Sci. Technol.*, 2014, **48**(11), 1145–1155.
- 101 J. F. Cahill, T. K. Darlington, X. L. Wang, J. Mayer, M. T. Spencer, J. C. Holecek, B. E. Reed and K. A. Prather, *Aerosol Sci. Technol.*, 2014, **48**(9), 948–956.
- 102 D. Suzuki, F. Esaka, Y. Miyamoto and M. Magara, *Appl. Radiat. Isot.*, 2015, **96**, 52–56.
- 103 F. Esaka, D. Suzuki and M. Magara, *Anal. Chem.*, 2015, **87**(5), 3107–3113.
- 104 S. Weinbruch, A. Worringer, M. Ebert, D. Scheuven, K. Kandler, U. Pfeffer and P. Bruckmann, *Atmos. Environ.*, 2014, **99**, 175–182.
- 105 M. Sommariva, M. Gateshki, J. A. Gertenbach, J. Bolze, U. Konig, B. S. Vasile and V. A. Surdu, *Powder Diff.*, 2014, **29**, S47–S53.
- 106 X. A. Guo, M. Wagner, A. Gutsche, J. Meyer, M. Seipenbusch and H. Nirschl, *J. Aerosol Sci.*, 2015, **85**, 17–29.



- 107 J. Reyes-Herrera, J. Miranda and O. G. de Lucio, *Microchem. J.*, 2015, **120**, 40–44.
- 108 T. Okuda, J. J. Schauer and M. M. Shafer, *Atmos. Environ.*, 2014, **97**, 552–555.
- 109 F. d'Acapito, S. M. Tagliani, F. Di Benedetto and A. Gianfagna, *Atmos. Environ.*, 2014, **99**, 582–586.
- 110 A. F. Longo, E. D. Ingall, J. M. Diaz, M. Oakes, L. E. King, A. Nenes, N. Mihalopoulos, K. Violaki, A. Avila, C. R. Benitez-Nelson, J. Brandes, I. McNulty and D. J. Vine, *Geophys. Res. Lett.*, 2014, **41**(11), 4043–4049.
- 111 A. de Santiago, A. F. Longo, E. D. Ingall, J. M. Diaz, L. E. King, B. Lai, R. J. Weber, A. G. Russell and M. Oakes, *Environ. Sci. Technol.*, 2014, **48**(16), 8988–8994.
- 112 L. L. van Loon, C. Throssell and M. D. Dutton, *Environ. Sci.: Processes Impacts*, 2015, **17**(5), 922–931.
- 113 S. Beauchemin, P. E. Rasmussen, T. MacKinnon, M. Chenier and K. Boros, *Environ. Sci. Technol.*, 2014, **48**(16), 9022–9029.
- 114 L. Z. Zhang, G. Tian, J. S. Li and B. L. Yu, *Appl. Spectrosc.*, 2014, **68**(10), 1095–1107.
- 115 C. Reidl-Leuthner, A. Viernstein, K. Wieland, W. Tomischko, L. Sass, G. Kinger, J. Ofner and B. Lendl, *Anal. Chem.*, 2014, **86**(18), 9058–9064.
- 116 C. Reidl-Leuthner, J. Ofner, W. Tomischko, H. Lohninger and B. Lendl, *Atmos. Environ.*, 2015, **112**, 189–195.
- 117 R. A. Robinson, T. D. Gardiner, F. Innocenti, A. Finlayson, P. T. Woods and J. F. M. Few, *Environ. Sci.: Processes Impacts*, 2014, **16**(8), 1957–1966.
- 118 R. van Geldern, M. E. Nowak, M. Zimmer, A. Szizyalski, A. Myrntinen, J. A. C. Barth and H. J. Jost, *Anal. Chem.*, 2014, **86**(24), 12191–12198.
- 119 J. Pavlovic, J. S. Kinsey and M. D. Hays, *Atmos. Meas. Tech.*, 2014, **7**(9), 2829–2838.
- 120 P. Panteliadis, T. Hafkenscheid, B. Cary, E. Diapouli, A. Fischer, O. Favez, P. Quincey, M. Viana, R. Hitzengerger, R. Vecchi, D. Saraga, J. Sciare, J. L. Jaffrezou, A. John, J. Schwarz, M. Giannoni, J. Novak, A. Karanasiou, P. Fermo and W. Maenhaut, *Atmos. Meas. Tech.*, 2015, **8**(2), 779–792.
- 121 L. W. A. Chen, J. C. Chow, X. L. Wang, J. A. Robles, B. J. Sumlin, D. H. Lowenthal, R. Zimmermann and J. G. Watson, *Atmos. Meas. Tech.*, 2015, **8**(1), 451–461.
- 122 L. Drinovec, G. Mocnik, P. Zotter, A. S. H. Prevot, C. Ruckstuhl, E. Coz, M. Rupakheti, J. Sciare, T. Muller, A. Wiedensohler and A. D. A. Hansen, *Atmos. Meas. Tech.*, 2015, **8**(5), 1965–1979.
- 123 Q. Q. Wang, F. M. Yang, L. F. Wei, G. J. Zheng, Z. J. Fan, S. Rajagopalan, R. D. Brook, F. K. Duan, K. B. He, Y. L. Sun and J. R. Brook, *Atmos. Environ.*, 2014, **95**, 520–524.
- 124 J. A. Forder, *Ann. Occup. Hyg.*, 2014, **58**(7), 889–898.
- 125 C. H. Yu, A. P. Patton, A. Zhang, Z.-H. Fan, C. P. Weisel and P. J. Liou, *J. Occup. Environ. Hyg.*, 2015, **12**(9), 577–587.
- 126 S. N. Vardag, S. Hammer, M. Sabasch, D. W. T. Griffith and I. Levin, *Atmos. Meas. Tech.*, 2015, **8**(2), 579–592.
- 127 J. Adetunji, *Atmos. Environ.*, 2014, **98**, 591–598.
- 128 H. Y. Guo, Z. Y. Zhang, B. S. Xing, A. Mukherjee, C. Musante, J. C. White and L. L. He, *Environ. Sci. Technol.*, 2015, **49**(7), 4317–4324.
- 129 H. M. Al-Saidi and A. A. A. Emara, *J. Saudi Chem. Soc.*, 2014, **18**(6), 745–761.
- 130 I. Hagarova, *Chem. Listy*, 2014, **108**(10), 949–955.
- 131 E. Stanisz, J. Werner and A. Zgola-Grzeskowiak, *TrAC, Trends Anal. Chem.*, 2014, **61**, 54–66.
- 132 B. Hu, M. He and B. B. Chen, *Anal. Bioanal. Chem.*, 2015, **407**(10), 2685–2710.
- 133 M. Rutkowska, K. Dubalska, P. Konieczka and J. Namiesnik, *Molecules*, 2014, **19**(6), 7581–7609.
- 134 N. S. La Colla, C. E. Domini, J. E. Marcovecchio and S. E. Botte, *J. Environ. Manage.*, 2015, **151**, 44–55.
- 135 T. Minami, W. Konagaya, L. J. Zheng, S. Takano, M. Sasaki, R. Murata, Y. Nakaguchi and Y. Sohrin, *Anal. Chim. Acta*, 2015, **854**, 183–190.
- 136 H. Y. Peng, N. Zhang, M. He, B. B. Chen and B. Hu, *Talanta*, 2015, **131**, 266–272.
- 137 A. Dados, E. Kartsiouli, T. Chatzimitakos, C. Papastefanou and C. D. Stalikas, *Talanta*, 2014, **130**, 142–147.
- 138 H. Tazoe, T. Yamagata, H. Obata and H. Nagai, *Anal. Chim. Acta*, 2014, **852**, 74–81.
- 139 J. P. Zou, X. G. Ma, Y. F. Dang and Y. Chen, *J. Anal. At. Spectrom.*, 2014, **29**(9), 1692–1697.
- 140 H. T. Zheng, B. T. Jia, Z. L. Zhu, Z. Y. Tang and S. H. Hu, *Anal. Methods*, 2014, **6**(21), 8569–8576.
- 141 T. T. Shih, I. H. Hsu, S. N. Chen, P. H. Chen, M. J. Deng, Y. Chen, Y. W. Lin and Y. C. Sun, *Analyst*, 2015, **140**(2), 600–608.
- 142 L. F. Meng, C. S. Chen and Y. L. Yang, *Anal. Lett.*, 2015, **48**(3), 453–463.
- 143 Y. A. Zhang, C. Zhong, Q. Y. Zhang, B. B. Chen, M. He and B. Hu, *RSC Adv.*, 2015, **5**(8), 5996–6005.
- 144 M. Krawczyk, M. Jeszka-Skowron and H. Matusiewicz, *Microchem. J.*, 2014, **117**, 138–143.
- 145 N. Thakur, S. A. Kumar, A. K. Pandey, S. D. Kumar and A. V. R. Reddy, *Anal. Methods*, 2014, **6**(19), 7823–7830.
- 146 K. C. Hsu, C. F. Lee, W. C. Tseng, Y. Y. Chao and Y. L. Huang, *Talanta*, 2014, **128**, 408–413.
- 147 C. Bazan, R. Gil, P. Smichowski and P. Pacheco, *Microchem. J.*, 2014, **117**, 40–45.
- 148 S. Poehle, K. Schmidt and A. Koschinsky, *Deep Sea Res., Part I*, 2015, **98**, 83–93.
- 149 C. Karadas and D. Kara, *Water, Air, Soil Pollut.*, 2014, **225**(5), 10.
- 150 C. Karadas and D. Kara, *Water, Air, Soil Pollut.*, 2014, **225**(11), 10.
- 151 R. Rodriguez, L. Leal, S. Miranda, L. Ferrer, J. Avivar, A. Garcia and V. Cerda, *Talanta*, 2015, **133**, 88–93.
- 152 A. Beiraghi, M. Shokri, S. Seidi and B. M. Godajdar, *J. Chromatogr. A*, 2015, **1376**, 1–8.
- 153 M. Shamsipur, N. Fattahi, Y. Assadi, M. Sadeghi and K. Sharafi, *Talanta*, 2014, **130**, 26–32.
- 154 A. C. Grijalba, L. B. Escudero and R. G. Wuilloud, *Anal. Methods*, 2015, **7**(2), 490–499.



- 155 H. Fazelirad, M. A. Taher and M. Nasiri-Majd, *J. Anal. At. Spectrom.*, 2014, **29**(12), 2343–2348.
- 156 I. Lopez-Garcia, Y. Vicente-Martinez and M. Hernandez-Cordoba, *J. Anal. At. Spectrom.*, 2015, **30**(2), 375–380.
- 157 C. Mitani, A. Kotzamanidou and A. N. Anthemidis, *J. Anal. At. Spectrom.*, 2014, **29**(8), 1491–1498.
- 158 H. Sereshti, M. Kermani, M. Karimi and S. Samadi, *Clean: Soil, Air, Water*, 2014, **42**(8), 1089–1097.
- 159 I. Celik, D. Kara, C. Karadas, A. Fisher and S. J. Hill, *Talanta*, 2015, **134**, 476–481.
- 160 K. Pytlakowska, M. Dabioch and R. Sitko, *Analyst*, 2014, **139**(16), 3911–3917.
- 161 P. J. Worsfold, M. C. Lohan, S. J. Ussher and A. R. Bowie, *Mar. Chem.*, 2014, **166**, 25–35.
- 162 B. Sadee, M. E. Foulkes and S. J. Hill, *J. Anal. At. Spectrom.*, 2015, **30**(1), 102–118.
- 163 M. Jablonska-Czapla, *Int. J. Anal. Chem.*, 2015, article ID 171478.
- 164 B. Markiewicz, I. Komorowicz, A. Sajnog, M. Belter and D. Baralkiewicz, *Talanta*, 2015, **132**, 814–828.
- 165 C. T. Liu and A. N. Tang, *Anal. Lett.*, 2015, **48**(7), 1031–1043.
- 166 N. S. Keller, A. Stefasson and B. Sigfusson, *Talanta*, 2014, **128**, 466–472.
- 167 K. Hagiwara, T. Inui, Y. Koike, M. Aizawa and T. Nakamura, *Talanta*, 2015, **134**, 739–744.
- 168 T. Huynh, H. H. Harris, H. Zhang and B. N. Noller, *Environ. Chem.*, 2015, **12**(2), 102–111.
- 169 J. Sun, Z. G. Yang, H. W. Lee and L. Wang, *Anal. Methods*, 2015, **7**(6), 2653–2658.
- 170 D. B. Wu and T. Pichler, *Anal. Methods*, 2014, **6**(14), 5112–5119.
- 171 H. Matsumiya, H. Inoue and M. Hiraide, *Talanta*, 2014, **128**, 500–504.
- 172 G. Acosta, A. Spisso, L. P. Fernandez, L. D. Martinez, P. H. Pacheco and R. A. Gil, *J. Pharm. Biomed. Anal.*, 2015, **106**, 79–84.
- 173 C. C. Brombach, B. Chen, W. T. Corns, J. Feldmann and E. M. Krupp, *Spectrochim. Acta, Part B*, 2015, **105**, 103–108.
- 174 Z. Nie, L. N. Zheng, W. Y. Feng and C. L. Liu, *Anal. Methods*, 2014, **6**(20), 8380–8387.
- 175 I. Lopez-Garcia, Y. Vicente-Martinez and M. Hernandez-Cordoba, *Spectrochim. Acta, Part B*, 2014, **101**, 93–97.
- 176 K. Proulx and K. J. Wilkinson, *Environ. Chem.*, 2014, **11**(4), 392–401.
- 177 P. Krystek, P. S. Bauerlein and P. J. F. Kooij, *J. Pharm. Biomed. Anal.*, 2015, **106**, 116–123.
- 178 R. Lohmayer, G. M. S. Reithmaier, E. Bura-Nakic and B. Planer-Friedrich, *Anal. Chem.*, 2015, **87**(6), 3388–3395.
- 179 L. Huang, D. Yang, X. Q. Guo and Z. L. Chen, *J. Chromatogr. A*, 2014, **1368**, 217–221.
- 180 X. J. Mao, W. Y. Fan, M. He, B. B. Chen and B. Hu, *J. Anal. At. Spectrom.*, 2015, **30**(1), 162–171.
- 181 E. Alasonati, B. Fabbri, I. Fettig, C. Yardin, M. E. D. Busto, J. Richter, R. Philipp and P. Fiscaro, *Talanta*, 2015, **134**, 576–586.
- 182 B. Gomez-Nieto, M. J. Gismera, M. T. Sevilla and J. R. Procopio, *Anal. Chim. Acta*, 2015, **854**, 13–19.
- 183 E. C. Jung, H. R. Cho, W. Cha, J. H. Park and M. H. Baik, *Rev. Anal. Chem.*, 2014, **33**(4), 245–254.
- 184 X. D. Yu, Y. Li, X. F. Gu, J. M. Bao, H. Z. Yang and L. Sun, *Environ. Monit. Assess.*, 2014, **186**(12), 8969–8980.
- 185 M. A. Aguirre, E. J. Selva, M. Hidalgo and A. Canals, *Talanta*, 2015, **131**, 348–353.
- 186 A. Matsumoto, A. Tamura, R. Koda, K. Fukami, Y. H. Ogata, N. Nishi, B. Thornton and T. Sakka, *Anal. Chem.*, 2015, **87**(3), 1655–1661.
- 187 M. Filella, D. J. Magnenat and M. Bensimon, *Anal. Methods*, 2014, **6**(20), 8090–8093.
- 188 A. Suzuki, H. Obata, A. Okubo and T. Gamo, *Mar. Chem.*, 2014, **166**, 114–121.
- 189 C. D. B. Amaral, R. S. Amais, L. L. Fialho, D. Schiavo, T. Amorim, A. R. A. Nogueira, F. R. P. Rocha and J. A. Nobrega, *Anal. Methods*, 2015, **7**(3), 1215–1220.
- 190 R. Clough, H. Sela, A. Milne, M. C. Lohan, S. Tokalioglu and P. J. Worsfold, *Talanta*, 2015, **133**, 162–169.
- 191 A. Y. Zhang, J. Zhang, R. F. Zhang and Y. Xue, *J. Anal. At. Spectrom.*, 2014, **29**(12), 2414–2418.
- 192 L. Yang, L. Zhou, Z. C. Hu and S. Gao, *Anal. Chem.*, 2014, **86**(18), 9301–9308.
- 193 M. Strok, H. Hintelmann and B. Dimock, *Anal. Chim. Acta*, 2014, **851**, 57–63.
- 194 H. Y. Lin, D. X. Yuan, B. Y. Lu, S. Y. Huang, L. M. Sun, F. Zhang and Y. Q. Gao, *J. Anal. At. Spectrom.*, 2015, **30**(2), 353–359.
- 195 R. E. Sturgeon, *Anal. Chem.*, 2015, **87**(5), 3072–3079.
- 196 H. L. Duan, Z. B. Gong and S. F. Yang, *J. Anal. At. Spectrom.*, 2015, **30**(2), 410–416.
- 197 C. L. He, G. L. Cheng, C. B. Zheng, L. Wu, Y. I. Lee and X. D. Hou, *Anal. Methods*, 2015, **7**(7), 3015–3021.
- 198 D. Picon, P. Carrero, M. Valero, Y. de Pena and L. Gutierrez, *Talanta*, 2015, **136**, 136–144.
- 199 G. V. Pashkova and A. G. Revenko, *Appl. Spectrosc. Rev.*, 2015, **50**(6), 443–472.
- 200 J. Kruse, M. Abraham, W. Amelung, C. Baum, R. Bol, O. Kuhn, H. Lewandowski, J. Niederberger, Y. Oelmann, C. Ruger, J. Santner, M. Siebers, N. Siebers, M. Spohn, J. Vestergren, A. Vogts and P. Leinweber, *J. Plant Nutr. Soil Sci.*, 2015, **178**(1), 43–88.
- 201 D. J. Butcher, *Appl. Spectrosc. Rev.*, 2015, **50**(1), 27–45.
- 202 P. Porizka, P. Prochazkova, D. Prochazka, L. Sladkova, J. Novotny, M. Petrlik, M. Brada, O. Samek, Z. Pilat, P. Zemanek, V. Adam, R. Kizek, K. Novotny and J. Kaiser, *Sensors*, 2014, **14**(9), 17725–17752.
- 203 K. H. Laursen, J. K. Schjoerring, S. D. Kelly and S. Husted, *TrAC, Trends Anal. Chem.*, 2014, **59**, 73–82.
- 204 A. D. Batista, M. K. Sasaki, F. R. P. Rocha and E. A. G. Zagatto, *Analyst*, 2014, **139**(15), 3666–3682.
- 205 I. Ugulu, *Appl. Spectrosc. Rev.*, 2015, **50**(2), 113–151.
- 206 C. D. B. Amaral, J. A. Nobrega and A. R. A. Nogueira, *Microchem. J.*, 2014, **117**, 122–126.
- 207 S. Loppi, C. Faleri and L. Paoli, *Bull. Environ. Contam. Toxicol.*, 2014, **93**(3), 350–353.
- 208 S. C. Jantzi and J. R. Almirall, *Appl. Spectrosc.*, 2014, **68**(9), 963–974.



- 209 S. Arnoldussen and B. van Os, *Catena*, 2015, **128**, 16–30.
- 210 M. Welna, A. Szymczycha-Madeja and P. Pohl, *TrAC, Trends Anal. Chem.*, 2015, **65**, 122–136.
- 211 H. O. Qu, T. K. Mudalige and S. W. Linder, *J. Agric. Food Chem.*, 2015, **63**(12), 3153–3160.
- 212 M. N. Herod, R. J. Cornett, I. D. Clark, W. E. Kieser and G. St Jean, *J. Environ. Radioact.*, 2014, **138**, 323–330.
- 213 K. Miranda, A. L. Vieira and J. A. G. Neto, *Anal. Methods*, 2014, **6**(23), 9503–9508.
- 214 L. Carrasco and E. Vassileva, *Anal. Chim. Acta*, 2015, **853**, 167–178.
- 215 D. Zhao, H. B. Li, J. Y. Xu, J. Luo and L. Ma, *Sci. Total Environ.*, 2015, **523**, 138–145.
- 216 S. Terfi and F. Sadi, *Anal. Lett.*, 2015, **48**(7), 1190–1197.
- 217 M. F. Mesko, R. S. Picoloto, L. R. Ferreira, V. C. Costa, C. M. P. Pereira, P. Colepiccolo, E. I. Muller and E. M. M. Flores, *J. Anal. At. Spectrom.*, 2015, **30**(1), 260–266.
- 218 C. A. Bizzi, J. A. Nobrega, J. S. Barin, J. S. S. Oliveira, L. Schmidt, P. A. Mello and E. M. M. Flores, *Anal. Chim. Acta*, 2014, **837**, 16–22.
- 219 A. M. Hernandez-Martinez, C. Padron-Sanz, M. E. T. Padron, Z. S. Ferrera and J. J. S. Rodriguez, *J. Anal. At. Spectrom.*, 2015, **30**(2), 435–442.
- 220 P. Mamatha, G. Venkateswarlu, A. V. N. Swamy and A. C. Sahayam, *Anal. Methods*, 2014, **6**(24), 9653–9657.
- 221 C. N. Lou, W. Q. Liu and X. D. Liu, *J. Chromatogr. B: Anal. Technol. Biomed. Life Sci.*, 2014, **969**, 29–34.
- 222 E. Bernalte, S. Salmanighabeshi, F. Rueda-Holgado, M. R. Palomo-Marin, C. Marin-Sanchez, F. Cereceda-Balic and E. Pinilla-Gil, *Int. J. Environ. Sci. Technol.*, 2015, **12**(3), 817–826.
- 223 M. Frena, D. P. C. Quadros, I. N. B. Castilho, J. S. de Gois, D. L. G. Borges, B. Welz and L. A. S. Madureira, *Microchem. J.*, 2014, **117**, 1–6.
- 224 M. V. B. Krishna and D. Karunasagar, *Anal. Methods*, 2015, **7**(5), 1997–2005.
- 225 B. D. Duval, S. M. Natali and B. A. Hungate, *Commun. Soil Sci. Plant Anal.*, 2015, **46**(3), 318–326.
- 226 F. Guerra, A. R. Trevizam, R. C. Fior and T. Muraoka, *Sci. Agric.*, 2014, **71**(5), 410–415.
- 227 J. Sun, L. Ma, Z. G. Yang, H. Lee and L. Wang, *J. Sep. Sci.*, 2015, **38**(6), 943–950.
- 228 D. Garcia-Casillas, S. Garcia-Salgado and M. A. Quijano, *Anal. Methods*, 2014, **6**(20), 8403–8412.
- 229 P. W. G. van Geffen, T. K. Kyser, C. J. Oates and C. Ihlenfeld, *Geochem.: Explor., Environ., Anal.*, 2015, **15**(1), 27–38.
- 230 M. Q. Wang, H. Wu, Y. Liao, F. Fang, Y. Y. Gao and Y. Xu, *J. Geochem. Explor.*, 2015, **148**, 231–240.
- 231 M. Rosende, L. M. Magalhaes, M. A. Segundo and M. Miro, *Anal. Chim. Acta*, 2014, **842**, 1–10.
- 232 N. Boisa, N. Elom, J. R. Dean, M. E. Deary, G. Bird and J. A. Entwistle, *Environ. Int.*, 2014, **70**, 132–142.
- 233 N. C. Galvan-Tejada, V. Pena-Ramirez, L. Mora-Palomino and C. Siebe, *J. Plant Nutr. Soil Sci.*, 2014, **177**(5), 792–802.
- 234 J. M. Rosas-Castor, L. Portugal, L. Ferrer, J. L. Guzman-Mar, A. Hernandez-Ramirez, V. Cerda and L. Hinojosa-Reyes, *Anal. Chim. Acta*, 2015, **874**, 1–10.
- 235 Y. L. Zhang, M. Miro and S. D. Kolev, *Environ. Sci. Technol.*, 2015, **49**(5), 2733–2740.
- 236 K. Barkonikos, I. N. Pasiadis and N. S. Thomaidis, *Talanta*, 2014, **129**, 165–170.
- 237 M. Y. Burylin, *J. Anal. Chem.*, 2015, **70**(1), 39–43.
- 238 R. Dobrowolski, J. Dobrzynska and B. Gawronska, *Environ. Monit. Assess.*, 2015, **187**(1), 8.
- 239 M. C. B. Alonso, M. N. Pardal, M. L. Pedrouso, J. R. Aboal, J. A. Fernandez and P. Bermejo-Barrera, *At. Spectrosc.*, 2015, **36**(1), 42–48.
- 240 P. Mandjukov, A. M. Orani, E. Han and E. Vassileva, *Spectrochim. Acta, Part B*, 2015, **103**, 24–33.
- 241 A. M. Orani, E. Han, P. Mandjukov and E. Vassileva, *Spectrochim. Acta, Part B*, 2015, **103**, 131–143.
- 242 P. Coufalik and J. Komarek, *J. Anal. Chem.*, 2014, **69**(12), 1123–1129.
- 243 B. Caballero-Segura, P. Avila-Perez, C. E. B. Diaz, J. J. R. Garcia, G. Zarazua, R. Soria and H. B. Ortiz-Oliveros, *Int. J. Environ. Anal. Chem.*, 2014, **94**(13), 1288–1301.
- 244 R. McIlwaine, S. F. Cox and R. Doherty, *Environ. Sci. Pollut. Res.*, 2015, **22**(8), 6364–6371.
- 245 G. L. Scheffler and D. Pozebon, *J. Anal. At. Spectrom.*, 2015, **30**(2), 468–478.
- 246 F. Kaveh and D. Beauchemin, *J. Anal. At. Spectrom.*, 2014, **29**(8), 1371–1377.
- 247 F. Kaveh, C. J. Oates and D. Beauchemin, *Geochem.: Explor., Environ., Anal.*, 2014, **14**(4), 305–313.
- 248 N. Sadiq and D. Beauchemin, *Anal. Chim. Acta*, 2014, **851**, 23–29.
- 249 P. Masson, *Spectrochim. Acta, Part B*, 2014, **102**, 24–27.
- 250 S. G. Silva, J. A. Nobrega, B. T. Jones and G. L. Donati, *J. Anal. At. Spectrom.*, 2014, **29**(8), 1499–1503.
- 251 S. Karlsson, V. Sjoberg and A. Ogar, *Talanta*, 2015, **135**, 124–132.
- 252 C. T. Kamala, V. Balaram, V. Dharmendra, M. Satyanarayanan, K. S. V. Subramanyam and A. Krishnaiah, *Environ. Monit. Assess.*, 2014, **186**(11), 7097–7113.
- 253 T. Frentiu, E. Darvasi, S. Butaciu, M. Ponta, D. Petreus, A. I. Mihaltan and M. Frentiu, *Talanta*, 2014, **129**, 72–78.
- 254 T. Frentiu, S. Butaciu, E. Darvasi, M. Ponta, M. Senila, E. Levei and M. Frentiu, *J. Anal. At. Spectrom.*, 2015, **30**(5), 1161–1168.
- 255 T. Frentiu, S. Butaciu, M. Ponta, E. Darvasi, M. Senila, D. Petreus and M. Frentiu, *J. Anal. At. Spectrom.*, 2014, **29**(10), 1880–1888.
- 256 Q. Li, Z. Zhang and Z. Wang, *Anal. Chim. Acta*, 2014, **845**, 7–14.
- 257 C. C. Brombach, Z. Gajdosechova, B. Chen, A. Brownlow, W. T. Corns, J. Feldmann and E. M. Krupp, *Anal. Bioanal. Chem.*, 2015, **407**(3), 973–981.
- 258 S. G. Silva, J. A. Nobrega, B. T. Jones and G. L. Donati, *Microchem. J.*, 2014, **117**, 250–254.
- 259 Y. X. Liu, Q. X. Li, N. Ma, X. L. Sun, J. F. Bai and Q. Zhang, *Anal. Chem.*, 2014, **86**(23), 11570–11577.



- 260 L. Bendakovska, A. Krejcova, T. Cernohorsky and K. Zvonickova, *Chem. Listy*, 2014, **108**, S154–S159.
- 261 B. S. Matteson, S. K. Hanson, J. L. Miller and W. J. Oldham, *J. Environ. Radioact.*, 2015, **142**, 62–67.
- 262 M. M. Wolle, G. M. M. Rahman, H. M. S. Kingston and M. Pamuku, *J. Anal. At. Spectrom.*, 2014, **29**(9), 1640–1647.
- 263 B. P. Jackson, A. Liba and J. Nelson, *J. Anal. At. Spectrom.*, 2015, **30**(5), 1179–1183.
- 264 E. Bolea-Fernandez, L. Balcaen, M. Resano and F. Vanhaecke, *Anal. Bioanal. Chem.*, 2015, **407**(3), 919–929.
- 265 Y. Gao, M. Xu, R. E. Sturgeon, Z. Mester, Z. M. Shi, R. Galea, P. Saull and L. Yang, *Anal. Chem.*, 2015, **87**(8), 4495–4502.
- 266 R. F. Wei, Q. J. Guo, H. J. Wen, J. X. Yang, M. Peters, C. W. Zhu, J. Ma, G. X. Zhu, H. Z. Zhang, L. Y. Tian, C. Y. Wang and Y. X. Wan, *Anal. Methods*, 2015, **7**(6), 2479–2487.
- 267 J. Durisova, L. Ackerman, L. Strnad, V. Chrastny and J. Borovicka, *Geostand. Geoanal. Res.*, 2015, **39**(2), 209–220.
- 268 W. Guo, S. H. Hu, Z. W. Wu, G. Y. Lan, L. L. Jin, X. G. Pang, J. C. Zhan, B. Chen and Z. Y. Tang, *J. Anal. At. Spectrom.*, 2015, **30**(4), 986–993.
- 269 B. C. Russell, I. W. Croudace, P. E. Warwick and J. A. Milton, *Anal. Chem.*, 2014, **86**(17), 8719–8726.
- 270 J. Zheng, W. T. Bu, K. Tagami, Y. Shikamori, K. Nakano, S. Uchida and N. Ishii, *Anal. Chem.*, 2014, **86**(14), 7103–7110.
- 271 J. S. Becker, A. Matusch and B. Wu, *Anal. Chim. Acta*, 2014, **835**, 1–18.
- 272 D. Pozebon, G. L. Scheffler, V. L. Dressler and M. A. G. Nunes, *J. Anal. At. Spectrom.*, 2014, **29**(12), 2204–2228.
- 273 S. R. Oliveira and M. A. Z. Arruda, *J. Anal. At. Spectrom.*, 2015, **30**(2), 389–395.
- 274 Y. Gao, S. van de Velde, P. N. Williams, W. Baeyens and H. Zhang, *TrAC, Trends Anal. Chem.*, 2015, **66**, 63–71.
- 275 A. Kreuzeder, J. Santner, H. Zhang, T. Prohaska and W. W. Wenzel, *Environ. Sci. Technol.*, 2015, **49**(3), 1594–1602.
- 276 A. Rugova, M. Puschenreiter, J. Santner, L. Fischer, S. Neubauer, G. Koellensperger and S. Hann, *J. Sep. Sci.*, 2014, **37**(14), 1711–1719.
- 277 R. Koplik, I. Klimesova, K. Malisova and O. Mestek, *Czech J. Food Sci.*, 2014, **32**(3), 249–259.
- 278 H. Pietila, P. Peramaki, J. Piispanen, M. Starr, T. Nieminen, M. Kantola and L. Ukonmaanaho, *Chemosphere*, 2015, **124**, 47–53.
- 279 G. F. Koopmans, T. Hiemstra, I. C. Regelink, B. Molleman and R. N. J. Comans, *J. Chromatogr. A*, 2015, **1392**, 100–109.
- 280 Y. B. Dan, W. L. Zhang, R. M. Xue, X. M. Ma, C. Stephan and H. L. Shi, *Environ. Sci. Technol.*, 2015, **49**(5), 3007–3014.
- 281 J. El Haddad, L. Canioni and B. Bousquet, *Spectrochim. Acta, Part B*, 2014, **101**, 171–182.
- 282 G. G. A. de Carvalho, D. Santos, M. D. Gomes, L. C. Nunes, M. B. B. Guerra and F. J. Krug, *Spectrochim. Acta, Part B*, 2015, **105**, 130–135.
- 283 K. Devey, M. Mucalo, G. Rajendram and J. Lane, *Commun. Soil Sci. Plant Anal.*, 2015, **46**, 72–80.
- 284 X. N. Liu, Q. Zhang, Z. S. Wu, X. Y. Shi, N. Zhao and Y. J. Qiao, *Sensors*, 2015, **15**(1), 642–655.
- 285 J. El Haddad, D. Bruyere, A. Ismael, G. Gallou, V. Laperche, K. Michel, L. Canioni and B. Bousquet, *Spectrochim. Acta, Part B*, 2014, **97**, 57–64.
- 286 A. M. Popov, T. A. Labutin, S. M. Zaytsev, I. V. Seliverstova, N. B. Zorov, I. A. Kal'ko, Y. N. Sidorina, I. A. Bugaev and Y. N. Nikolaev, *J. Anal. At. Spectrom.*, 2014, **29**(10), 1925–1933.
- 287 E. C. Ferreira, E. J. Ferreira, P. R. Villas-Boas, G. S. Senesi, C. M. Carvalho, R. A. Romano, L. Martin-Neto and D. Milori, *Spectrochim. Acta, Part B*, 2014, **99**, 76–81.
- 288 D. C. Weindorf, N. Bakr and Y. D. Zhu, in *Advances in Agronomy*, ed. D. L. Sparks, Elsevier Academic Press Inc, San Diego, 2014, vol. 128, pp. 1–45.
- 289 N. W. Brand and C. J. Brand, *Geochem.: Explor., Environ., Anal.*, 2014, **14**(2), 125–138.
- 290 G. E. M. Hall, G. F. Bonham-Carter and A. Buchar, *Geochem.: Explor., Environ., Anal.*, 2014, **14**(2), 99–123.
- 291 C. A. Shand and R. Wendler, *J. Geochem. Explor.*, 2014, **143**, 31–42.
- 292 D. C. Arne, R. A. Mackie and S. A. Jones, *Geochem.: Explor., Environ., Anal.*, 2014, **14**(3), 233–244.
- 293 B. Lemiere, V. Laperche, L. Haouche and P. Auger, *Geochem.: Explor., Environ., Anal.*, 2014, **14**(3), 257–264.
- 294 R. M. Conrey, M. Goodman-Elgar, N. Bettencourt, A. Seyfarth, A. van Hoose and J. A. Wolff, *Geochem.: Explor., Environ., Anal.*, 2014, **14**(3), 291–301.
- 295 A. M. W. Hunt and R. J. Speakman, *J. Archaeol. Sci.*, 2015, **53**, 626–638.
- 296 M. I. Kaniu and K. H. Angeyo, *Geoderma*, 2015, **241**, 32–40.
- 297 A. Sharma, D. C. Weindorf, T. Man, A. A. A. Aldabaa and S. Chakraborty, *Geoderma*, 2014, **232**, 141–147.
- 298 F. L. Melquiades and F. R. dos Santos, *Spectrosc. Lett.*, 2015, **48**(4), 286–289.
- 299 A. Sharma, D. C. Weindorf, D. D. Wang and S. Chakraborty, *Geoderma*, 2015, **239**, 130–134.
- 300 S. Swanhart, D. C. Weindorf, S. Chakraborty, N. Bakr, Y. D. Zhu, C. Nelson, K. Shook and A. Acree, *Soil Sci.*, 2014, **179**(9), 417–423.
- 301 D. D. Wang, S. Chakraborty, D. C. Weindorf, B. Li, A. Sharma, S. Paul and M. N. Ali, *Geoderma*, 2015, **243**, 157–167.
- 302 S. Chakraborty, D. C. Weindorf, B. Li, A. A. A. Aldabaa, R. K. Ghosh, S. Paul and M. N. Ali, *Sci. Total Environ.*, 2015, **514**, 399–408.
- 303 A. A. A. Aldabaa, D. C. Weindorf, S. Chakraborty, A. Sharma and B. Li, *Geoderma*, 2015, **239**, 34–46.
- 304 A. Horta, B. Malone, U. Stockmann, B. Minasny, T. F. A. Bishop, A. B. McBratney, R. Pallasser and L. Pozza, *Geoderma*, 2015, **241**, 180–209.
- 305 K. Ploykrachang, J. Hasegawa, K. Kondo, H. Fukuda and Y. Oguri, *Nucl. Instrum. Methods Phys. Res., Sect. B*, 2014, **331**, 261–265.
- 306 M. B. B. Guerra, E. de Almeida, G. G. A. Carvalho, P. F. Souza, L. C. Nunes, D. Santos and F. J. Krug, *J. Anal. At. Spectrom.*, 2014, **29**(9), 1667–1674.



- 307 P. Vavpetic, K. Vogel-Mikus, L. Jeromel, N. O. Potocnik, P. Pongrac, D. Drobne, Z. P. Tkalec, S. Novak, M. Kos, S. Koren, M. Regvar and P. Pelicon, *Nucl. Instrum. Methods Phys. Res., Sect. B*, 2015, **348**, 147–151.
- 308 V. Romero, I. Costas-Mora, I. Lavilla and C. Bendicho, *Spectrochim. Acta, Part B*, 2015, **107**, 125–131.
- 309 A. T. Reis, A. C. Duarte, B. Henriques, C. Coelho, C. B. Lopes, C. L. Mieiro, D. S. Tavares, L. Ahmad, J. P. Coelho, L. S. Rocha, N. Cruz, R. J. R. Monteiro, R. Rocha, S. Rodrigues and E. Pereira, *TrAC, Trends Anal. Chem.*, 2015, **64**, 137–149.
- 310 B. Marie, L. Marin, P. Y. Martin, T. Gulon, J. Carignan and C. Cloquet, *Geostand. Geoanal. Res.*, 2015, **39**(1), 71–86.
- 311 M. Soylak and I. Murat, *J. AOAC Int.*, 2014, **97**(4), 1189–1194.
- 312 J. A. Baig, L. Elci, M. I. Khan and T. G. Kazi, *J. AOAC Int.*, 2014, **97**(5), 1421–1425.
- 313 D. Mendil, M. Karatas and M. Tuzen, *Food Chem.*, 2015, **177**, 320–324.
- 314 Z. Bahadir, V. N. Bulut, D. Ozdes, C. Duran, H. Bektas and M. Soylak, *J. Ind. Eng. Chem.*, 2014, **20**(3), 1030–1034.
- 315 B. E. D. Costa, N. M. M. Coelho and L. M. Coelho, *Food Chem.*, 2015, **178**, 89–95.
- 316 S. Khan, T. G. Kazi and M. Soylak, *Anal. Lett.*, 2015, **48**(11), 1751–1766.
- 317 M. Soylak and E. Yilmaz, *Anal. Lett.*, 2015, **48**(3), 464–476.
- 318 Z. X. Zheng and W. L. Huang, *Environ. Eng. Manage. J.*, 2014, **13**(5), 1041–1046.
- 319 M. Aghamohammadi, M. Faraji, P. Shahdousti, H. Kalhor and A. Saleh, *Phytochem. Anal.*, 2015, **26**(3), 209–214.
- 320 S. S. Arain, T. G. Kazi, A. J. Arain, H. I. Afridi, J. A. Baig, K. D. Brahman, Naeemullah and S. A. Arain, *Spectrochim. Acta, Part A*, 2015, **138**, 387–394.
- 321 S. Li, M. Wang, B. Y. Yang, Y. Z. Zhong and L. Feng, *PLoS One*, 2014, **9**(9), 9.
- 322 P. Liang, J. Yu, E. J. Yang and Y. J. Mo, *Food Analytical Methods*, 2014, **7**(7), 1506–1512.
- 323 L. M. Zhang, X. L. Li, X. Y. Wang, W. T. Wang, X. S. Wang and H. Y. Han, *Anal. Methods*, 2014, **6**(15), 5578–5583.
- 324 E. Stanisz, A. Zgola-Grzeskowiak and H. Matusiewicz, *Talanta*, 2014, **129**, 254–262.
- 325 T. Li and J. H. Yang, *J. Iran. Chem. Soc.*, 2015, **12**(2), 367–370.
- 326 N. Jalbani and M. Soylak, *Food Chem.*, 2015, **167**, 433–437.
- 327 W. I. Mortada, I. M. Kenawy and M. M. Hassanien, *Anal. Methods*, 2015, **7**(5), 2114–2120.
- 328 P. Liang, J. Yu, E. J. Yang and Y. J. Mo, *Food Analytical Methods*, 2015, **8**(1), 236–242.
- 329 B. B. Chen, Y. L. Wu, X. Q. Guo, M. He and B. Hu, *J. Anal. At. Spectrom.*, 2015, **30**(4), 875–881.
- 330 A. M. D. de Jesus, M. A. Aguirre, M. Hidalgo, A. Canals and E. R. Pereira, *J. Anal. At. Spectrom.*, 2014, **29**(10), 1813–1818.
- 331 Y. Wang, Y. Y. Liu, J. Han, L. Wang, T. Chen and L. Ni, *Anal. Methods*, 2015, **7**(6), 2339–2346.
- 332 Z. A. Allothman, N. H. Al-Shaalan, M. A. Habila, Y. E. Unsal, M. Tuzen and M. Soylak, *Environ. Monit. Assess.*, 2015, **187**(2), 8.
- 333 W. P. Jia, Y. Hu, F. Li and D. M. Han, *At. Spectrosc.*, 2015, **36**(2), 96–101.
- 334 S. Bahar and R. Zakerian, *Iran. J. Chem. Chem. Eng.*, 2014, **33**(4), 51–58.
- 335 C. Labrecque and D. Lariviere, *Anal. Methods*, 2014, **6**(23), 9291–9298.
- 336 S. Z. Chen, S. P. Zhu and D. B. Lu, *Food Chem.*, 2015, **169**, 156–161.
- 337 Naeemullah, T. G. Kazi and M. Tuzen, *Food Chem.*, 2015, **172**, 161–165.
- 338 F. Sabermahani, R. Askari, S. J. Hosseini-fard and M. Saeidi, *Scientia Iranica*, 2014, **21**(6), 2012–2020.
- 339 Y. L. Zhang and S. B. Adeloju, *Talanta*, 2015, **137**, 148–155.
- 340 V. A. Lemos, G. S. do Nascimento and L. S. Nunes, *Water, Air, Soil Pollut.*, 2015, **226**(2), 10.
- 341 S. Sivrikaya, M. Imamoglu and D. Kara, *At. Spectrosc.*, 2014, **35**(4), 168–176.
- 342 Z. A. Allothman, E. Yilmaz, M. Habila and M. Soylak, *Ecotoxicol. Environ. Saf.*, 2015, **112**, 74–79.
- 343 A. Tadjarodi, A. Abbaszadeh, M. Taghizadeh, N. Shekari and A. A. Asgharinezhad, *Mater. Sci. Eng., C*, 2015, **49**, 416–421.
- 344 H. R. Fouladian and M. Behbahani, *Food Analytical Methods*, 2015, **8**(4), 982–993.
- 345 D. Ozdes and C. Durans, *At. Spectrosc.*, 2014, **35**(3), 118–126.
- 346 S. K. Behzad, A. Balati, M. M. Amini and M. Ghanbari, *Microchim. Acta*, 2014, **181**(15–16), 1781–1788.
- 347 T. Dasbasi, S. Sacmaci, A. Ulgen and S. Kartal, *Food Chem.*, 2015, **174**, 591–596.
- 348 P. Azizi, M. Golshekan, S. Shariati and J. Rahchamani, *Environ. Monit. Assess.*, 2015, **187**(4), 11.
- 349 A. Islam, A. Ahmad and M. A. Laskar, *J. AOAC Int.*, 2015, **98**(1), 165–175.
- 350 N. Jalbani, R. M. Alosmanov and M. Soylak, *At. Spectrosc.*, 2014, **35**(4), 163–167.
- 351 B. C. Russell, P. E. Warwick and I. W. Croudace, *Anal. Chem.*, 2014, **86**(23), 11890–11896.
- 352 D. Cagirdi, H. Altundag, M. Imamoglu and M. Tuzen, *J. AOAC Int.*, 2014, **97**(4), 1137–1142.
- 353 F. Sabermahani and M. A. Taher, *J. AOAC Int.*, 2014, **97**(6), 1713–1718.
- 354 S. Baytak, R. Mert and A. R. Turker, *Int. J. Environ. Anal. Chem.*, 2014, **94**(10), 975–987.
- 355 Y. E. Unsal, M. Soylak, M. Tuzen and B. Hazer, *Anal. Lett.*, 2015, **48**(7), 1163–1179.
- 356 V. Okumus, S. Ozdemir, E. Kilinc, A. Dundar, U. Yuksel and Z. Baysal, *Bioresour. J.*, 2015, **19**(1), 47–55.
- 357 L. O. dos Santos and V. A. Lemos, *Water, Air, Soil Pollut.*, 2014, **225**(9), 8.
- 358 L. A. Escudero, A. J. Blanchet, L. L. Sombra, J. A. Salonia and J. A. Gasquez, *Microchem. J.*, 2014, **116**, 92–97.
- 359 A. Saljooqi, T. Shamspur, M. Mohamadi and A. Mostafavi, *J. Sep. Sci.*, 2014, **37**(14), 1856–1861.
- 360 E. Ghorbani-Kalhor, M. Behbahani, J. Abolhasani and R. H. Khanmiri, *Food Analytical Methods*, 2015, **8**(5), 1326–1334.
- 361 M. Soylak and S. Yigit, *At. Spectrosc.*, 2015, **36**(1), 49–53.



- 362 E. Yavuz, S. Tokalioglu, H. Sahan and S. Patat, *Talanta*, 2014, **128**, 31–37.
- 363 H. C. Wu, T. Y. Su, T. L. Tsai, S. B. Jong, M. H. Yang and Y. C. Tyan, *RSC Adv.*, 2014, **4**(74), 39226–39230.
- 364 Z. Z. Cheng, M. Liu, H. K. Huang, T. X. Gu, W. D. Yan and H. L. Wen, *Geostand. Geoanal. Res.*, 2015, **39**(2), 221–232.
- 365 A. M. W. Hunt, D. K. Dvoracek, M. D. Glascock and R. J. Speakman, *J. Radioanal. Nucl. Chem.*, 2014, **302**(1), 505–512.
- 366 A. Audetat, D. Garbe-Schonberg, A. Kronz, T. Pettke, B. Rusk, J. J. Donovan and H. A. Lowers, *Geostand. Geoanal. Res.*, 2015, **39**(2), 171–184.
- 367 W. A. Brand, T. B. Coplen, J. Vogl, M. Rosner and T. Prohaska, *Pure Appl. Chem.*, 2014, **86**(3), 425–467.
- 368 K. A. Iles, J. M. Hergt, K. N. Sircombe, J. D. Woodhead, S. Bodorkos and I. S. Williams, *Chem. Geol.*, 2015, **402**, 140–152.
- 369 A. K. Kennedy, J. F. Wotzlav, U. Schaltegger, J. L. Crowley and M. Schmitz, *Can. Mineral.*, 2014, **52**(3), 409–421.
- 370 F. Jourdan, A. Frew, A. Joly, C. Mayers and N. J. Evans, *Geochim. Cosmochim. Acta*, 2014, **141**, 113–126.
- 371 S. Burger, S. F. Boulyga, M. V. Penkin, D. Bostick, S. Jovanovic, R. Lindvall, G. Rasmussen and L. Riciputi, *J. Radioanal. Nucl. Chem.*, 2014, **301**(3), 711–729.
- 372 M. Lin, Y. G. Zhao, L. F. Zhao, L. L. Li, F. Wang, L. C. Zhu, X. N. Hu and W. Ning, *J. Anal. At. Spectrom.*, 2015, **30**(2), 396–402.
- 373 N. Miliszkiewicz, S. Walas and A. Tobiasz, *J. Anal. At. Spectrom.*, 2015, **30**(2), 327–338.
- 374 Y. Q. Ke, X. F. Yao, S. H. Hu, W. Guo, Q. H. Hu, Z. L. Zhu and Z. C. Hu, *Anal. Lett.*, 2015, **48**(5), 830–842.
- 375 T. Luo, Y. Wang, Z. C. Hu, D. Gunther, Y. S. Liu, S. Gao, M. Li and S. H. Hu, *J. Anal. At. Spectrom.*, 2015, **30**(4), 941–949.
- 376 K. P. Jochum, B. Stoll, U. Weis, D. E. Jacob, R. Mertz-Kraus and M. O. Andreae, *Geostand. Geoanal. Res.*, 2014, **38**(3), 265–292.
- 377 Z. Li, Z. C. Hu, Y. S. Liu, S. Gao, M. Li, K. Q. Zong, H. H. Chen and S. H. Hu, *Chem. Geol.*, 2015, **400**, 11–23.
- 378 F. X. d'Abzac, A. D. Czaja, B. L. Beard, J. J. Schauer and C. M. Johnson, *Geostand. Geoanal. Res.*, 2014, **38**(3), 293–309.
- 379 M. Oeser, S. Weyer, I. Horn and S. Schuth, *Geostand. Geoanal. Res.*, 2014, **38**(3), 311–328.
- 380 J. A. Schuessler and F. von Blanckenburg, *Spectrochim. Acta, Part B*, 2014, **98**, 1–18.
- 381 Z. C. Hu, W. Zhang, Y. S. Liu, S. Gao, M. Li, K. Q. Zong, H. H. Chen and S. H. Hu, *Anal. Chem.*, 2015, **87**(2), 1152–1157.
- 382 L. X. Feng and J. Wang, *J. Anal. At. Spectrom.*, 2014, **29**(11), 2183–2189.
- 383 B. Fernandez, P. Rodriguez-Gonzalez, J. I. G. Alonso, J. Malherbe, S. Garcia-Fonseca, R. Pereiro and A. Sanz-Medel, *Anal. Chim. Acta*, 2014, **851**, 64–71.
- 384 A. Gundlach-Graham, E. A. Dennis, S. J. Ray, C. G. Enke, C. J. Barinaga, D. W. Koppelaar and G. M. Hieftje, *J. Anal. At. Spectrom.*, 2015, **30**(1), 139–147.
- 385 X. D. Che, F. Y. Wu, R. C. Wang, A. Gerdes, W. Q. Ji, Z. H. Zhao, J. H. Yang and Z. Y. Zhu, *Ore Geol. Rev.*, 2015, **65**, 979–989.
- 386 C. C. Wohlgemuth-Ueberwasser, U. Soderlund, V. Pease and M. K. M. Nilsson, *J. Anal. At. Spectrom.*, 2015, **30**(5), 1191–1196.
- 387 X. D. Deng, J. W. Li and G. Wen, *Chem. Geol.*, 2014, **382**, 95–110.
- 388 L. Lin, Z. C. Hu, L. Yang, W. Zhang, Y. S. Liu, S. Gao and S. H. Hu, *Chem. Geol.*, 2014, **386**, 22–30.
- 389 Y. H. Yang, F. Y. Wu, J. H. Yang, D. M. Chew, L. W. Xie, Z. Y. Chu, Y. B. Zhang and C. Huang, *Chem. Geol.*, 2014, **385**, 35–55.
- 390 J. Lewis, C. D. Coath and A. W. G. Pike, *Chem. Geol.*, 2014, **390**, 173–181.
- 391 C. Huang, Y. H. Yang, J. H. Yang and L. W. Xie, *J. Anal. At. Spectrom.*, 2015, **30**(4), 994–1000.
- 392 U. Schaltegger, A. K. Schmitt and M. S. A. Horstwood, *Chem. Geol.*, 2015, **402**, 89–110.
- 393 G. Gehrels, *Annu. Rev. Earth Planet. Sci.*, 2014, **42**, 127–149.
- 394 Q. G. Crowley, K. Heron, N. Riggs, B. Kamber, D. Chew, B. McConnell and K. Benn, *Minerals*, 2014, **4**(2), 503–518.
- 395 A. von Quadt, D. Gallhofer, M. Guillon, I. Peytcheva, M. Waelle and S. Sakata, *J. Anal. At. Spectrom.*, 2014, **29**(9), 1618–1629.
- 396 J. I. Kimura, Q. Chang, K. Itano, T. Iizuka, B. S. Vaglarov and K. Tani, *J. Anal. At. Spectrom.*, 2015, **30**(2), 494–505.
- 397 K. D. Zhao, S. Y. Jiang, H. F. Ling and M. R. Palmer, *Chem. Geol.*, 2014, **389**, 110–121.
- 398 J. P. Bernal, L. A. Solari, A. Gomez-Tuena, C. Ortega-Obregon, L. Mori, M. Vega-Gonzalez and D. G. Espinosa-Arbelaes, *Quaternary Geochronology*, 2014, **23**, 46–55.
- 399 B. Paul, J. D. Woodhead, C. Paton, J. M. Hergt, J. Hellstrom and C. A. Norris, *Geostand. Geoanal. Res.*, 2014, **38**(3), 253–263.
- 400 R. Hennekam, T. Jilbert, P. R. D. Mason, G. J. de Lange and G. J. Reichart, *Chem. Geol.*, 2015, **403**, 42–51.
- 401 C. J. Kelly, C. R. M. McFarlane, D. A. Schneider and S. E. Jackson, *Geostand. Geoanal. Res.*, 2014, **38**(4), 389–407.
- 402 G. S. Senesi, *Earth-Sci. Rev.*, 2014, **139**, 231–267.
- 403 S. J. Qiao, Y. Ding, D. Tian, L. Yao and G. Yang, *Appl. Spectrosc. Rev.*, 2015, **50**(1), 1–26.
- 404 N. J. McMillan, S. Rees, K. Kochelek and C. McManus, *Geostand. Geoanal. Res.*, 2014, **38**(3), 329–343.
- 405 Z. Q. Hao, C. M. Li, M. Shen, X. Y. Yang, K. H. Li, L. B. Guo, X. Y. Li, Y. F. Lu and X. Y. Zeng, *Opt. Express*, 2015, **23**(6), 7795–7801.
- 406 L. W. Sheng, T. L. Zhang, G. H. Niu, K. Wang, H. S. Tang, Y. X. Duan and H. Li, *J. Anal. At. Spectrom.*, 2015, **30**(2), 453–458.
- 407 C. Alvarez, J. Pisonero and N. Bordel, *Spectrochim. Acta, Part B*, 2014, **100**, 123–128.
- 408 P. Porizka, A. Demidov, J. Kaiser, J. Keivanian, I. Gornushkin, U. Panne and J. Riedel, *Spectrochim. Acta, Part B*, 2014, **101**, 155–163.
- 409 G. Vitkova, L. Prokes, K. Novotny, P. Porizka, J. Novotny, D. Vsiansky, L. Celko and J. Kaiser, *Spectrochim. Acta, Part B*, 2014, **101**, 191–199.



- 410 P. Pease and V. Tchakerian, *Aeolian Research*, 2014, **15**, 203–216.
- 411 C. P. M. Roux, J. Rakovsky, O. Musset, F. Monna, J. F. Buoncristiani, P. Pellenard and C. Thomazo, *Spectrochim. Acta, Part B*, 2015, **103**, 63–69.
- 412 C. Fabre, A. Cousin, R. C. Wiens, A. Ollila, O. Gasnault, S. Maurice, V. Sautter, O. Forni, J. Lasue, R. Tokar, D. Vaniman and N. Melikechi, *Spectrochim. Acta, Part B*, 2014, **99**, 34–51.
- 413 P. J. Gasda, T. E. Acosta-Maeda, P. G. Lucey, A. K. Misra, S. K. Sharma and G. J. Taylor, *Appl. Spectrosc.*, 2015, **69**(2), 173–192.
- 414 M. Tulej, A. Riedo, M. B. Neuland, S. Meyer, P. Wurz, N. Thomas, V. Grimaudo, P. Moreno-Garcia, P. Broekmann, A. Neubeck and M. Ivarsson, *Geostand. Geoanal. Res.*, 2014, **38**(4), 441–466.
- 415 J. Solé, *Chem. Geol.*, 2014, **388**, 9–22.
- 416 Y. Cho, S. Sugita, S. Kameda, Y. N. Miura, K. Ishibashi, S. Ohno, S. Kamata, T. Arai, T. Morota, N. Namiki and T. Matsui, *Spectrochim. Acta, Part B*, 2015, **106**, 28–35.
- 417 B. A. Cohen, J. S. Miller, Z. H. Li, T. D. Swindle and R. A. French, *Geostand. Geoanal. Res.*, 2014, **38**(4), 421–439.
- 418 B. Thornton, T. Takahashi, T. Sato, T. Sakka, A. Tamura, A. Matsumoto, T. Nozaki, T. Ohki and K. Ohki, *Deep Sea Research*, 2015, **195**, 20–36.
- 419 T. F. Boucher, M. V. Ozanne, M. L. Carmosino, M. D. Dyar, S. Mahadevan, E. A. Breves, K. H. Lepore and S. M. Clegg, *Spectrochim. Acta, Part B*, 2015, **107**, 1–10.
- 420 Y. Wang and I. D. Brindle, *J. Anal. At. Spectrom.*, 2014, **29**(10), 1904–1911.
- 421 F. D'Agostino, E. Oliveri, E. Bagnato, F. Falco, S. Mazzola and M. Sprovieri, *Anal. Chim. Acta*, 2014, **852**, 8–12.
- 422 G. M. S. Sampaio and J. Enzweiler, *Geostand. Geoanal. Res.*, 2015, **39**(1), 105–119.
- 423 W. J. Li, X. D. Jin, B. Y. Gao, C. L. Wang and L. C. Zhang, *Anal. Methods*, 2014, **6**(15), 6125–6132.
- 424 A. Ishikawa, R. Senda, K. Suzuki, C. W. Dale and T. Meisel, *Chem. Geol.*, 2014, **384**, 27–46.
- 425 J. Li, P. P. Zhao, J. G. Liu, X. C. Wang, A. Y. Yang, G. Q. Wang and J. F. Xu, *Geostand. Geoanal. Res.*, 2015, **39**(1), 17–30.
- 426 Z. Y. Chu, Y. Yan, Z. Chen, J. H. Guo, Y. H. Yang, C. F. Li and Y. B. Zhang, *Geostand. Geoanal. Res.*, 2015, **39**(2), 151–169.
- 427 O. Evdokimova, P. Zaitceva, N. Pechishcheva, A. Pupyshev and K. Shunyaev, *Curr. Anal. Chem.*, 2014, **10**(4), 449–456.
- 428 M. Krishnakumar, K. Satyanarayana and K. Mukkanti, *At. Spectrosc.*, 2015, **36**(2), 74–81.
- 429 T. Vogt, D. Bauer, M. Neuroth and M. Otto, *Fuel*, 2015, **152**, 96–102.
- 430 Y. Makonnen and D. Beauchemin, *Spectrochim. Acta, Part B*, 2014, **99**, 87–93.
- 431 T. Chen, Z. C. Hu, S. H. Liu, Y. S. Liu, S. Gao, M. Li, K. Q. Zong, H. H. Chen and S. H. Hu, *Spectrochim. Acta, Part B*, 2015, **106**, 36–44.
- 432 M. Liezers, O. T. Farmer, M. P. Dion, M. L. Thomas and G. C. Eiden, *Int. J. Mass Spectrom.*, 2015, **376**, 58–64.
- 433 J. Teran-Baamonde, J. M. Andrade, R. M. Soto-Ferreiro, A. Carlosena and D. Prada, *J. Anal. At. Spectrom.*, 2015, **30**(5), 1197–1206.
- 434 W. Doherty, *Spectrochim. Acta, Part B*, 2015, **107**, 56–60.
- 435 W. Doherty, P. C. Lightfoot and D. E. Ames, *Spectrochim. Acta, Part B*, 2014, **98**, 28–38.
- 436 A. Gourgiotis, S. Beraïl, P. Louvat, H. Isnard, J. Moureau, A. Nonell, G. Manhes, J. L. Birck, J. Gaillardet, C. Pecheyran, F. Chartier and O. F. X. Donard, *J. Anal. At. Spectrom.*, 2014, **29**(9), 1607–1617.
- 437 K. van Hoecke, V. Devulder, P. Claeys, P. Degryse and F. Vanhaecke, *J. Anal. At. Spectrom.*, 2014, **29**(10), 1819–1826.
- 438 P. Louvat, J. Moureau, G. Paris, J. Bouchez, J. Noireaux and J. Gaillardet, *J. Anal. At. Spectrom.*, 2014, **29**(9), 1698–1707.
- 439 S. Misra, R. Owen, J. Kerr, M. Greaves and H. Elderfield, *Geochim. Cosmochim. Acta*, 2014, **140**, 531–552.
- 440 K. Kaczmarek, I. Horn, G. Nehrke and J. Bijma, *Chem. Geol.*, 2015, **392**, 32–42.
- 441 R. Chakrabarti, *Curr. Sci.*, 2015, **108**(2), 246–254.
- 442 Y. J. An and F. Huang, *J. Earth Sci.*, 2014, **25**(5), 822–840.
- 443 T. Breton and G. Quitté, *J. Anal. At. Spectrom.*, 2014, **29**(12), 2284–2293.
- 444 E. K. Skierszkan, M. Amini and D. Weis, *Anal. Bioanal. Chem.*, 2015, **407**(7), 1925–1935.
- 445 D. Malinovsky, P. J. H. Dunn, P. Petrov and H. Goenaga-Infante, *Anal. Bioanal. Chem.*, 2015, **407**(3), 869–882.
- 446 J. B. Creech and B. Paul, *Geostand. Geoanal. Res.*, 2015, **39**(1), 7–15.
- 447 J. M. Koornneef, I. Nikogosian, M. J. van Bergen, R. Smeets, C. Bouman and G. R. Davies, *Chem. Geol.*, 2015, **397**, 14–23.
- 448 C. Sarkar, D. G. Pearson, L. M. Heaman and S. J. Woodland, *Chem. Geol.*, 2015, **395**, 27–40.
- 449 M. Wiedenbeck, L. P. Bedard, R. Bugoi, M. Horan, K. Linge, S. Merchel, L. F. G. Morales, D. Savard, A. K. Souders and P. Sylvester, *Geostand. Geoanal. Res.*, 2014, **38**(4), 467–512.
- 450 R. Chatterjee and J. C. Lassiter, *Chem. Geol.*, 2015, **396**, 112–123.
- 451 Z. Y. Chu, C. F. Li, E. Hegner, Z. Chen, Y. Yan and J. H. Guo, *Anal. Chem.*, 2014, **86**(22), 11141–11150.
- 452 D. J. Condon, B. Schoene, N. M. McLean, S. A. Bowring and R. R. Parrish, *Geochim. Cosmochim. Acta*, 2015, **164**, 464–480.
- 453 N. M. McLean, D. J. Condon, B. Schoene and S. A. Bowring, *Geochim. Cosmochim. Acta*, 2015, **164**, 481–501.
- 454 A. Das and D. W. Davis, *Chem. Geol.*, 2014, **385**, 1–6.
- 455 H. Z. Wei, S. Y. Jiang, T. L. Yang, J. H. Yang, T. Yang, X. Yan, B. P. Ling, Q. Liu and H. P. Wu, *J. Anal. At. Spectrom.*, 2014, **29**(11), 2104–2107.
- 456 M. T. McCulloch, M. Holcomb, K. Rankenburg and J. A. Trotter, *Rapid Commun. Mass Spectrom.*, 2014, **28**(24), 2704–2712.
- 457 P. A. Sossi, G. P. Halverson, O. Nebel and S. M. Eggins, *Geostand. Geoanal. Res.*, 2015, **39**(2), 129–149.
- 458 M. Schiller, E. van Kooten, J. C. Holst, M. B. Olsen and M. Bizzarro, *J. Anal. At. Spectrom.*, 2014, **29**(8), 1406–1416.



- 459 C. F. Li, J. H. Guo, Y. H. Yang, Z. Y. Chu and X. C. Wang, *J. Anal. At. Spectrom.*, 2014, **29**(8), 1467–1476.
- 460 Y. J. An, F. Wu, Y. X. Xiang, X. Y. Nan, X. Yu, J. H. Yang, H. M. Yu, L. W. Xie and F. Huang, *Chem. Geol.*, 2014, **390**, 9–21.
- 461 J. Li, X. R. Liang, L. F. Zhong, X. C. Wang, Z. Y. Ren, S. L. Sun, Z. F. Zhang and J. F. Xu, *Geostand. Geoanal. Res.*, 2014, **38**(3), 345–354.
- 462 C. Pin, A. Gannoun and A. Dupont, *J. Anal. At. Spectrom.*, 2014, **29**(10), 1858–1870.
- 463 J. Krajko, Z. Varga, E. Yalcintas, M. Wallenius and K. Mayer, *Talanta*, 2014, **129**, 499–504.
- 464 C. F. Li, X. C. Wang, Y. L. Li, Z. Y. Chu, J. H. Guo and X. H. Li, *J. Anal. At. Spectrom.*, 2015, **30**(4), 895–902.
- 465 J. I. Kimura, T. Nozaki, R. Senda and K. Suzuki, *J. Anal. At. Spectrom.*, 2014, **29**(8), 1483–1490.
- 466 M. R. Raven, J. F. Adkins, J. P. Werne, T. W. Lyons and A. L. Sessions, *Org. Geochem.*, 2015, **80**, 53–59.
- 467 P. von Strandmann, C. D. Coath, D. C. Catling, S. W. Poulton and T. Elliott, *J. Anal. At. Spectrom.*, 2014, **29**(9), 1648–1659.
- 468 M. A. Millet and N. Dauphas, *J. Anal. At. Spectrom.*, 2014, **29**(8), 1444–1458.
- 469 S. Okabayashi, S. Sakata and T. Hirata, *Anal. Chim. Acta*, 2015, **853**, 469–476.
- 470 R. Khan, Y. Yokozuka, S. Terai, N. Shirai and M. Ebihara, *J. Anal. At. Spectrom.*, 2015, **30**(2), 506–514.
- 471 Y. T. Lin, L. Feng, J. T. Hao, Y. Liu, S. Hu, J. C. Zhang and W. Yang, *J. Anal. At. Spectrom.*, 2014, **29**(9), 1686–1691.
- 472 N. T. Kita, P. E. Sobol, J. R. Kern, N. E. Lord and J. W. Valley, *J. Anal. At. Spectrom.*, 2015, **30**(5), 1207–1213.
- 473 S. Hu, Y. T. Lin, J. C. Zhang, J. L. Hao, W. Yang and L. W. Deng, *J. Anal. At. Spectrom.*, 2015, **30**(4), 967–978.
- 474 G. Othmane, S. Hull, M. Fayek, O. Rouxel, M. L. Geagea and T. K. Kyser, *Chem. Geol.*, 2015, **395**, 41–49.
- 475 H. R. Marschall and B. D. Monteleone, *Geostand. Geoanal. Res.*, 2015, **39**(1), 31–46.
- 476 B. D. Pauly, L. B. Williams, R. L. Bervig, P. Schiffman and R. A. Zierenberg, *Clays Clay Miner.*, 2014, **62**(3–4), 224–234.
- 477 D. Rubatto, B. Putlitz, L. Gauthiez-Putallaz, C. Crepisson, I. S. Buick and Y. F. Zheng, *Chem. Geol.*, 2014, **380**, 84–96.
- 478 G. Q. Tang, X. H. Li, Q. L. Li, Y. Liu, X. X. Ling and Q. Z. Yin, *J. Anal. At. Spectrom.*, 2015, **30**(4), 950–956.
- 479 J. C. Zhang, Y. T. Lin, W. Yang, W. J. Shen, J. L. Hao, S. Hu and M. J. Cao, *J. Anal. At. Spectrom.*, 2014, **29**(10), 1934–1943.
- 480 T. Ushikubo, K. H. Williford, J. Farquhar, D. T. Johnston, M. J. van Kranendonk and J. W. Valley, *Chem. Geol.*, 2014, **383**, 86–99.
- 481 Y. Liu, Q. L. Li, G. Q. Tang, X. H. Li and Q. Z. Yin, *J. Anal. At. Spectrom.*, 2015, **30**(4), 979–985.
- 482 Q. Liu, X. L. Hou, W. J. Zhou and Y. C. Fu, *J. Am. Soc. Mass Spectrom.*, 2015, **26**(5), 725–733.
- 483 L. L. Cui and X. Wang, *Anal. Methods*, 2014, **6**(22), 9173–9178.
- 484 L. L. Cui and X. Wang, *Int. J. Mass Spectrom.*, 2014, **372**, 46–50.
- 485 F. Fourel, F. Martineau, M. Seris and C. Lecuyer, *Geostand. Geoanal. Res.*, 2015, **39**(1), 47–53.
- 486 P. S. Ross, A. Bourke and B. Fresia, *Geochem.: Explor., Environ., Anal.*, 2014, **14**(2), 171–185.
- 487 S. J. Piercey and M. C. Devine, *Geochem.: Explor., Environ., Anal.*, 2014, **14**(2), 139–148.
- 488 M. F. Gazley, C. M. Tutt, L. I. Brisbout, L. A. Fisher and G. Duclaux, *Geochem.: Explor., Environ., Anal.*, 2014, **14**(3), 223–231.
- 489 P. S. Ross, A. Bourke and B. Fresia, *Geochem.: Explor., Environ., Anal.*, 2014, **14**(2), 187–196.
- 490 L. Fisher, M. F. Gazley, A. Baensch, S. J. Barnes, J. Cleverley and G. Duclaux, *Geochem.: Explor., Environ., Anal.*, 2014, **14**(2), 149–159.
- 491 M. le Vaillant, S. J. Barnes, L. Fisher, M. L. Fiorentini and S. Caruso, *Geochem.: Explor., Environ., Anal.*, 2014, **14**(3), 199–209.
- 492 G. J. Simandl, R. S. Stone, S. Paradis, R. Fajber, H. M. Reid and K. Grattan, *Miner. Deposita*, 2014, **49**(8), 999–1012.
- 493 G. J. Simandl, S. Paradis, R. S. Stone, R. Fajber, R. D. Kressall, J. Crozier and L. J. Simandi, *Geochem.: Explor., Environ., Anal.*, 2014, **14**(3), 211–221.
- 494 G. J. Simandl, R. Fajber and S. Paradis, *Geochem.: Explor., Environ., Anal.*, 2014, **14**(2), 161–169.

